EVOLUTION
INTERNATIONAL JOURNAL OF ORGANIC EVOLUTION
SSE
SOCIETY for the STUDY of EVOLUTION

Evolution of aerial spider webs coincided with repeated structural optimization of silk anchorages

Journal:	*Evolution*
Manuscript ID	19-0218
Manuscript Type:	Original Article
Keywords:	animal architecture, evolutionary biomechanics, extended phenotype, spider silk

Evolution of aerial spider webs coincided with repeated structural optimization of silk anchorages

Abstract

Physical structures built by animals challenge our understanding of biological processes and inspire the development of smart materials and green architecture. It is thus indispensable to understand the drivers, constraints and dynamics that lead to the emergence and modification of building behaviour. Here, we demonstrate that spider web diversification repeatedly followed strikingly similar evolutionary trajectories, guided by physical constraints. We found that the evolution of suspended webs that intercept flying prey coincided with small changes in silk anchoring behaviour with considerable effects on the robustness of web attachment. The use of nanofiber based capture threads (cribellate silk) conflicts with the behavioural enhancement of web attachment, and the repeated loss of this trait was frequently followed by physical improvements of web anchor structure. These findings suggest that the evolution of building behaviour may be constrained by major physical traits limiting its role in rapid adaptation to a changing environment.

Keywords

animal architecture; macro-evolution; evolutionary biomechanics; extended phenotype; spider silk; bio-inspiration

Introduction

From efficient tunnel networks of ant colonies and strikingly effective thermal control of termite mounds to the aesthetic assembly of bower bird displays and ecosystem-forming beaver dams: the complexity, efficiency and far reaching effects of animal buildings excite and inspire (Hansell 2005) - their study may even drive technical innovation towards a greener future (Turner and Soar 2008). Our understanding of how building behaviour evolves within an ecological context is limited because animal architectures blur the boundaries of an organism's phenotype (Dawkins 1982; Odling-Smee et al. 2003; Bailey 2012).

Spider webs are flagship examples of animal architectures, and their enormous diversity in shape render them an ideal system in which to unravel the evolutionary dynamics of building behaviour. Hypotheses of spider web evolution have been formulated for more than a hundred years, with a focus on the role of putatively singular events, such as the emergence of distinct building routines, specific silk proteins or viscid silk (Coddington 1986; Eberhard 1990; Bond and Opell 1998; Coddington 2005; Blackledge et al. 2009). In contrast, recent (Bond et al. 2014; Fernández et al. 2014; Fernández et al. 2018) and controversial (Garrison et al. 2016; Eberhard 2018a) phylogenomic studies favour a more dynamic scenario, where similar behavioural routines have repeatedly evolved. The core of the controversy is the question whether the evolution of behavioural building routines is dynamic and repeatable or slow and determined by contingent events. The answer to this question goes beyond spider webs: if the evolution of behaviour is less constrained than the evolution of physiological and morphological traits it could facilitate rapid responses to environmental changes, thereby setting the course of evolutionary trajectories (Wcislo 1989; Odling-Smee et al. 2003; Ord and Summers 2015).

Here, we approach the inference of spider web evolution from a previously neglected angle: the idea that a robust foundation is the basis for a stable building (Hansell 2005). It has been proposed that the evolution of tape-like thread anchorages at the base of modern spiders (Araneomorphae) ~300 MYA dramatically changed silk usage: spiders were no longer restricted to spinning substrate-bound sheets, but could produce complex three dimensional structures by spatially arranging single lines (Coddington 2005; Wolff et al. 2017). Despite this early insight, subsequent work has focussed on the role web geometry and silk proteins in the evolution of webs, neglecting the role of web anchorages.

Since anchor strength underlies global mechanical rules, it is possible to derive parameter estimates for its physical optimization (Pugno et al. 2013). A previous parametric study by two of us revealed that a single parameter in anchor structure (i.e. the location of the dragline joint) explains most of the variation in anchor strength (Wolff and Herberstein 2017).

We hypothesized that lineages that achieve optimal anchor strength by behavioural means, also achieve web types with greater mechanical integrity. To test this, we quantified silk anchor structure and web types in 105 spider species of 45 families, covering all major clades of the modern spiders. We first built a numerical model to identify the optimum in anchor structure and tested if it matched the adaptive peaks in the macro-evolutionary signal. We then related silk anchor performance to anchor building behaviour and the morphology of the spinning apparatus. Specifically, we tested how the innate spinneret choreography during anchor production affects anchor structure (Wolff et al. 2017), and how the configuration of the spinning apparatus affects the kinematic properties of the system. Here we distinguished between such spiders that bear a spinning plate, the so-called *cribellum*, in the anterior part of the spinning apparatus (cribellate spiders) and such, in which this organ is reduced and non-functional (ecribellate spiders). The cribellum is used to produce sophisticated adhesive capture threads, representing bundles of nano-fibres, and we hypothesized that it restricts the mobility of the spinnerets involved in silk anchor production. Finally, we aimed to determine the sequence of silk anchor enhancement and aerial web evolution: did an evolutionary enhancement of silk anchors occur after the evolution of aerial webs, or did enhanced anchors precede the evolution of aerial webs? Such time sequences could provide insights into whether silk anchor mechanics constrain or facilitate the evolution of web architectures.

Material and Methods

Material sourcing and fieldwork

Spiders were collected in Eastern Australia (NSW, QLD, VIC and TAS), New Zealand (North Island), Germany, Italy, the U.S.A., Argentina and Morocco, or obtained from lab stocks (3 species) and kept in the lab in plastic jars or boxes with slightly moistened tissue (complete list of species and collection data in Tab. S9). We aimed for three individuals per species, while we did not expect differences in our target traits between sexes and developmental stages (confirmed by intraspecific comparison of anchor structure in *Argiope keyserlingi* and *Nephila plumipes*, unpub.). However, for some species only single individuals could be obtained (samples sizes are given in Tab. S9 and Fig. 2). Silk samples were collected on glass slides that were left in the enclosures for 2-7 days. Silk samples were stored in dry boxes and are deposited at the Department of Biological Sciences, Macquarie University (MQ). Voucher specimens of spiders are deposited at the Australian Museum (AM), the Zoological Museum of the University of Greifswald (UG), the Natural History Museum of Argentina (MA), Canterbury Museum (CM) and private collections (see Tab. S9 for details).

For each species we recorded the web type based on field and lab observations: 0, no web (hunting spider); 1, substrate bound web (capture area ± parallel and directly attached to the substrate surface); 2, aerial web (capture area suspended, indirectly attached to substrate, and its shape ± independent of substrate topography). These categories were chosen, because they represent different demands of a robust anchorage.

Morphology of spinning apparatus

Spiders were investigated under dissection microscopes to score two states of the spinning apparatus: 0, ecribellate; 1, cribellate.

Kinematics of spinning apparatus

Spinning choreography was studied in a subset of 71 species following the methods described in (Wolff and Herberstein 2017), using a Basler Ace 640×480pix USB 3.0 high speed video camera (Basler AG, Ahrensburg, Germany), equipped with a Navitar Precise Eye extension tube including a 1.33× magnification lens (Navitar, Inc., Rochester, NY, USA). A 0.25× accessory lens was used for larger spiders (body length >10 mm). The resulting field of view was 1.3 × 1.0 mm at a pixel size of 2.1 µm for the basic configuration, and 5.3 × 4.0 mm at a pixel size of 8.3 µm for the configuration with the 0.25× lens. Videos were recorded with 500 frames per second, using the *TroublePix* software (NorPix, Inc., Montreal, QC, Canada) with continuous looping and post event trigger.

Videos were processed with *ImageJ 1.5* (Schneider et al. 2012) as detailed in (Wolff and Herberstein 2017). The movements of both anterior lateral spinnerets were manually tracked using the *MTrackJ* plugin (Meijering et al. 2012), taking the centre of the piriform spigot field on the anterior lateral spinneret apex as a reference. Each spinning sequence consists of a set of stereotypic spinneret trajectories. Single trajectories were extracted, their tracking coordinates positioned in a generalized grid and partitioned into 50 landmarks defined by regularly spaced time intervals (for details on this procedure we refer to (Wolff and Herberstein 2017; Wolff et al. 2017)). This procedure ensures that the relative orientation of the kinematic track shapes towards the animal's body axis is maintained. From these shapes we calculated the relative track proportions h_r as the y-dimension divided by the x-dimension of the aligned track shape, where the minimal x-coordinate denotes the proximal turning point of the adducted spinneret (where the dragline is usually placed) and the maximal x-coordinate the lateral turning point of the abducted spinneret. This variable reflects under which angle piriform silk is spread away from the dragline joint.

The final dragline location may not only be determined by the trajectories of single kinematic elements, but also how these are applied along the animal's body axis. Some spiders perform a back-and-forth movement of the abdomen to further modulate dragline placement. This behaviour was recorded as a binary character: 0, absent; 1, present.

Structure and morphometrics of silk anchors

Nine to twenty silk anchors per individual spider were imaged with Leica M205A (Leica Microsystems GmbH, Wetzlar, Germany) and Motic (Motic Inc. Ltd., Hong Kong) stereo microscopes with mounted cameras.

Morphometrics of silk anchors was performed on micrographs in *ImageJ*. We calculated the dragline placement variable c_d as follows: distance d between the dragline joint (point were the dragline leaves the anchor) and the anterior border of the anchor divided by the longitudinal dimension of the anchor. In anchors of some basal species the individual dragline fibres do not leave the anchor as a bundle, but separately in different locations. In these cases the pair of fibres located closest to the frontal border of the anchor was taken into consideration and their d-values were averaged. Details on the morphometric characterization of silk anchors are described in (Wolff and Herberstein 2017).

Numerical model

The elastic membrane was modelled by discretising it in a network of elastic bonds (i.e. springs) in a square-diagonal lattice, using a generalized non-linear 3D co-rotational truss formulation (Cook et al. 2001). A homogenization procedure was adopted, imposing the equivalence of the strain energy density of the lattice with that of a corresponding homogeneous membrane (Ostoja-Starzewski 2002; Brely et al. 2015). We used a standardized anchor geometry with length l = 1 mm, width w = 1 mm, thickness t = 1 µm, and with the dragline fused with the membrane over a length of c_l = 0.33 mm. To account for differences in silk properties, we performed separate simulations for a combination of membrane and dragline stiffness values, as empirically observed in the basal sheet web spider *H. troglodytes* and the aerial web builder *N. plumipes*: Young's modulus of piriform silk membrane E_p = 0.25 GPa for *Hickmania* and E_p = 1.7 GPa for *Nephila* (see tensile test methodologies and results in S1), and Young's modulus of dragline E_d = 10 GPa for *Hickmania* and E_d = 15 GPa for *Nephila* (after (Piorkowski et al. 2018) and (Swanson et al. 2006)).

The interface was modelled assuming a 3D exponential-like traction-separation law (cohesive zone model) of the form $T_i = \Delta_i \frac{\phi_i}{\delta_i^2} \cdot \exp\left(\sum_j - \frac{\Delta_j^2}{\delta_j^2}\right)$ where ϕ_i, Δ_i and δ_i are the work of

separation, the crack gap value and the characteristic length (i.e. the gap value corresponding to the maximum traction) (Salehani and Irani 2018). The resulting system of coupled non-linear equations in matrix form was solved using an algorithm based on the Newton-Raphson method (Ostrowski 1973) implemented in C++ and run on the OCCAM HPC cluster at the University of Torino. The adhesive energy of the interface, calculated as the integral of the cohesive law, was taken to be equal to $\phi = 0.5$ MPa·mm.

We simulated the maximal pull-off forces for different c_d between 0.0 and 0.5. To further study the effect of c_d on anchor robustness we simulated maximal pull-off forces for different pull-off angles (loading angles) between 15° (± parallel to substrate along spinning direction) and 165° (± parallel to substrate against spinning direction, e.g. dragline flipped over) for a c_d of 0.0, 0.2 and 0.4.

Phylogenetic inference

The phylogenetic tree was estimated using three mitochondrial (12S, 16S, COI) and three nuclear (histone H3, 18S, 28S) markers, taken from the study of Wheeler et al. (2017) and supplemented with sequences from GenBank (Tab. S11). The clades obtained as monophyletic in the genomic analyses of Fernández et al. (2018) (Araneae), Kallal et al. (2018) (Araneidae), Cheng and Piel (2018) (oval calamistrum clade), and Maddison et al. (2017) (Salticidae) were constrained for monophyly, as a backbone tree. The reason for such constrained analysis is that our six-markers dataset will not have sufficient signal to overturn the results based on hundreds to thousands of markers from the genomic analyses.

We lacked sequence data for 58 of the studied species but were able to use sequences from closely related species to obtain a good estimate of phylogenetic placement and branch lengths (Tab. S10). For an additional set of 20 species we did not have close relatives, or a close relative was already in the dataset; these were connected randomly in internal branches according to their taxonomic placement (Tab. S10). Two non-araneomorph terminals were added to root the tree, representing the lineages Mesothelae and Mygalomorphae; these were excluded from the comparative analyses.

Alignment of sequences was performed with *MAFFT* version 7 online service (Katoh et al. 2017). Model selection was made with *jModeltest* (Darriba et al. 2012). Secondary dating of main tree nodes was assigned as mean and 95% HPD taken from Fernández et al. (2018) and analysed in *BEAST2* (Bouckaert et al. 2014) under a relaxed lognormal clock model (Drummond et al. 2006), using the CIPRES Science Gateway (Miller et al. 2010) for 50 million generations. After a pilot run, GTR models were simplified to HYK to achieve convergence.

The 20 species without sequence data were free to connect anywhere along any branch within taxonomically constrained clades; to avoid for very short tip branches, we placed a uniform prior for the clade age, with minimum 2 mya for congeners and 5 mya for higher taxa.

To account for the uncertainty of the phylogenetic estimation, we obtained 100 trees randomly drawn from the post-burnin posterior sample of the Bayesian analysis in *BEAST2*. The subsequent comparative analyses are averaged over these 100 trees, and thus incorporate the uncertainty in phylogenetic parameters.

Macro-evolutionary framework

We used phylogenetic comparative methods to infer adaptive peaks and constraints and test evolutionary associations of silk anchor structure, spinning apparatus, spinning kinematics and web building behaviour, using multiple packages in the software environment *R*.

To select the best model for ancestral character estimation (*ACE*), we calculated the corrected Akaike information criterion weights (*AICcw*) using *geiger* 2.0.6 (Pennell et al. 2014). For spinning apparatus state, we fitted an Equal Rates model (*ER*), an All Rates Different model (*ARD*) and a customized model with supressed state 1 to 2 transitions (following Dollo's law, see (Alfaro et al. 2018)), of which the Dollo's law model had the strongest support (*AICcw* = 0.640). For web type ER, SYM and ARD models were fitted, of which the ER model was preferred (*AICcw* = 0.583). ACE was performed with stochastic character mapping in *phytools* (Revell 2012), on the consensus tree with 100 repeats and across a sample of 100 trees with 1 simmap per tree.

To infer evolutionary dynamics of the continuous variables dragline placement c_d and spinning track dimensions h_r we used a multi-step model-selection process. To test if changes in discreet characters led to differential evolutionary dynamics, we fitted different Brownian Motion (*BM*) and generalized Ornstein-Uhlenbeck-based Hansen models (*OU*) using the package *OUwie* 1.50 (Beaulieu and O'Meara 2014). We built a set of models for spinning apparatus state (*c*) and web type (*w*, web type was binary discretized for this purpose in aerial web: 0, no; 1, yes) using a randomly drawn simmap of *c*- and *w*-regimes for each of the 100 trees from our sample. We tested a single-regime BM (*BM1*) and OU model (*OU1*), and per regime type each a two-σ^2 (*BMS*) BM model, and OU models with two θ (*OUM*), two θ and two σ^2 (*OUMV*), two θ and two α (*OUMA*), and two θ, two σ^2 and two σ^2 (*OUMVA*). The *AICcw* was used to compare the fit between all 12 models for each tree. *AICcw* and model parameters were then summarized across all 100 trees and their median and variance assessed to select for the model(s) that could best explain the data. For each c_d and h_r we ran two loops across the

tree sample to check for the effect of the stochastic component in this procedure, and found comparable results (i.e. similar models were favoured and no major differences in median parameter estimates).

While prior clade assignments are useful to compare defined groups, they may miss some hidden patterns caused by unstudied effects. We therefore additionally used the methods *SURFACE* (Ingram and Mahler 2013) and *bayou* (Uyeda and Harmon 2014) on the consensus tree (S3). *SURFACE* performs stepwise AIC estimation to identify regime shifts in θ assuming evolution under the OU process with constant σ^2 and α. *bayou* uses a reverse-jump Markov chain Monte Carlo procedure for the similar purpose. By this, we also checked, if evolution of our variables was driven by singular events (i.e. the occurrence of only a single shift), which may bias PGLS inference (Uyeda et al. 2018). Priors in *bayou* analyses were defined as follows: for α a half-Cauchy distribution with *scale* = 0.1; for σ^2 a half-Cauchy distribution with *scale* = 0.01; for θ a uniform distribution delimited by *min* = 0 and *max* = 1; and a conditional Poisson for the number of shifts. Because the results of *bayou* can be sensitive to the mean number of shifts in the prior (Ho and Ané 2014; Uyeda and Harmon 2014), we ran each two chains over 500,000 generations for prior means of 10, 15, 20, and 25 shifts with equal shift probability and one shift maximum per branch, discarding the first 30% as burn-in. For c_d chains with priors of 20 and 25 shifts and for h_r chains with priors of 15, 20 and 25 shifts arrived at a similar posterior (S6). Results are reported from these chains only (means of converged chains given, and graphical representation of shifts for c_d from a randomly chosen chain with a prior of 25 shifts and for h_r from a randomly chosen chain with a prior of 20 shifts).

Trait correlation

To reveal patterns of trait correlation we used phylogenetic generalized least squares models (PGLS), which accounts for the non-independence of observations due to common evolutionary history (Felsenstein 1985; Grafen 1989; Freckleton et al. 2002), across pairwise combinations of our variables: (1) $c_d \sim$ *spinning apparatus*; (2) $c_d \sim$ *web type*; (3) $h_r \sim$ *spinning apparatus*; and (4) $h_r \sim$ *web type*. Further, we performed PGLS regressions between $c_d \sim h_r$. PGLS analyses were performed with the R package *phylolm* (Tung Ho and Ané 2014) and branch length transformation were optimized by setting *lambda* value through maximum likelihood. To account for phylogenetic uncertainty in PGLS results (Donoghue and Ackerly 1996) we repeated each model across our posterior sample of 100 phylogenetic trees. The influence of phylogenetic uncertainty on results was estimated by the variation in model

parameters across all runs. Phylogenetic sensitivity analyses were performed for each PGLS model with the R package *sensiPhy* (Paterno et al. 2018).

Geometric Morphometrics

To test if the shape of spinning paths differed between spiders with different spinning apparatus and web type, and if it correlates with c_d and h_r, geometric morphometrics was performed using the R package *geomorph* (Adams and Otárola-Castillo 2013). For this purpose aligned spinneret trajectories were discretized into 50 landmarks with similar time steps, as described in (Wolff et al. 2017). We used both an alignment towards the median axis between the paired spinnerets which keeps the angular orientation of the trajectories (see (Wolff et al. 2017)), and General Procrustes Alignment (GPA), which omits this information and extracts the pure shape. We then performed Phylogenetic Procrustes ANOVA against the variable 'spinning apparatus' and 'web type' and Phylogenetic Procrustes Regression against variables c_d and h_r using the consensus tree.

Results

Physical constraints and optima of silk anchorages

Our broad comparative study of anchor structures across the spider tree of life confirmed that there is a general structure of web anchors, consisting of a dragline attached to the substrate with numerous, sub-micron sized, glue coated fibres (*piriform silk*) combined into a patch-like film. The major interspecific differences are the shape of the piriform silk film and the structure of the dragline joint. The dragline can be embedded all the way through this film, or be attached centrally only. The attachment position of the dragline greatly affects where and how load is transmitted onto the underlying film. The more central the dragline placement c_d (i.e. the dragline centrality) the better the anchor can withstand stress from a variably loaded silk line. Preliminary studies have revealed that this is the most significant determinant of web anchor robustness (Wolff and Herberstein 2017).

To identify the optimum of the dragline placement parameter, we built a numerical model based on the theory of thin film contact mechanics (Pugno 2011), approximating silk anchorages as tape like films. Previous models of web anchor mechanics, such as the staple-pin model (Sahni et al. 2012; Pugno et al. 2013), do not account for the observed variation in dragline joint structure and presume independent peeling events of single piriform fibres, which, however, have not been empirically observed in peel-off tests with attachment discs from orb web spiders (Araneidae) and wandering spiders (Ctenidae) (Wolff et al. 2015; Wolff

2017; Wolff and Herberstein 2017). In our comparative analysis reported here, we did not observe a single case of an attachment disc composed of parallel piriform fibres that did not overlap with each other, confirming that the staple-pin model is not appropriate to describe the mechanics of spider web anchorages. We therefore developed a new model, approximating the piriform silk film as a single tape-like element, where load is shared and transmitted between piriform fibres.

To apply our results to a range of silk properties found in spiders, we repeated simulations for parameters measured in the Tasmanian cave spider (*Hickmania troglodytes*), representing an ancient lineage, and in golden orb web spiders (*Nephila plumipes*), a representative of derived aerial web builders. We found that anchor strength improved if its geometrical structure is allowed to maximize the peeling line (total length of the detachment front) before detachment, which occurred in the range c_d = 0.3–0.5 mm/mm for typical anchorage parameters (Fig. 1a). The exact optimum within this range depends, amongst others, on the material properties of the silk. For draglines as stiff as the anchor silk (or point-like dragline joints) c_d = 0.5 and it decreased with an increase in stiffness difference between dragline and anchor silk. During detachment, the stress concentrations and subsequent delamination front approximated a circular shape that became more elliptical as the peeling angle increased (Fig. 1b). The c_d value determined a delay in the detachment front reaching the anchorage edges (for typical anchorage shapes), leading to an overall increase in robustness. This is in agreement with empirical data on silk anchors of orb web spiders (S2) and up-scaled physical models (Wolff and Herberstein 2017). Notably, the effect of the pulling angle on anchor resistance was reduced at optimal c_d (Fig. 1c,d). This indicates that the benefit of high c_d is realised in dynamic loading situation, such as in aerial webs.

Evolutionary dynamics of spider web traits

Spider webs are diverse in shape and function but for the purpose of our analyses we categorised the web phenotypes into: ‘substrate webs’, ‘aerial webs’ and ‘webless foragers’ (see methods for definition). Aerial webs were hereby characterized by a capture area (sheet or tangle) that is fully suspended (i.e. indirectly attached to the substrate by supporting lines) and has a shape that does not resemble the substrate topography, such as in orb webs, cob webs and canopy webs. This categorization followed the assumption that such aerial webs often have an increased demand in anchor robustness, because of the use of a limited number of anchor lines and higher exposure to mechanical impacts, such as wind, rain and flying animals. Our phylogenetic analyses indicated that substrate webs are the ancestral state in the

Araneomorphae and aerial webs have evolved five to six times independently: at the basis of Araneoidea, in Uloboridae, Deinopidae, Pholcidae, and within Desidae (Fig. 2; S4).

We found, that lineages with anchors near the physical optimum of $c_d = 0.3–0.5$ included all aerial web builders that lack a cribellum, one cribellate substrate web building species (*Megadictyna thilenii*), and some ecribellate hunting spiders belonging to Mimetidae, Arkyidae, Thomisidae, Oxyopidae, Trechaleidae, Philodromidae, Salticidae and Toxopidae. We found multiple support for six shifts in the evolutionary regime of c_d (Fig. 2; S5): *shift 1* in Pholcidae (posterior probability $pp = 0.494$); *shift 2* in the grate-shaped tapetum clade (excl. Zoropsidae) ($pp = 0.474$); *shift 3* at the basis of Salticidae ($pp = 0.405$); *shift 4* at the basis of Entelegynae ($pp = 370$); *shift 5* at the basis of Araneoidea ($pp = 0.336$); and *shift 6* within Desidae (*Cambridgea*) ($pp = 0.309$). Shift 5 and 6 (both aerial web spinners; adaptive optimum $\theta \sim 0.36$ mm/mm), and shifts 1, 2 and 3 (aerial web spinning and hunting spiders; $\theta \sim 0.30$ mm/mm) were convergent, shifting towards similar evolutionary optima (Fig. 3f). Shifts 2, 5 and 6 coincided with cribellum loss and shifts 1 and 5 with the evolution of aerial webs. Notably all supported shifts led towards an elevated adaptive optimum θ. Our data suggest that the evolutionary trend towards an elevated c_d happened stepwise, for instance the exceptional c_d in Araneoidea evolved from an estimated root optimum of $\theta \sim 0.18$ mm/mm, with the first shift around 250 MYA towards $\theta \sim 0.24$ mm/mm, and the second one around 180 MYA towards $\theta \sim 0.36$ mm/mm. The exact location of these shifts differed between *SURFACE* and *bayou* methods, and an additional shift at the basis of Nicodamidoidea+Araneoidea around 200 MYA is possible (Fig. 2; S5; S6).

We found strong correlations between c_d and the configuration of the spinning apparatus. Spiders with a cribellum (the basal state) produced a significantly smaller c_d ($p = 0.005$; S7) and cribellum loss repeatedly led to an increase of c_d (Fig. 2). Furthermore, c_d correlated with spinning choreography, i.e. the relative height of the spinneret trajectory geometry h_r ($p = 0.004$; S7): h_r is on average 1.6 times larger in ecribellate spiders ($p < 0.001$; S7). These results were highly robust to phylogenetic uncertainty (S7). Notably, the shape of the spinning path did not differ between cribellate and ecribellate spiders ($p_r = 0.316$) (S8). This indicates that it is not the shape of the spinning path, but its orientation and proportions that affect c_d. Our kinematic and morphological studies revealed that the cribellum mechanically constrains the mobility of the anchor producing spinnerets (the anterior lateral spinnerets) by blocking them on the anterior side. As a result, most cribellate spiders spread the spinnerets more laterally, leading to smaller h_r and c_d.

To further investigate if the configuration of the spinning apparatus (c) and web building behaviour (w) had an effect on the evolutionary dynamics of c_d, we compared the fit of single and two-regime Brownian Motion (BM) and Ornstein-Uhlenbeck (OU) models. To account for phylogenetic uncertainty, we repeated the analyses across a sample of 100 phylogenetic trees.

We found strong support for a scenario, where the evolution of anchor structure was highly dynamic in substrate web builders and hunters, but stabilized around an elevated optimum in aerial web builders. Among all models, OUw models provided the best explanation for the extant variation of c_d (*AICcw* (OUMVAw) = 0.667±0.339; *AICcw* (OUMAw) = 0.163±0.295; Fig. 3a). Under these models c_d evolved at an increased adaptive optimum with a high adaptive potential in aerial web builders, while c_d of substrate web building and hunting spiders followed a stochastic evolution (i.e. $t½ >> T$; Fig. 3b,c). There was support that cribellum loss affected the evolution of c_d (mean *ΔAICc* (OUMc-BM1) = 3.43, mean *ΔAICc* (OUMc-OU1) = 4.34). The best fit among OUc-models was the OUMc, a model under which c_d of ecribellate spiders had a higher adaptive optimum θ but evolutionary rates σ^2 and adaptive potential α did not differ between cribellate and ecribellate spiders. The inferred mean $t½$ was close to the total height of the tree T, which represents a moderate α (Cooper et al. 2016).

Similar analyses on the spinning track proportions h_r indicated five shifts in the evolutionary regime (Fig. 2; S5). All but one shift coincided with cribellum loss, and three shifts co-occurred with aerial webs. Branches accommodating shifts 1, 3, 4 and 5 also had shifts in c_d, indicating a causal link. The constitution of the spinning apparatus had clearly affected the evolution of h_r (*AICcw*(OUMAc) = 0.442 ±0.247; *AICcw*(OUMVAc) = 0.388 ±0.269), whereas OUw models were indistinguishable from BM models (Fig. 3d). The contrasting results for c_d indicate that h_r alone does not explain c_d. There is, at least, one additional behavioural component affecting c_d, which is the movement of the body while a series of alternating spinneret movements are performed. The highest c_d values (excluding the hunting spider *Australomisidia*) were found in spiders that perform a back-and-forth movement of the abdomen during anchor production. This behaviour has evolved independently in the Araneoidea and within the New Zealand Desidae.

Discussion

This study is the first to assess attachment as a component in the evolution of animal architectures. We have shown that small changes in anchor structure profoundly affect web attachment. Notably, structural optimization does not necessarily come at a higher material cost, as the effect of dragline placement is significant for similar sized silk films. It therefore appears

counter-intuitive that not all extant spiders exhibit an optimized anchor structure and that anchor building behaviour evolved slowly and stepwise. Our results indicate this is due to two reasons.

First, the evolution of anchor structure is relaxed in substrate web builders and wandering spiders. Substrate web builder rely less on robust silk anchorages, because their webs are attached with numerous anchor lines and are usually less exposed to the environment than aerial webs. Hunting spiders may have different demands on silk anchorages, depending on whether draglines are used for locomotion, or whether silk is merely used in substrate-bound sheets for shelters and eggs sacs. This may explain the high variation and lability of c_d in hunting spiders.

Second, the evolution of anchor building behaviour may be constrained by physical traits. Our data suggest that the cribellum organ, a sophisticated spinning plate that produces nanofiber-based capture threads, is one example of such a physical constraint on behavioural evolution. This is important since it provides an explanation for an old enigmatic problem in the understanding of spider web evolution: why nano-fibre capture silk was lost so frequently across the spider tree, resulting in cribellate spiders being largely outnumbered by ecribellate spiders, and why only few cribellate spiders evolved aerial webs, even though cribellate silk can be highly efficient in prey capture (Opell 1994; Opell and Schwend 2009; Bott et al. 2017). Our results indicate that the cribellum represents a significant physical constraint on the spinning of robust anchorages limiting the capability to build efficient suspended webs.

We found that all changes in the evolutionary mode of anchor spinning behaviour followed or coincided with the loss of the cribellum. However, not all events of cribellum loss were followed by changes in the evolutionary dynamics of spinning behaviour, indicating that further changes of physical traits, such as the arrangement of muscles and spinneret articulation, might have been necessary to alter spinning behaviour in a way to optimize anchor structure. Cribellum loss may thus rather be an important pre-condition for further evolutionary enhancement of silk attachment.

Multiple support for an exceptional (i.e. faster and more stabilized) evolution of anchor structure in aerial web builders suggests its adaptive value for such webs. Aerial webs repeatedly evolved after or with evolutionary shifts in silk anchor structure and anchor spinning behaviour occurred, supporting the idea that web anchor performance affects the evolution of web architecture.

Limited anchor performance may thus in itself be an important constraint in the evolution of web building behaviour, and its improvement may have accelerated spider web diversification: web architecture is phylogenetically labile and enormously variable in

ecribellate orb-web and cobweb spiders (Blackledge and Gillespie 2004; Eberhard et al. 2008; Kuntner et al. 2010), lineages in which anchor structure has reached the physical optimum. Such a rapid turnover of web building behaviour may mask evolutionary histories in these lineages. Concluding that similarities in building routines indicate a common origin can be problematic in these cases, since the probability of parallelism is high (Ord and Summers 2015; York and Fernald 2017). Nevertheless, we note that the idea of an independent origin of orb webs in Araneoidea and Uloboridae as indicated by this and a previous study (Fernández et al. 2018), has recently received some scepticism (Garrison et al. 2016; Coddington et al. 2018; Eberhard 2018b). In particular, it was argued that the loss of complex traits such as orb web building is more likely than their emergence, and the phylogenetic framework should account for that. Here, we tested three different evolutionary models, of which the *Equal Rates* model was statistically preferred. However, because our category 'aerial web' contains different architectural shapes of webs, our results are not suited to draw definitive conclusions on the homology of a single architectural type, such as orbs – a question that is outside the scope of this study. If assuming an early origin of the orb web at the root of Entelegynae, an early shift in the macro-evolutionary optimum of silk anchor structure (shift 4) would have coincided with the evolution of this ancient (cribellar) orb web. Thus, we refrain from drawing conclusions on the chronological order of web and web anchor evolution. Reconstructing the evolution of biomechanics and building routines of web elements other than anchors could help to resolve the chronology of evolutionary events that have preceded complex web architectures.

To the best of our knowledge, this is the first study that integrates physical and macro-evolutionary modelling to explain the evolution of animal architectures. Using web anchorages as an example, we demonstrate that to understand the evolution of complex behaviour, like web building, it is essential to identify the interdependencies of behavioural and physical traits. Future works should therefore study the evolution of animal architectures and the morphology of their architects in combination.

We conclude that the evolution of behaviour and extended phenotypes may be not as free as previously suggested (West-Eberhard 1989; Odling-Smee et al. 2003; Duckworth 2009; Bailey et al. 2018), but may rather be tightly bound to evolutionary changes in physical traits. In the case of spider webs the evolutionary removal of such physical constraints may have led to an evolutionary cascade resulting in an enormous diversity of web architectures and outstanding ecological success.

References

Adams, D. C. and E. Otárola-Castillo. 2013. geomorph: an R package for the collection and analysis of geometric morphometric shape data. Methods in Ecology and Evolution 4:393-399.

Alfaro, R. E., C. E. Griswold, and K. B. Miller. 2018. Comparative spigot ontogeny across the spider tree of life. PeerJ 6:e4233.

Bailey, N. W. 2012. Evolutionary models of extended phenotypes. Trends Ecol Evol 27:561-569.

Bailey, N. W., L. Marie-Orleach, and A. J. Moore. 2018. Indirect genetic effects in behavioral ecology: does behavior play a special role in evolution? Behav Ecol 29:1-11.

Beaulieu, J. and B. O'Meara. 2014. OUwie: analysis of evolutionary rates in an OU framework. R package version 1.

Blackledge, T. A. and R. G. Gillespie. 2004. Convergent evolution of behavior in an adaptive radiation of Hawaiian web-building spiders. Proceedings of the National Academy of Sciences 101:16228-16233.

Blackledge, T. A., N. Scharff, J. A. Coddington, T. Szüts, J. W. Wenzel, C. Y. Hayashi, and I. Agnarsson. 2009. Reconstructing web evolution and spider diversification in the molecular era. Proceedings of the National Academy of Sciences 106:5229-5234.

Bond, J. E., N. L. Garrison, C. A. Hamilton, R. L. Godwin, M. Hedin, and I. Agnarsson. 2014. Phylogenomics resolves a spider backbone phylogeny and rejects a prevailing paradigm for orb web evolution. Curr Biol 24:1765-1771.

Bond, J. E. and B. D. Opell. 1998. Testing adaptive radiation and key innovation hypotheses in spiders. Evolution 52:403-414.

Bott, R. A., W. Baumgartner, P. Bräunig, F. Menzel, and A.-C. Joel. 2017. Adhesion enhancement of cribellate capture threads by epicuticular waxes of the insect prey sheds new light on spider web evolution. Proc. R. Soc. B 284:20170363.

Bouckaert, R., J. Heled, D. Kühnert, T. Vaughan, C.-H. Wu, D. Xie, M. A. Suchard, A. Rambaut, and A. J. Drummond. 2014. BEAST 2: a software platform for Bayesian evolutionary analysis. Plos Comput Biol 10:e1003537.

Brely, L., F. Bosia, and N. M. Pugno. 2015. A hierarchical lattice spring model to simulate the mechanics of 2-D materials-based composites. Frontiers in Materials 2:51.

Cheng, D.-Q. and W. H. Piel. 2018. The origins of the Psechridae: Web-building lycosoid spiders. Mol Phylogenet Evol 125:213-219.

Coddington, J. A. 1986. The monophyletic origin of the orb web. Pp. 319-363 *in* W. A. Shear, ed. Spiders. Webs, Behavior, and Evolution. Stanford University Press, Stanford,CA.

Coddington, J. A. 2005. Phylogeny and classification of spiders. Pp. 18-24 *in* D. Ubick, P. Paquin, P. E. Cushing, and V. Roth, eds. Spiders of North America: an identification manual. . American Arachnological Society.

Coddington, J. A., I. Agnarsson, C. Hamilton, and J. E. J. P. P. Bond. 2018. Spiders did not repeatedly gain, but repeatedly lost, foraging webs. 6:e27341v27341.

Cook, R. D., D. S. Malkus, and M. E. Plesha. 2001. Concepts and applications of finite element analysis. John Wiley & Sons.

Cooper, N., G. H. Thomas, C. Venditti, A. Meade, and R. P. Freckleton. 2016. A cautionary note on the use of Ornstein Uhlenbeck models in macroevolutionary studies. Biol J Linn Soc 118:64–77.

Darriba, D., G. L. Taboada, R. Doallo, and D. Posada. 2012. jModelTest 2: more models, new heuristics and parallel computing. Nature methods 9:772.

Dawkins, R. 1982. The extended phenotype: The long reach of the gene. Oxford: Oxford University Press.

Donoghue, M. J. and D. D. Ackerly. 1996. Phylogenetic uncertainties and sensitivity analyses in comparative biology. Phil. Trans. R. Soc. Lond. B 351:1241-1249.

Drummond, A. J., S. Y. Ho, M. J. Phillips, and A. Rambaut. 2006. Relaxed phylogenetics and dating with confidence. PLoS biology 4:e88.

Duckworth, R. A. 2009. The role of behavior in evolution: a search for mechanism. Evolutionary ecology 23:513-531.

Eberhard, W. G. 1990. Function and phylogeny of spider webs. Annual review of Ecology and Systematics 21:341-372.

Eberhard, W. G. 2018a. Modular patterns in behavioural evolution: webs derived from orbs. Behaviour 155:531-566.

Eberhard, W. G., I. Agnarsson, and H. W. Levi. 2008. Web forms and the phylogeny of theridiid spiders (Araneae: Theridiidae): chaos from order. Systematics and biodiversity 6:415.

Eberhard, W. G. J. B. 2018b. Modular patterns in behavioural evolution: webs derived from orbs. 155:531-566.

Felsenstein, J. 1985. Phylogenies and the comparative method. The American Naturalist 125:1-15.

Fernández, R., G. Hormiga, and G. Giribet. 2014. Phylogenomic analysis of spiders reveals nonmonophyly of orb weavers. Curr Biol 24:1772-1777.

Fernández, R., R. J. Kallal, D. Dimitrov, J. A. Ballesteros, M. A. Arnedo, G. Giribet, and G. Hormiga. 2018. Phylogenomics, diversification dynamics, and comparative transcriptomics across the spider tree of life. Curr Biol 28:1489-1497.

Freckleton, R. P., P. H. Harvey, and M. Pagel. 2002. Phylogenetic analysis and comparative data: a test and review of evidence. The American Naturalist 160:712-726.

Garrison, N. L., J. Rodriguez, I. Agnarsson, J. A. Coddington, C. E. Griswold, C. A. Hamilton, M. Hedin, K. M. Kocot, J. M. Ledford, and J. E. Bond. 2016. Spider phylogenomics: untangling the Spider Tree of Life. PeerJ 4:e1719.

Grafen, A. 1989. The phylogenetic regression. Phil. Trans. R. Soc. Lond. B 326:119-157.

Hansell, M. H. 2005. Animal architecture. Oxford University Press, New York.

Ho, L. S. T. and C. Ané. 2014. Intrinsic inference difficulties for trait evolution with Ornstein-Uhlenbeck models. Methods in Ecology and Evolution 5:1133-1146.

Ingram, T. and D. L. Mahler. 2013. SURFACE: detecting convergent evolution from comparative data by fitting Ornstein-Uhlenbeck models with stepwise Akaike Information Criterion. Methods in Ecology and Evolution 4:416-425.

Kallal, R. J., R. Fernández, G. Giribet, and G. Hormiga. 2018. A phylotranscriptomic backbone of the orb-weaving spider family Araneidae (Arachnida, Araneae) supported by multiple methodological approaches. Mol Phylogenet Evol 126:129-140.

Katoh, K., J. Rozewicki, and K. D. Yamada. 2017. MAFFT online service: multiple sequence alignment, interactive sequence choice and visualization. Briefings in bioinformatics.

Kuntner, M., S. Kralj-Fišer, and M. Gregorič. 2010. Ladder webs in orb-web spiders: ontogenetic and evolutionary patterns in Nephilidae. Biol J Linn Soc 99:849-866.

Maddison, W. P., S. C. Evans, C. A. Hamilton, J. E. Bond, A. R. Lemmon, and E. M. Lemmon. 2017. A genome-wide phylogeny of jumping spiders (Araneae, Salticidae), using anchored hybrid enrichment. Zookeys:89.

Meijering, E., O. Dzyubachyk, and I. Smal. 2012. Methods for Cell and Particle Tracking. Methods in Enzymology 504:183-200.

Miller, M. A., W. Pfeiffer, and T. Schwartz. 2010. Creating the CIPRES Science Gateway for inference of large phylogenetic trees. Pp. 1-8. Gateway Computing Environments Workshop (GCE), 2010. Ieee.

Odling-Smee, F. J., H. Odling-Smee, K. N. Laland, M. W. Feldman, and F. Feldman. 2003. Niche construction: the neglected process in evolution. Princeton university press.

Opell, B. 1994. The ability of spider cribellar prey capture thread to hold insects with different surface features. Funct Ecol:145-150.

Opell, B. D. and H. S. Schwend. 2009. Adhesive efficiency of spider prey capture threads. Zoology 112:16-26.

Ord, T. J. and T. C. Summers. 2015. Repeated evolution and the impact of evolutionary history on adaptation. Bmc Evol Biol 15:137.

Ostoja-Starzewski, M. 2002. Lattice models in micromechanics. Applied Mechanics Reviews 55:35-60.

Ostrowski, A. M. 1973. The Newton-Raphson Method," Pure Appl. Math. Pp. 53-55 *in* A. M. Ostrowski, ed. Third Edition of Solution of Equations and Systems of Equations. Elsevier.

Paterno, G. B., C. Penone, and G. D. Werner. 2018. sensiPhy: An r-package for sensitivity analysis in phylogenetic comparative methods. Methods in Ecology and Evolution 9:1461-1467.

Pennell, M. W., J. M. Eastman, G. J. Slater, J. W. Brown, J. C. Uyeda, R. G. FitzJohn, M. E. Alfaro, and L. J. Harmon. 2014. geiger v2. 0: an expanded suite of methods for fitting macroevolutionary models to phylogenetic trees. Bioinformatics 30:2216-2218.

Piorkowski, D., S. Blamires, N. Doran, C. P. Liao, C. L. Wu, and I. M. Tso. 2018. Ontogenetic shift toward stronger, tougher silk of a web-building, cave-dwelling spider. J Zool 304:81-89.

Pugno, N. M. 2011. The theory of multiple peeling. Int J Fracture 171:185-193.

Pugno, N. M., S. W. Cranford, and M. J. Buehler. 2013. Synergetic material and structure optimization yields robust spider web anchorages. Small 9:2747-2756.

Revell, L. J. 2012. phytools: an R package for phylogenetic comparative biology (and other things). Methods in Ecology and Evolution 3:217-223.

Sahni, V., J. Harris, T. A. Blackledge, and A. Dhinojwala. 2012. Cobweb-weaving spiders produce different attachment discs for locomotion and prey capture. Nat Commun 3.

Salehani, M. K. and N. Irani. 2018. A coupled mixed-mode cohesive zone model: An extension to three-dimensional contact problems. arXiv preprint arXiv:1801.03430.

Schneider, C. A., W. S. Rasband, and K. W. Eliceiri. 2012. NIH Image to ImageJ: 25 years of image analysis. Nat methods 9:671-675.

Swanson, B., T. Blackledge, J. Beltrán, and C. Hayashi. 2006. Variation in the material properties of spider dragline silk across species. Applied Physics A 82:213-218.

Tung Ho, L. s. and C. Ané. 2014. A linear-time algorithm for Gaussian and non-Gaussian trait evolution models. Systematic biology 63:397-408.

Turner, J. S. and R. C. Soar. 2008. Beyond biomimicry: What termites can tell us about realizing the living building *in* I. Wallis, L. Bilan, M. Smith, and A. S. Kaz, eds. First International Conference on Industrialized, Intelligent Construction at Loughborough University.

Uyeda, J. C. and L. J. Harmon. 2014. A novel Bayesian method for inferring and interpreting the dynamics of adaptive landscapes from phylogenetic comparative data. Systematic biology 63:902-918.

Uyeda, J. C., R. Zenil-Ferguson, and M. W. Pennell. 2018. Rethinking phylogenetic comparative methods. Systematic Biology:syy031.

Wcislo, W. T. 1989. Behavioral environments and evolutionary change. Annual Review of Ecology and Systematics 20:137-169.

West-Eberhard, M. J. 1989. Phenotypic plasticity and the origins of diversity. Annual review of Ecology and Systematics 20:249-278.

Wheeler, W. C., J. A. Coddington, L. M. Crowley, D. Dimitrov, P. A. Goloboff, C. E. Griswold, G. Hormiga, L. Prendini, M. J. Ramírez, and P. Sierwald. 2017. The spider tree of life: phylogeny of Araneae based on target-gene analyses from an extensive taxon sampling. Cladistics 33:574-616.

Wolff, J. O. 2017. Structural effects of glue application in spiders – What can we learn from silk anchors? Pp. 63-80 *in* L. Xue, L. Heepe, and S. N. Gorb, eds. Bio-inspired structured adhesives. Springer Science+Business Media, Dordrecht.

Wolff, J. O., I. Grawe, M. Wirth, A. Karstedt, and S. N. Gorb. 2015. Spider's super-glue: thread anchors are composite adhesives with synergistic hierarchical organization. Soft Matter 11:2394-2403.

Wolff, J. O. and M. E. Herberstein. 2017. 3D-printing spiders: back-and-forth glue application yields silk anchorages with high pull-off resistance under varying loading situations. J R Soc Interface 14:20160783.

Wolff, J. O., A. van der Meijden, and M. E. Herberstein. 2017. Distinct spinning patterns gain differentiated loading tolerance of silk thread anchorages in spiders with different ecology. Proceedings of the Royal Society B: Biological Sciences 284:20171124.

York, R. A. and R. D. Fernald. 2017. The Repeated Evolution of Behavior. Frontiers in Ecology and Evolution 4:143.

614 **Figures**
615

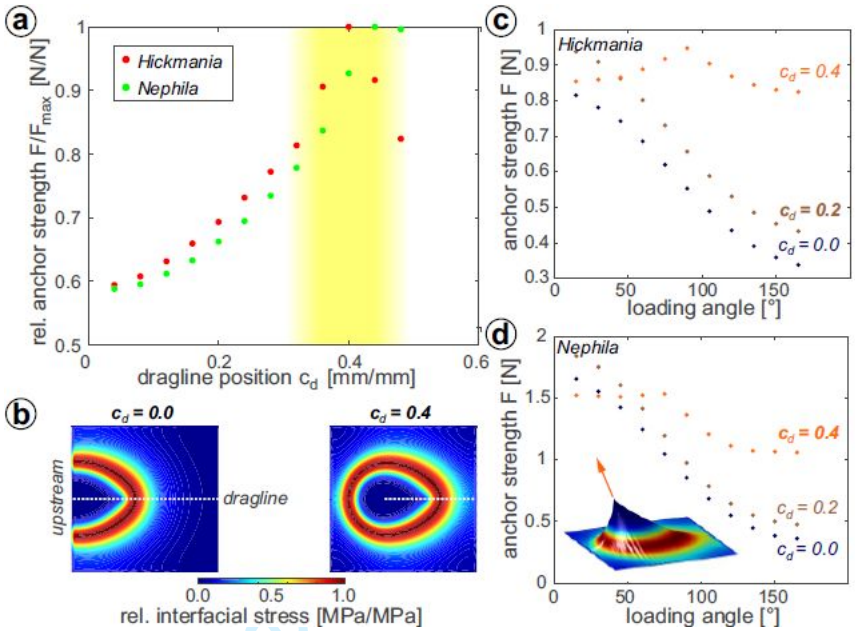

616
617

618 **Fig. 1. Optimization of web anchor performance**. ***(a)*** Simulated peak pull-off forces
619 (anchor strength) vs. different dragline positions for silk properties of Tasmanian cave spiders
620 (*Hickmania troglodytes*) and golden orb weavers (*Nephila plumipes*) under vertical load. The
621 yellow shade indicates the estimated range of c_d (for a variety of silk properties), where anchor
622 strength is maximized. ***(b)*** Exemplary maps of interfacial stress in the silk membrane (apical
623 view) for an orb weaver silk anchor with $c_d = 0.0$ and $c_d = 0.4$ under vertical load. Warm colours
624 indicate high stress. Anchors reach the peak pull-off force when the interfacial stress
625 concentration around the peeling line reaches the membrane edge. ***(c)*** Simulated anchor
626 strength for different dragline loading angles between 15° (± parallel to substrate along spinning
627 direction) and 165° (± parallel to substrate against spinning direction, i.e. dragline flipped over)
628 and three different values of c_d (different colours, bold font indicates the mean c_d naturally
629 found in this species) for silk properties of Tasmanian cave spiders. ***(d)*** Same as in (c) for silk
630 properties of golden orb weavers. Inset shows three-dimensional displacement map and stress
631 distribution in an anchor with $c_d = 0.4$, pulled at an angle of 75° (top-side view).
632

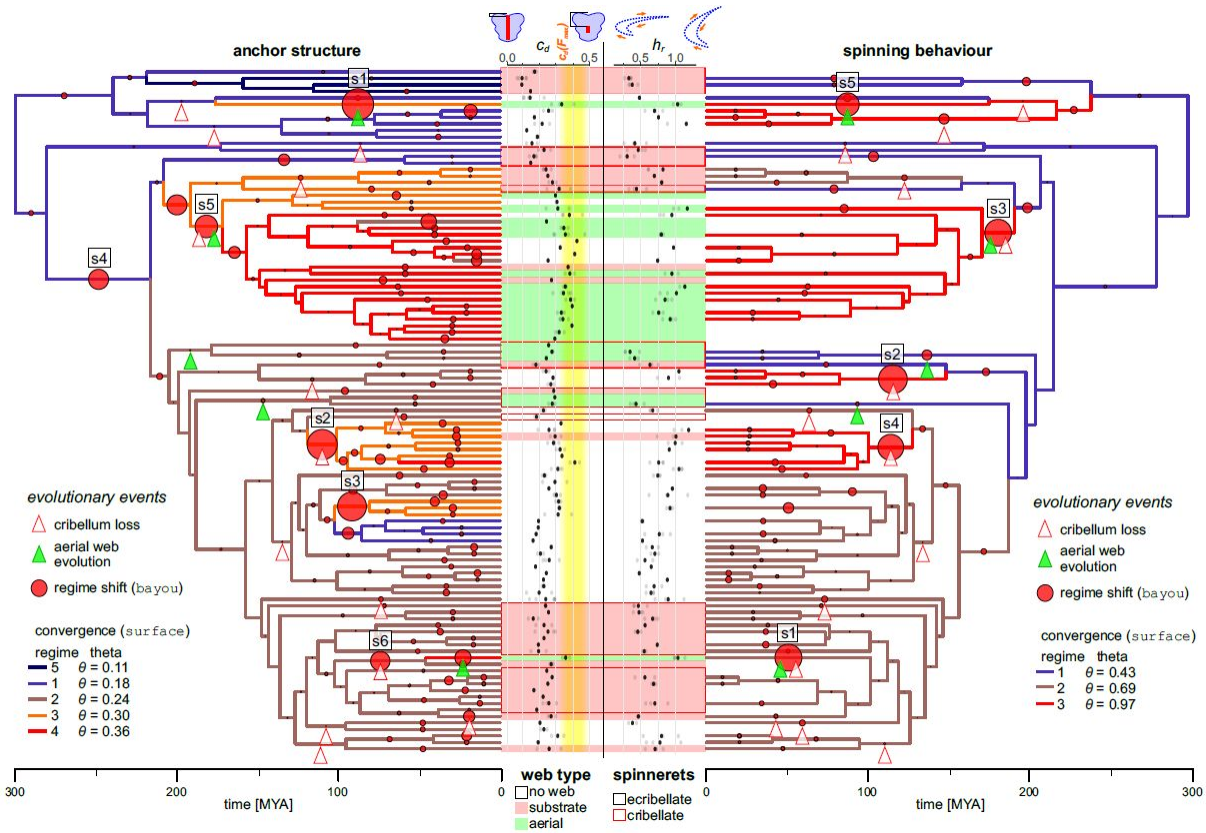

Fig. 2. Correlated evolution of web structure, behaviour and morphology. Shifts in the adaptive landscape of dragline placement c_d (left tree) and spinning choreography h_r (right tree). Branch colours denote convergent evolutionary regimes in the adaptive optimum θ as identified by *SURFACE*, with warmer colours indicating higher θs. The size of overlaid red pies indicates the posterior probability of a shift in θ in that branch, as found by *bayou*. Numbered shifts mark well supported shifts with $pp > 0.3$. White arrowheads with red outline indicate branches in which cribellum loss occurred, and green arrowheads indicate branches in which aerial web building has evolved (with a probability > 0.5). Dots at tips display c_d and h_r values measured in the extant species (grey dots represent means of individuals, black dot species means). The underlying shade indicates web building behaviour (white - no web, red - substrate web, green - aerial web) and the range of optimal anchor structure (yellow shade). Red boxes denote species with a cribellum. Schematics above symbolize anchors with a low and a high c_d (left; top view of anchor with membrane in blue and fused dragline in red) and spinning paths with a low and a high h_r (right; spinneret abducting to the right).

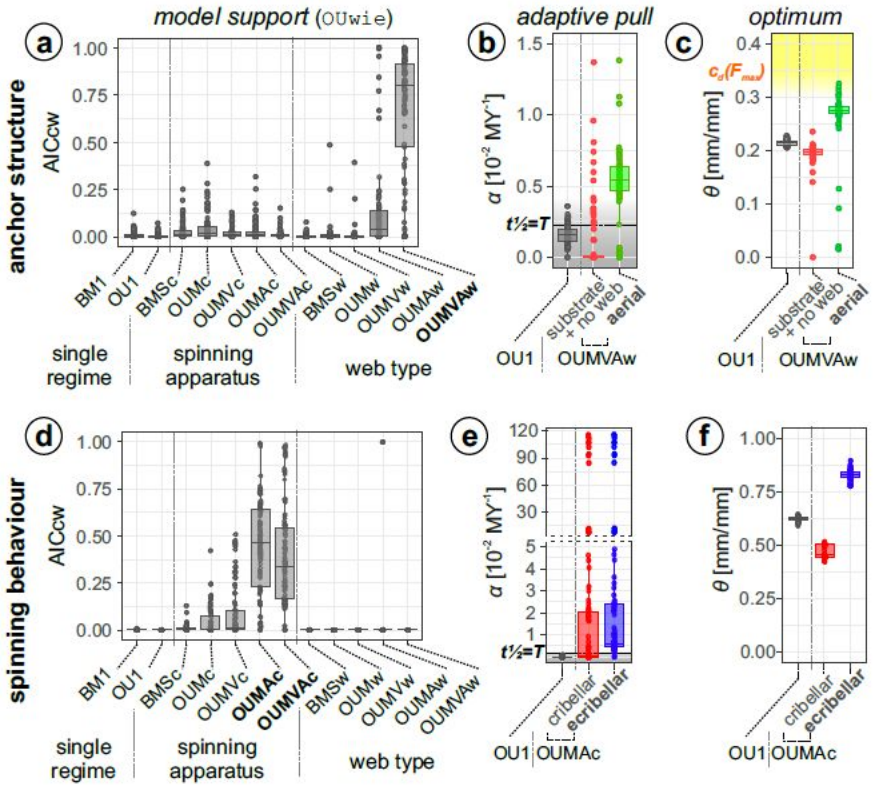

Fig. 3. Exceptional evolution of anchor structure in aerial web builders. ***(a)*** *AICc*-weight values for single- and two-regime evolutionary models of dragline placement c_d across 100 trees (best supporting model in bold font). A clear support for OUMAw and OUMVAw indicates that c_d evolved towards an elevated optimum and at a higher adaptive potential (and higher evolutionary rates) in aerial web builders. ***(b)*** Summary of adaptive potential α of c_d for single regime OU-models ('null'-model), and the two regimes of the best fitting OUw model across 100 trees (some extreme outliers not displayed). The black dotted line indicates an α for which the phylogenetic half-life $t½$ equals the total tree height T; below this threshold evolution becomes highly labile and BM-like (grey area). ***(c)*** Summary of the evolutionary optimum θ of c_d for single regime OU-models ('null'-model), and the two regimes of the best fitting OUw models across 100 trees. The yellow area indicates the theoretical physical optimum $c_d(F_{max})$. ***(d)*** Same as in (a) for spinning choreography h_r. A clear support for OUMAc and OUMVAc indicates that h_r evolved towards an elevated optimum and at a higher adaptive potential (and higher evolutionary rates) after cribellum loss. ***(e)*** Summary of adaptive potential α of h_r for single regime OU-models ('null'-model), and the two regimes of the best fitting OUc model across 100 trees. Same conventions as in (b). ***(f)*** Summary of the evolutionary optimum θ of h_r for single regime OU-models ('null'-model), and the two regimes of the best fitting OUc models across 100 trees. Same conventions as in (c).

Electronic Supplemental Material (*ESM*)

S1. Estimation of silk membrane stiffness.
S2. Comparing numerical model results of silk anchor efficiency with empirical data.
S3. Consensus tree.
S4. Ancestral character estimation
S5. Summary of SURFACE results.
S6. Summary of bayou results.
S7. Summary of PGLS results.
S8. Summary of geometric morphometrics results.
S9. Material list and sample sizes.
S10. Terminals mapping.
S11. Genbank identifiers.
S12. R code including data and tree files (zipped archive).

ESM.1. Estimation of silk membrane stiffness

Methods

To estimate realistic parameters for our numerical model of silk anchor mechanics, we performed exemplary lateral stress tests of anchors that had been carefully delaminated from polypropylene sheets. Each 7-8 anchors of the basal substrate web builder *H. troglodytes*, the hunting spider *I. villosa* and the aerial web builder *N. plumipes* were glued with cyanacrylate adhesive onto a cardboard strip, such that the central dragline was oriented along the apical edge of the strip. Thereby the glue was spread across one lateral wing of the membrane up to the dragline such that the dragline was fixed (Fig. S.1.1a). The cardboard strip was mounted into the Instron 5542 tensile tester (Instron, Norwood, USA) with a clamp and the stage with an attached ULC-0.5N load cell (Interface, Inc., Scottsdale, AZ, USA) was slowly driven towards the free side of the silk membrane. The lateral edge of the membrane was then glued onto another piece of cardboard that was attached to the load cell, leaving a free membrane sample of 0.11-1.00 mm gauge length. The stage was moved slightly downwards to prevent a pre-stress of the silk membrane during adhesive curing. The sample was stretched at a rate of 0.01 mm/s until rupture. The process was monitored with a Basler Ace 640×480pix camera (Basler AG, Ahrensburg, Germany) equipped with an extension tube, 1.33× and 0.25× lenses (Navitar, Inc., Rochester, NY, USA) at 15 frames per second to record membrane strain and crack propagation. For each species four tests showed an even fraction of the membrane and were further analysed. To calculate stress, we estimated a cross-sectional area of the membrane $A = w \times t$, where w is the width of the sample and t its thickness. Here, t is given by the observed density of the spinning trajectory (as found in the kinematic analysis), which determines how many layers of piriform silk are applied, with each layer corresponding to the mean diameter of piriform fibres (0.5 µm (Wolff et al., 2015)). The Young's Modulus of the membrane was derived from the initial slope of the stress strain curve.

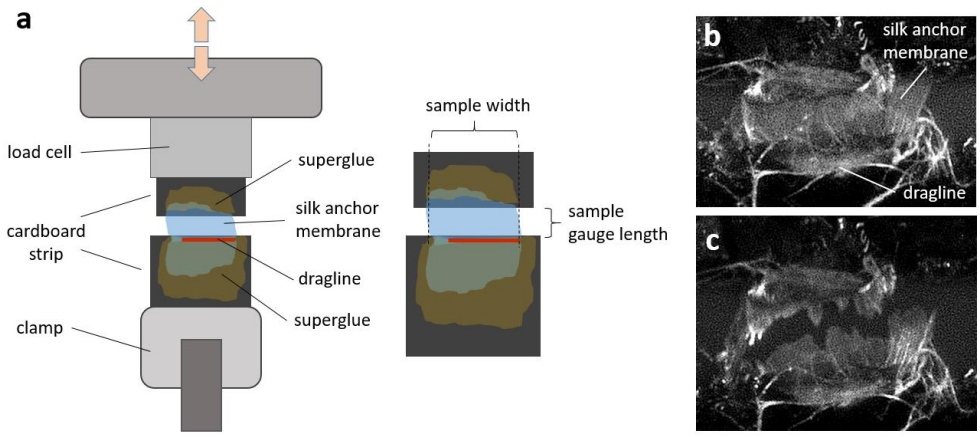

Fig. S1.1. (a) Schematic illustration of membrane stress tests to estimate membrane stiffness. (b) Video still of a stretched membrane of a *Nephila* silk anchor. (c) Similar silk membrane after rupture.

Results

Membranes of delaminated silk anchors generally had a 10-40 times lower stiffness than dragline silk of these or similar species (Piorkowski et al., 2018; Swanson et al., 2006). Silk membranes of *N. plumipes* were six times stiffer and stronger than the membranes of *I. villosa* and *H. troglodytes*, on average. This may be due to the grid-like overlay of fibres within the membrane (Wolff et al., 2015) caused by the specific back-and-forth spinning pattern in this spider.

Mechanical properties are summarized in Tab. S.1.1. below.

Tab. S1.1. Estimates of mechanical properties of silk anchor membranes from lateral stress tests.

Orb Weaver (*Nephila plumipes*)					
Sample no.	1	2	4	5	Mean ± s.d.
Length [mm]	0.33	0.31	0.67	0.25	
Width [mm]	1.93	1.17	1.29	1.28	
Extensibility [mm/mm]	0.05	0.11	0.53	0.33	0.26 ± 0.22
Strength [GPa]	0.149	0.214	0.168	0.319	0.212 ± 0.076
Young's Modulus [GPa]	3.02	2.28	0.25	1.17	**1.68** ± 1.22
Huntsman Spider (*Isopeda villosa*)					
Sample no.	3	4	7	8	Mean ± s.d.
Length [mm]	0.71	0.11	0.67	0.76	
Width [mm]	0.94	0.70	0.85	0.57	
Extensibility [mm/mm]	0.31	0.54	0.17	0.14	0.29 ± 0.18
Strength [GPa]	0.039	0.066	0.063	0.030	0.050 ± 0.018
Young's Modulus [GPa]	0.17	0.23	0.19	0.30	**0.22** ± 0.06
Tasmanian Cave Spider (*Hickmania troglodytes*)					
Sample no.	1	2	5	6	Mean ± s.d.
Length [mm]	1.00	0.32	0.66	0.16	
Width [mm]	1.35	0.50	1.00	0.81	
Extensibility [mm/mm]	0.19	0.33	0.14	0.32	0.25 ± 0.09
Strength [GPa]	0.016	0.075	0.023	0.028	0.035 ± 0.027
Young's Modulus [GPa]	0.29	0.27	0.34	0.09	**0.25** ± 0.11

For the numerical model of silk anchor mechanics, we used rounded numbers of the observed membrane and dragline stiffness parameters.

References

Piorkowski, D., Blamires, S., Doran, N., Liao, C. P., Wu, C. L. and Tso, I. M. (2018). Ontogenetic shift toward stronger, tougher silk of a web-building, cave-dwelling spider. *Journal of Zoology* **304**, 81-89.

Swanson, B., Blackledge, T., Beltrán, J. and Hayashi, C. (2006). Variation in the material properties of spider dragline silk across species. *Applied Physics A* **82**, 213-218.

Wolff, J. O., Grawe, I., Wirth, M., Karstedt, A. and Gorb, S. N. (2015). Spider's super-glue: thread anchors are composite adhesives with synergistic hierarchical organization. *Soft Matter* **11**, 2394-2403.

ESM.2. Comparing numerical model results of silk anchor efficiency with empirical data

Previous comparative measurements in silk anchors of orb weavers have revealed that centrality is the most (and only) significant variable of attachment disc structure that explains variation in maximal pull-off forces (Wolff & Herberstein, 2017). To derive a general relationship between centrality (front shift) and pull-off force, we used fracture mechanics theory to build a numerical model and simulated pull-off forces for different values of centrality (see main text). We found that the relationship resembles a curve, and pull-off force is maximized between c_d = 0.3 and c_d = 0.5.

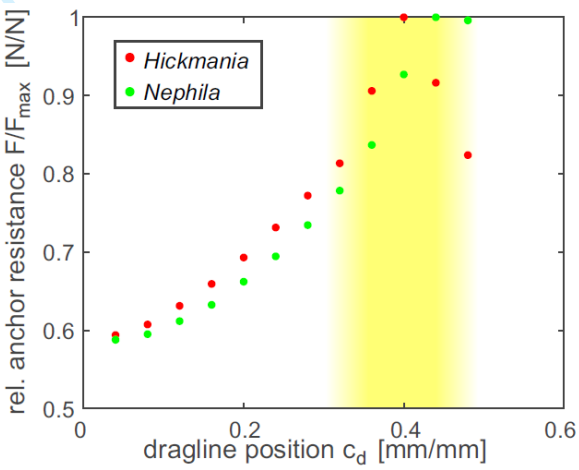

We re-analysed the data by Wolff and Herberstein (2017), and calculated c_d and F_{max}/A (maximal pull-off force normalized on projected anchor area).

We found that the relationship is consistent with the numerical results for *Nephila* anchors.

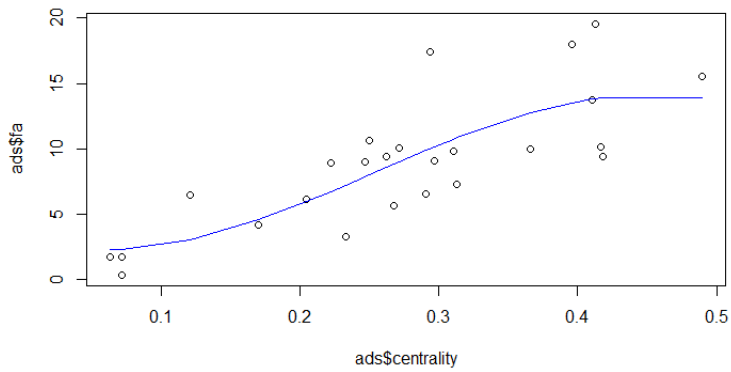

Fitting a sine curve:

```
Call:
lm(formula = ads$fa ~ xc + xs)

Residuals:
    Min      1Q  Median      3Q     Max
-4.5118 -2.7686 -0.3529  1.5837  7.4274

Coefficients:
            Estimate Std. Error t value Pr(>|t|)
(Intercept)    8.205      1.315   6.238 2.81e-06 ***
xc            -5.418      1.205  -4.496  0.00018 ***
```

```
xs            -2.474      1.608  -1.538  0.13827
---
Signif. codes:  0 ‘***’ 0.001 ‘**’ 0.01 ‘*’ 0.05 ‘.’ 0.1 ‘ ’ 1

Residual standard error: 3.273 on 22 degrees of freedom
Multiple R-squared:  0.6137, Adjusted R-squared:  0.5786
F-statistic: 17.48 on 2 and 22 DF,  p-value: 2.856e-05
```

Fitting a linear model:

```
Call:
lm(formula = ads$fa ~ ads$centrality)

Residuals:
    Min      1Q  Median      3Q     Max
-4.4656 -2.0683 -0.3826  1.2083  7.8337

Coefficients:
               Estimate Std. Error t value Pr(>|t|)
(Intercept)     -0.4676     1.6497  -0.283    0.779
ads$centrality  34.2819     5.5467   6.181 2.64e-06 ***
---
Signif. codes:  0 ‘***’ 0.001 ‘**’ 0.01 ‘*’ 0.05 ‘.’ 0.1 ‘ ’ 1

Residual standard error: 3.157 on 23 degrees of freedom
Multiple R-squared:  0.6242, Adjusted R-squared:  0.6078
F-statistic:  38.2 on 1 and 23 DF,  p-value: 2.636e-06
```

References

Wolff, Jonas O., and Marie E. Herberstein. "Three-dimensional printing spiders: back-and-forth glue application yields silk anchorages with high pull-off resistance under varying loading situations." *Journal of The Royal Society Interface* 14.127 (2017): 20160783.

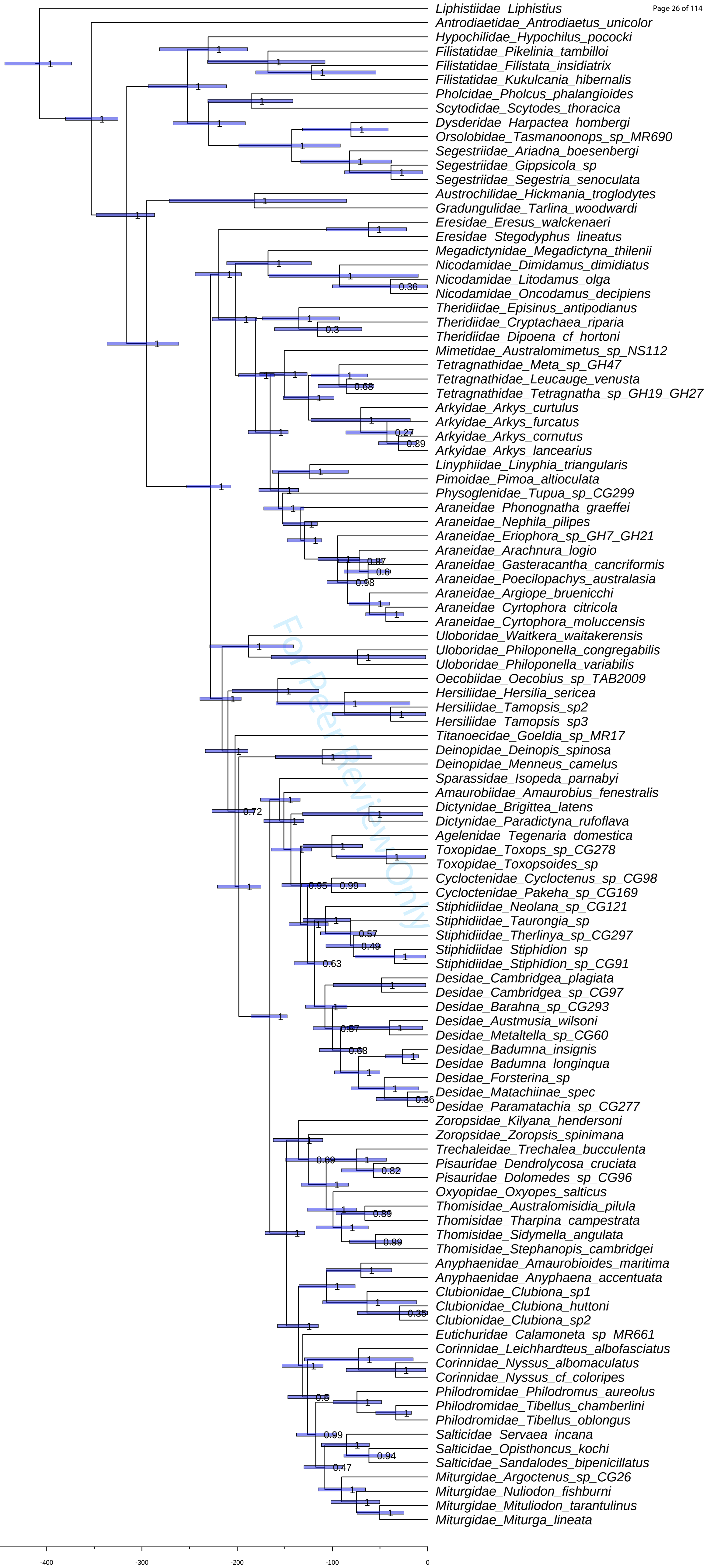

ESM.4. Ancestral Character Estimation of web type

Model comparison (AICc weights)

```
        ER        SYM        ARD
0.5825985 0.1818513 0.2355502
```

Stochastic Character Mapping

ER

100 times on consensus tree

```
make.simmap is sampling character histories conditioned on the transition matrix

Q =
              0            1            2
0 -0.002082653  0.001041326  0.001041326
1  0.001041326 -0.002082653  0.001041326
2  0.001041326  0.001041326 -0.002082653
(estimated using likelihood);
and (mean) root node prior probabilities
pi =
        0         1         2
0.3333333 0.3333333 0.3333333

100 trees with a mapped discrete character with states:
 0, 1, 2

trees have 25.19 changes between states on average

changes are of the following types:
      0,1  0,2  1,0  1,2  2,0  2,1
x->y 2.81 1.49 8.13 5.72 3.98 3.06

mean total time spent in each state is:
                 0            1            2    total
raw  4172.6046685 5053.3308585 2790.3464610 12016.28
prop    0.3472459    0.4205403    0.2322138     1.00
```

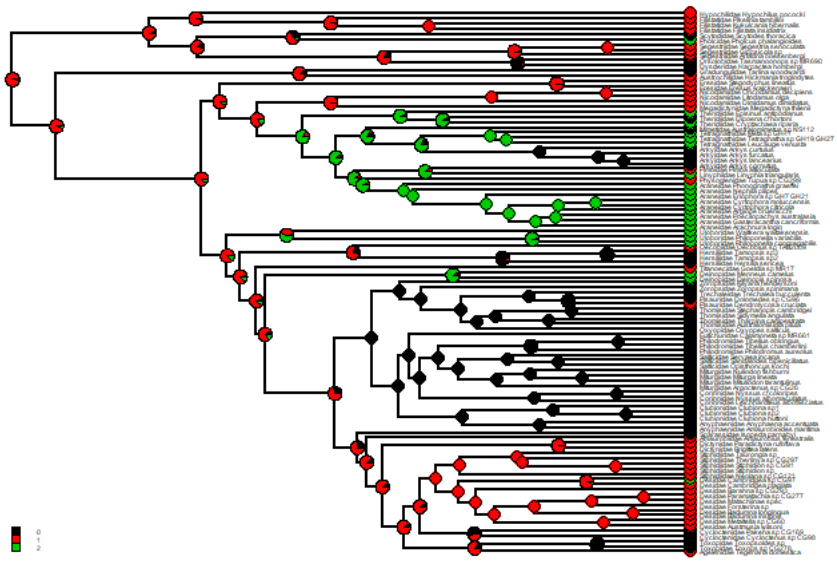

Including phylogenetic uncertainty (across 100 trees)

```
100 trees with a mapped discrete character with states:
 0, 1, 2

trees have 26.5 changes between states on average

changes are of the following types:
      0,1 0,2  1,0  1,2  2,0  2,1
x->y 3.24 1.6 7.92 5.96 4.51 3.27

mean total time spent in each state is:
                 0            1            2    total
raw  4158.8882447 4922.7032452 2813.0397605 11894.63
prop    0.3493514    0.4140903    0.2365583     1.00
```

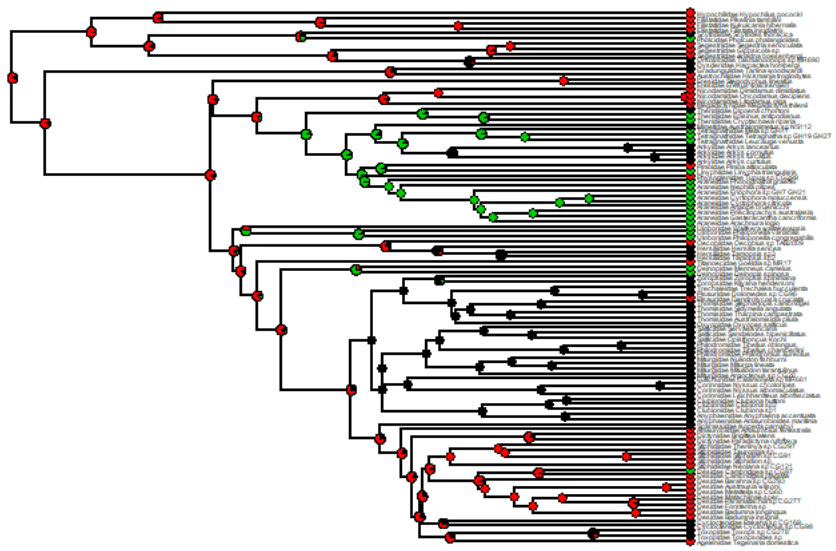

ARD

100 times on consensus tree

```
make.simmap is sampling character histories conditioned on the transition matrix

Q =
               0             1             2
0 -0.0004125627  0.0004125627  0.000000000
1  0.0016196521 -0.0029227069  0.001303055
2  0.0012480697  0.0010154840 -0.002263554
(estimated using likelihood);
and (mean) root node prior probabilities
pi =
        0         1         2
0.3333333 0.3333333 0.3333333

100 trees with a mapped discrete character with states:
 0, 1, 2

trees have 23.28 changes between states on average

changes are of the following types:
      0,1 0,2  1,0  1,2  2,0  2,1
x->y 1.58   0 8.61 6.71 3.46 2.92

mean total time spent in each state is:
                 0            1            2    total
raw  3945.137882 5263.4162177 2807.7278887 12016.28
prop    0.328316    0.4380237    0.2336603     1.00
```

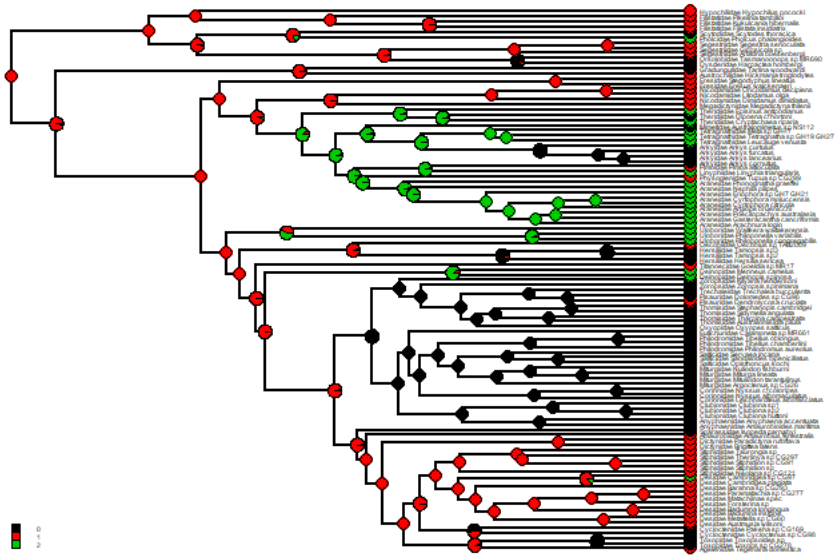

Ancestral Character Estimation of spinning apparatus state

Model comparison (AICc weights)

```
         ER         ARD      Dollo
0.00201729 0.35779483 0.64018788
```

Stochastic Character Mapping

Dollo's Law

100 times on consensus tree

```
make.simmap is sampling character histories conditioned on the transition matrix

Q =
             0            1
0 0.000000000  0.000000000
1 0.003021743 -0.003021743
(estimated using likelihood);
and (mean) root node prior probabilities
pi =
  0   1
0.5 0.5


100 trees with a mapped discrete character with states:
 0, 1

trees have 15.28 changes between states on average

changes are of the following types:
     0,1   1,0
x->y   0 15.28

mean total time spent in each state is:
                 0            1    total
raw  6932.4776368 5083.8043512 12016.28
prop    0.5769237    0.4230763     1.00
```

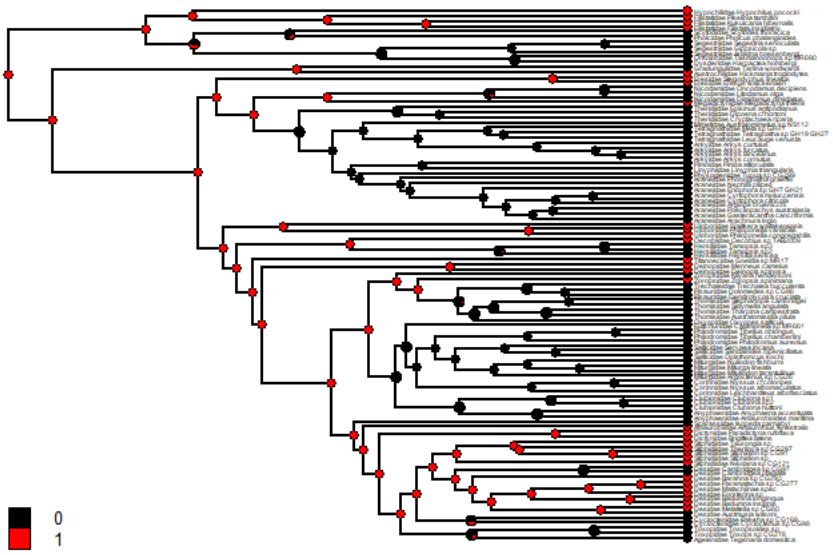

Including phylogenetic uncertainty (across 100 trees)

```
100 trees with a mapped discrete character with states:
 0, 1

trees have 16.26 changes between states on average

changes are of the following types:
     0,1   1,0
x->y   0 16.26

mean total time spent in each state is:
                 0            1    total
raw  6792.9713724 5101.6598780 11894.63
prop    0.5708267    0.4291733     1.00
```

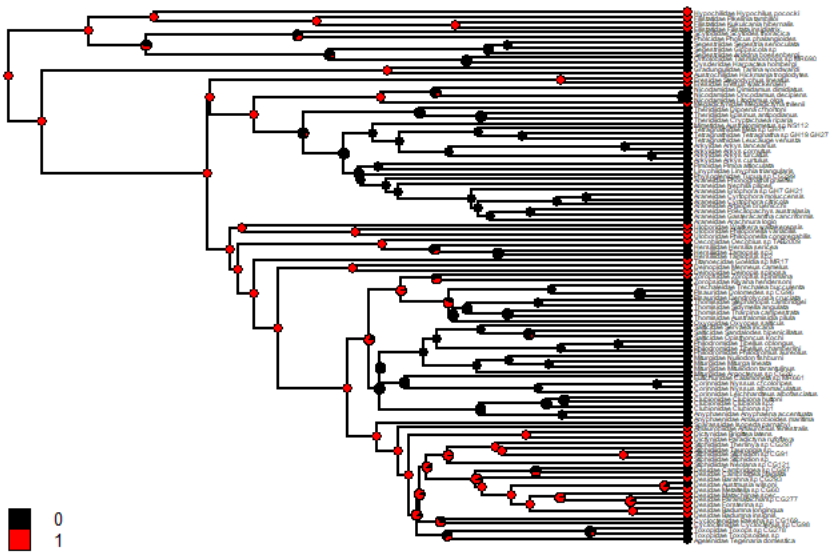

ESM.5. *Summary of SURFACE results.*

Centrality

```
> surfaceSummary(centrSurf$fwd, centrSurf$bwd)
$`n_steps`
[1] 19

$lnls
                [,1]     [,2]     [,3]     [,4]     [,5]     [,6]     [,7]     [,8]     [,9]
[,10]    [,11]    [,12]
centrality 148.9926 154.8584 160.7192 167.1772 173.0176 177.6523 182.3514 186.6792 190.2654 1
94.0089 197.7598 201.7447
               [,13]   [,14]    [,15]    [,16]    [,17]    [,18]    [,19]
centrality 205.9621 205.962 205.9537 205.9372 205.8607 205.7536 203.1835

$n_regimes_seq
                [,1] [,2] [,3] [,4] [,5] [,6] [,7] [,8] [,9] [,10] [,11] [,12] [,13] [,14] [,1
5] [,16] [,17] [,18] [,19]
k                  1    2    3    4    5    6    7    8    9    10    11    12    13    13
13    13    13    13    13
kprime             1    2    3    4    5    6    7    8    9    10    11    12    13    12
11    10     9     8     5
deltak             0    0    0    0    0    0    0    0    0     0     0     0     0     1
2     3     4     5     8
c                  0    0    0    0    0    0    0    0    0     0     0     0     0     2
4     6     7     9    12
kprime_conv        0    0    0    0    0    0    0    0    0     0     0     0     0     1
2     3     3     4     4
kprime_nonconv     1    2    3    4    5    6    7    8    9    10    11    12    13    11
9     7     6     4     1

$aics
        1         2         3         4         5         6         7         8         9
10        11        12
-289.5851 -296.8597 -303.9383 -312.0140 -318.6439 -322.6380 -326.5211 -329.4050 -330.5309 -33
1.6764 -332.5195 -333.4894
       13        14        15        16        17        18        19
-334.5558 -338.2875 -341.9074 -345.4187 -348.7215 -351.8776 -356.3670

$shifts
  1  39 102  53 110  37  59 195  62 128 134   3 165
"a" "b" "c" "b" "b" "f" "b" "f" "a" "c" "c" "l" "f"

$n_regimes
             k         kprime         deltak              c    kprime_conv kprime_nonconv
            13              5              8             12              4              1

$alpha
centrality
  1.746556

$phylhalflife
centrality
 0.3968652

$sigma_squared
 centrality
0.004265715

$theta
  centrality
a  0.1786923
b  0.2996083
c  0.2377853
f  0.3591632
l  0.1113329
```

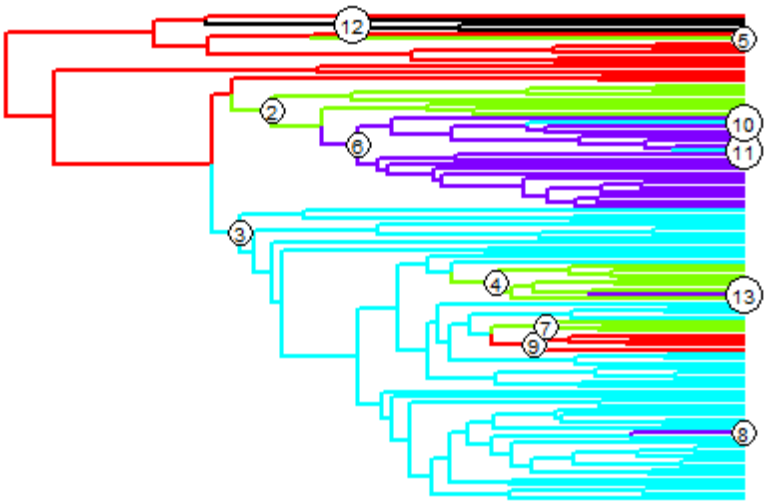

Spinning track proportions

```
> surfaceSummary(trackSurf$fwd, trackSurf$bwd)
$`n_steps`
[1] 11

$lnls
                    [,1]     [,2]     [,3]     [,4]    [,5]     [,6]    [,7]     [,8]     [,9]
[,10]    [,11]
smu_rel_height 9.751597 13.44973 17.18656 21.45115 24.6963 29.28001 35.3672 39.12883 39.08978
37.9916 37.35386

$n_regimes_seq
               [,1] [,2] [,3] [,4] [,5] [,6] [,7] [,8] [,9] [,10] [,11]
k                 1    2    3    4    5    6    7    8    8     8     8
kprime            1    2    3    4    5    6    7    8    7     4     3
deltak            0    0    0    0    0    0    0    0    1     4     5
c                 0    0    0    0    0    0    0    0    2     6     8
kprime_conv       0    0    0    0    0    0    0    0    1     2     3
kprime_nonconv    1    2    3    4    5    6    7    8    6     2     0

$aics
        1         2         3         4         5         6         7         8         9
10        11
-10.89713 -13.58695 -16.05053 -19.23564 -20.01329 -23.06002 -28.66033 -29.10381 -32.63240 -40
.48321 -42.32176

$shifts
  1  21  26  32   6  65  10  73
"a" "b" "b" "b" "b" "f" "f" "a"

$n_regimes
             k         kprime         deltak              c    kprime_conv kprime_nonconv
             8              3              5              8              3              0

$alpha
smu_rel_height
      0.351283

$phylhalflife
smu_rel_height
      1.973187

$sigma_squared
smu_rel_height
    0.01436403

$theta
  smu_rel_height
a      0.4272920
b      0.9686941
f      0.6853987
```

ESM.6. Summary of results from *Bayou*-Analysis

Centrality

We found multiple support for six shifts in the evolutionary regime of c_d (Fig. 2): *shift 1* in Pholcidae (posterior probability *pp* = 0.494); *shift 2* in the grate-shaped tapetum clade (excl. Zoropsidae) (*pp* = 0.474); *shift 3* at the basis of Salticidae (*pp* = 0.405); *shift 4* at the basis of Entelegynae (*pp* = 370); *shift 5* at the basis of Araneoidea (*pp* = 0.336); and *shift 6* within Desidae (*Cambridgea*) (*pp* = 0.309).

Statistics for all MCMC chains are given below.

dk=10

```
bayou MCMC chain: 5e+05 generations
50001 samples, first 15000 samples discarded as burnin


Summary statistics for parameters:
                    Mean         SD     Naive SE Time-series SE Effective Size    HPD95Lower  HPD95Upper
lnL        165.826135286 5.18216859 2.769906e-02    0.347153318       222.8335  1.547498e+02 176.2997813
prior      -24.752205853 6.44104264 3.442784e-02    0.430418184       223.9397 -3.768278e+01 -13.0924456
alpha        1.261797474 3.87243122 2.069842e-02    0.281845726       188.7750  3.305496e-04   4.6418679
sig2         0.004790455 0.01306605 6.983898e-05    0.001104616       139.9155  1.075320e-05   0.0185710
k            5.806639621 1.91730213 1.024812e-02    0.119146834       258.9501  3.000000e+00   9.0000000
ntheta       6.806639621 1.91730213 1.024812e-02    0.119146834       258.9501  4.000000e+00  10.0000000
root.theta   0.213671127 0.03001162 1.604143e-04    0.002781067       116.4544  1.520682e-01   0.2509984
all theta    0.275514976 0.12128322           NA             NA             NA            NA          NA


Branches with posterior probabilities higher than 0.1:
           pp magnitude.of.theta2 naive.SE.of.theta2 rel.location
75  0.7230444           0.3404147       0.0002616941    0.4976113
105 0.6942460           0.3235953       0.0003768009    0.4919371
5   0.3916062           0.1102863       0.0002470688    0.4609237
205 0.2239872           0.2400395       0.0001398414    0.5089253
158 0.1986744           0.3873070       0.0013185527    0.4075966
7   0.1620193           0.3478268       0.0013100235    0.4719392
77  0.1462774           0.3400975       0.0010462965    0.5077757
20  0.1441346           0.1268873       0.0003489537    0.4977884
208 0.1368493           0.1666876       0.0002588612    0.4887941
73  0.1338495           0.3426803       0.0002948124    0.4747188
124 0.1185075           0.3590558       0.0020705443    0.3917418
97  0.1152791           0.4398128       0.0018183241    0.4337498
78  0.1003371           0.1571498       0.0006974564    0.4855903
```

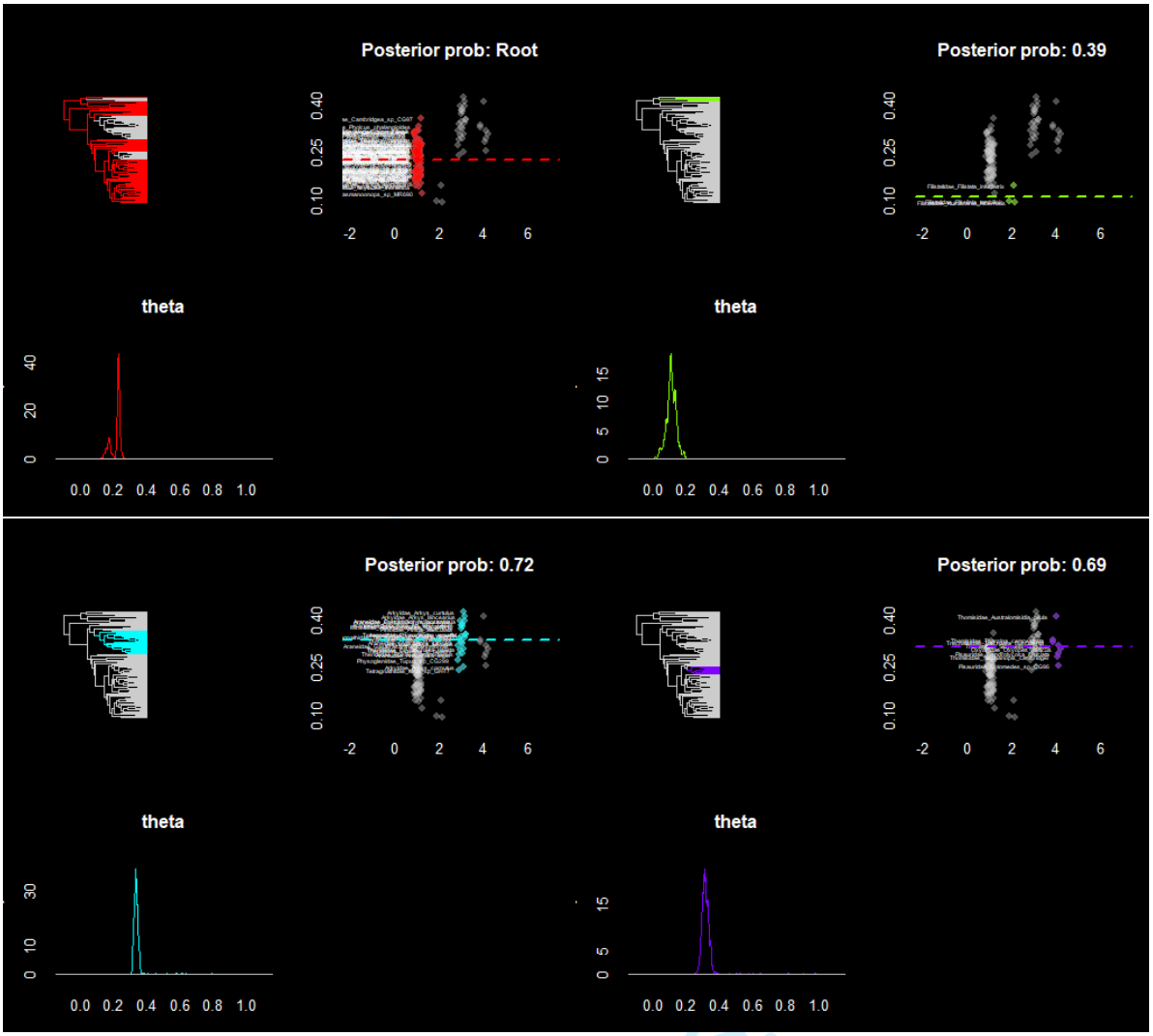

2nd run

```
bayou MCMC chain: 5e+05 generations
50001 samples, first 15000 samples discarded as burnin


Summary statistics for parameters:
                     Mean           SD     Naive SE Time-series SE Effective Size    HPD95Lower    HPD95Upper
lnL          1.580312e+02 6.0953712286 3.258020e-02   4.814163e-01      160.30934  1.468149e+02  1.700578e+02
prior       -3.414068e+01 9.0254451541 4.824166e-02   4.859780e-01      344.90864 -5.196350e+01 -1.912175e+01
alpha        5.819107e-03 0.0284022498 1.518121e-04   4.114094e-03       47.66034  1.436121e-06  7.984187e-03
sig2         3.676155e-05 0.0001120929 5.991445e-07   1.611899e-05       48.35937  1.054735e-05  4.184227e-05
k            1.000409e+01 3.0362250863 1.622884e-02   1.642275e-01      341.80328  4.000000e+00  1.500000e+01
ntheta       1.100409e+01 3.0362250863 1.622884e-02   1.642275e-01      341.80328  5.000000e+00  1.600000e+01
root.theta   2.205943e-01 0.0422409550 2.257810e-04   2.795953e-03      228.24834  1.277259e-01  2.994918e-01
all theta    4.603161e-01 0.2731071777           NA             NA             NA            NA            NA


Branches with posterior probabilities higher than 0.1:
           pp magnitude.of.theta2 naive.SE.of.theta2 rel.location
105 0.4282327           0.6322921        0.001573613    0.4229985
75  0.3684075           0.5404736        0.001492504    0.4903995
124 0.2717559           0.6812887        0.001940352    0.3293983
77  0.2682132           0.5426039        0.001699363    0.4747756
205 0.2082452           0.4098543        0.002108421    0.5236186
7   0.2024170           0.6327453        0.002476646    0.2629357
158 0.1740758           0.7231331        0.002869299    0.2163453
73  0.1689332           0.5909194        0.002224458    0.4356041
174 0.1671047           0.6511175        0.002912173    0.3689094
38  0.1109079           0.2530948        0.004040710    0.3158326
97  0.1099366           0.6938910        0.003954666    0.2826855
116 0.1072224           0.6092654        0.003961196    0.4399017
103 0.1059082           0.6648438        0.003097093    0.2301801
```

1st run 2nd run

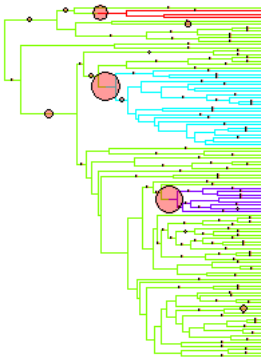

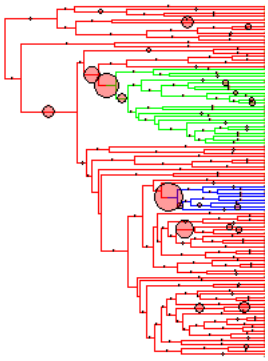

dk=15

1st run

```
bayou MCMC chain: 5e+05 generations
50001 samples, first 15000 samples discarded as burnin


Summary statistics for parameters:
                     Mean          SD     Naive SE Time-series SE Effective Size    HPD95Lower    HPD95Upper
lnL          1.594930e+02  7.33308861 3.919589e-02   0.5951762864      151.80379  1.461434e+02  1.738977e+02
prior       -4.584691e+01 10.20752700 5.455997e-02   0.5995534219      289.85801 -6.317080e+01 -2.469958e+01
alpha        4.410990e-02  0.34109074 1.823155e-03   0.0428580416       63.33958  7.087212e-06  2.300219e-02
sig2         1.729462e-04  0.00118225 6.319213e-06   0.0001538536       59.04774  8.442185e-06  9.273385e-05
k            1.415376e+01  4.06393874 2.172205e-02   0.2430759647      279.51832  5.000000e+00  2.100000e+01
ntheta       1.515376e+01  4.06393874 2.172205e-02   0.2430759647      279.51832  6.000000e+00  2.200000e+01
root.theta   2.257205e-01  0.04382645 2.342556e-04   0.0031898781      188.76631  1.312206e-01  3.098228e-01
all theta    4.653516e-01  0.27487349           NA             NA             NA            NA            NA


Branches with posterior probabilities higher than 0.1:
           pp magnitude.of.theta2 naive.SE.of.theta2 rel.location
105 0.5088852          0.63869334        0.001506174    0.3914692
75  0.3684075          0.54639934        0.001513793    0.4575997
124 0.3674933          0.68550651        0.001608974    0.2773560
7   0.2900977          0.67070679        0.002285416    0.2331472
174 0.2745557          0.67043257        0.002382592    0.3146514
77  0.2576424          0.54312690        0.001762578    0.5035017
205 0.2178161          0.40336996        0.001731546    0.5534020
158 0.2113022          0.70264475        0.002534607    0.2650521
73  0.1854180          0.58997745        0.002047026    0.4372530
38  0.1373921          0.29780230        0.003370798    0.2523120
39  0.1364493          0.28989318        0.003390127    0.2151234
10  0.1311068          0.67723079        0.003536286    0.2168928
114 0.1229073          0.57307180        0.004172357    0.4177948
5   0.1187361          0.09554681        0.001394889    0.3270057
111 0.1179933          0.57944125        0.003822961    0.3641653
167 0.1167648          0.61663877        0.004370802    0.2645987
68  0.1136792          0.35982707        0.004086645    0.3650892
78  0.1125079          0.19048829        0.002760002    0.3315407
162 0.1121650          0.61799740        0.003801353    0.3221223
55  0.1105937          0.42072058        0.004266147    0.4141708
208 0.1051083          0.16365957        0.002491905    0.3720691
40  0.1039083          0.62336539        0.004686015    0.3322986
157 0.1028513          0.37427597        0.004148040    0.3382965
182 0.1025941          0.61691698        0.004261719    0.2260338
113 0.1005371          0.48761225        0.004675290    0.3961859
126 0.1001657          0.57750085        0.003680377    0.4000864
```

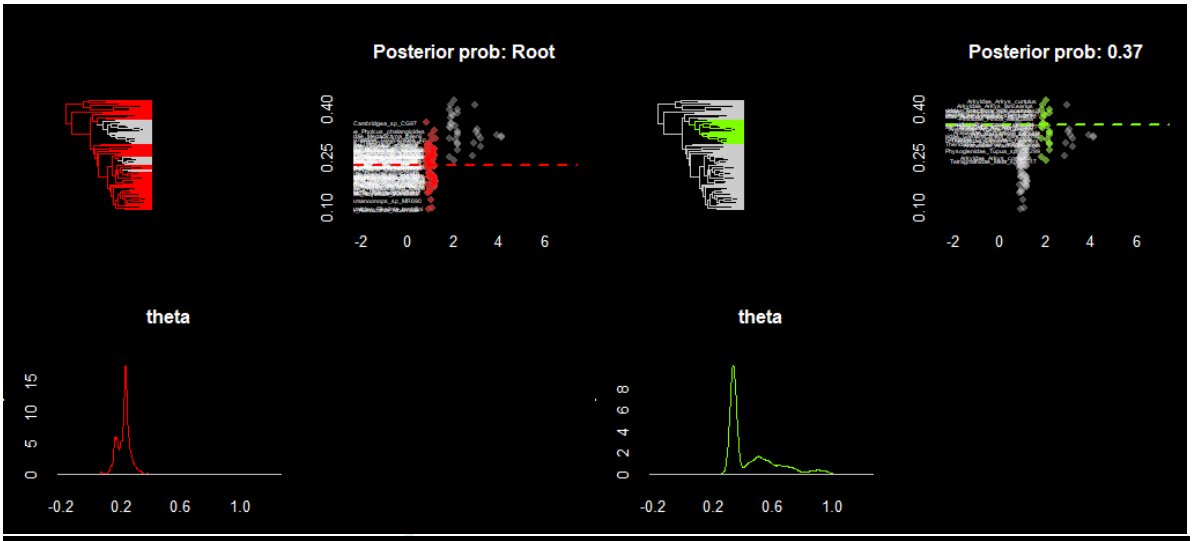

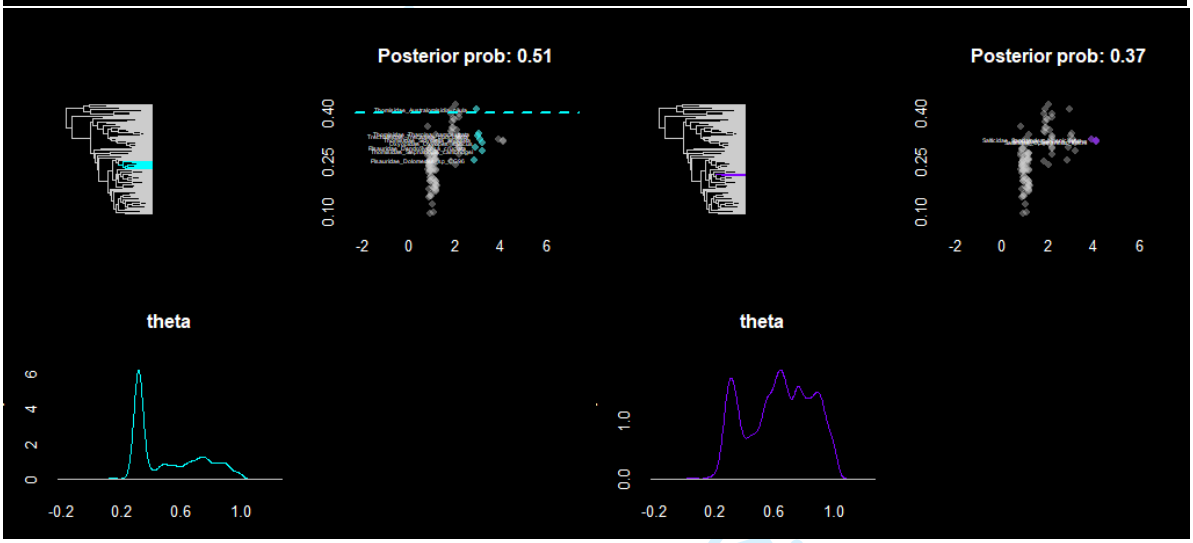

2nd run

```
bayou MCMC chain: 5e+05 generations

50001 samples, first 15000 samples discarded as burnin


Summary statistics for parameters:
                    Mean           SD     Naive SE Time-series SE Effective Size    HPD95Lower    HPD95Upper
lnL        162.355873724  7.85479977 0.0419844713    0.790483517       98.73806  1.473363e+02 176.385021285
prior      -40.493855630 11.44856446 0.0611934028    0.998182562      131.54735 -6.317221e+01 -22.178569305
alpha        0.653034692  4.98801918 0.0266613223    0.247836494      405.06593  3.172934e-08   1.994958325
sig2         0.002490205  0.01893404 0.0001012038    0.001123609      283.95925  8.237006e-06   0.007623954
k           11.601937032  4.87399816 0.0260518717    0.477985287      103.97805  3.000000e+00  20.000000000
ntheta      12.601937032  4.87399816 0.0260518717    0.477985287      103.97805  4.000000e+00  21.000000000
root.theta   0.212481150  0.04308519 0.0002302934    0.003041398      200.68246  1.377568e-01   0.288388349
all theta    0.425076934  0.26117940           NA             NA             NA            NA            NA


Branches with posterior probabilities higher than 0.1:
           pp magnitude.of.theta2 naive.SE.of.theta2 rel.location
105 0.5775670           0.5156189        0.001509455    0.4536456
75  0.4906862           0.4515565        0.001221860    0.4905556
124 0.3103823           0.5870177        0.002143099    0.3185833
7   0.3031541           0.5549989        0.002399259    0.3293857
205 0.2996400           0.3322102        0.001437984    0.4904793
77  0.2364436           0.4774504        0.001817618    0.4449244
158 0.2169590           0.6147119        0.002943515    0.3052464
174 0.2029884           0.6268177        0.002837692    0.3699016
73  0.1529055           0.5281421        0.002529442    0.4967491
97  0.1412205           0.6201739        0.003522575    0.3429068
5   0.1292783           0.1060067        0.001335984    0.3666868
208 0.1272213           0.2013855        0.002085698    0.4225844
78  0.1268499           0.1941159        0.002221723    0.3844341
38  0.1251643           0.3107900        0.003681683    0.2952714
```

```
116 0.1039655          0.5308964        0.003883170    0.3663483
10  0.1038512          0.6106724        0.004650042    0.2051190
```

1st run 2nd run

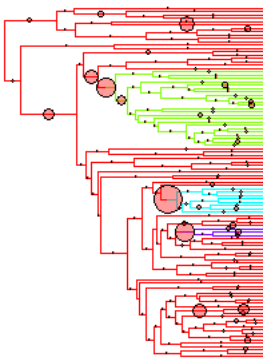

dk=20

1st run

```
bayou MCMC chain: 5e+05 generations
50001 samples, first 15000 samples discarded as burnin


Summary statistics for parameters:
                      Mean           SD     Naive SE Time-series SE Effective Size    HPD95Lower    HPD95Upper
lnL          1.613735e+02 8.296503e+00 4.434541e-02   7.058833e-01      138.14157  1.455210e+02  1.772630e+02
prior       -5.785089e+01 9.518090e+00 5.087488e-02   5.111926e-01      346.68138 -7.766378e+01 -4.177376e+01
alpha        1.909046e-03 1.278900e-03 6.835815e-06   1.378223e-04       86.10617  6.515770e-06  4.197143e-03
sig2         1.979462e-05 5.043979e-06 2.696043e-08   1.969712e-07      655.75379  1.060847e-05  2.985477e-05
k            1.911376e+01 4.238527e+00 2.265523e-02   2.275394e-01      346.98986  1.100000e+01  2.700000e+01
ntheta       2.011376e+01 4.238527e+00 2.265523e-02   2.275394e-01      346.98986  1.200000e+01  2.800000e+01
root.theta   2.156545e-01 4.807421e-02 2.569601e-04   3.463834e-03      192.62391  1.207540e-01  3.046784e-01
all theta    4.720302e-01 2.759516e-01           NA              NA             NA            NA            NA


Branches with posterior probabilities higher than 0.1:
           pp magnitude.of.theta2 naive.SE.of.theta2 rel.location
7   0.4612022           0.6866834        0.001765727    0.2467851
105 0.4451174           0.6686136        0.001412760    0.3399521
124 0.4263756           0.6942185        0.001420096    0.2613805
75  0.3381521           0.5840537        0.001515838    0.4537847
205 0.3039541           0.4086429        0.001446467    0.4818938
77  0.3035541           0.5659425        0.001511648    0.3973248
174 0.2934118           0.6717428        0.002076803    0.3407633
158 0.2473573           0.7645885        0.002252506    0.1757241
38  0.2405863           0.2421728        0.002192625    0.2160274
10  0.2075596           0.6707606        0.002866616    0.1558525
123 0.1871036           0.1588267        0.001413957    0.1940317
73  0.1866750           0.6294419        0.001939571    0.3174921
167 0.1833038           0.6704709        0.003002495    0.2251404
78  0.1805897           0.1869158        0.002109374    0.3235077
39  0.1670476           0.2915119        0.003263349    0.2413745
182 0.1590481           0.6441422        0.003463762    0.2116708
40  0.1586195           0.6574563        0.003668248    0.2433032
99  0.1575624           0.7647194        0.002542939    0.2757742
97  0.1561054           0.7662817        0.002882567    0.2748960
116 0.1503914           0.5898044        0.003478196    0.3826298
162 0.1418490           0.6026422        0.003471753    0.2962035
126 0.1365636           0.5782486        0.003275045    0.3124141
111 0.1364493           0.6395457        0.003373857    0.3102875
34  0.1361636           0.4661136        0.003760419    0.4265737
103 0.1334209           0.6944975        0.002662718    0.2716785
91  0.1329353           0.4643242        0.003749103    0.3573912
57  0.1318782           0.3786699        0.003656724    0.3071919
68  0.1291926           0.3848192        0.003750713    0.3393363
157 0.1236786           0.3350900        0.003748761    0.3081097
114 0.1235644           0.6038941        0.003865275    0.2794883
94  0.1195932           0.6155378        0.003757755    0.3468050
128 0.1179075           0.5794396        0.004396414    0.1730970
198 0.1175647           0.4714160        0.003913374    0.3836449
134 0.1157362           0.4309224        0.004080971    0.4244093
101 0.1155648           0.5798809        0.004382647    0.4247714
```

136	0.1136792	0.5404059	0.004554523	0.3041582
44	0.1136506	0.6681865	0.004193582	0.1997562
36	0.1120222	0.5406163	0.003768132	0.3863949
102	0.1119936	0.6566518	0.003409054	0.2619235
152	0.1119079	0.4773175	0.004521663	0.3798154
161	0.1097652	0.2709676	0.003898034	0.2788746
92	0.1086795	0.4087701	0.004150842	0.3452907
139	0.1085938	0.4325678	0.004473724	0.3804871
35	0.1073082	0.5242727	0.004144945	0.3625968
203	0.1062796	0.3532611	0.001805183	0.4396342
106	0.1040512	0.2665533	0.003935944	0.3572946
50	0.1039369	0.6234392	0.004001767	0.3788676
160	0.1016799	0.5575227	0.004767799	0.2942689
29	0.1012514	0.5419677	0.004263449	0.3936401
42	0.1011942	0.5094773	0.004505566	0.3101032
98	0.1011942	0.5992102	0.004253846	0.3540355
55	0.1009085	0.4516611	0.004794680	0.3179066
208	0.1008228	0.1738312	0.002505040	0.3217908
125	0.1003086	0.3151696	0.004709635	0.2501843

2nd run

```
bayou MCMC chain: 5e+05 generations
50001 samples, first 15000 samples discarded as burnin


Summary statistics for parameters:
                     Mean           SD     Naive SE Time-series SE Effective Size    HPD95Lower    HPD95Upper
lnL          1.598232e+02 7.682216e+00 4.106200e-02   6.363818e-01       145.7262  1.464346e+02  1.747977e+02
prior       -5.885307e+01 9.333439e+00 4.988791e-02   4.847635e-01       370.7008 -7.766283e+01 -4.177377e+01
alpha        1.565559e-03 8.472627e-04 4.528680e-06   7.410575e-05       130.7171  4.839453e-05  3.072955e-03
sig2         1.954644e-05 4.643708e-06 2.482096e-08   1.745129e-07       708.0679  1.102065e-05  2.892003e-05
k            1.955917e+01 4.160716e+00 2.223933e-02   2.160530e-01       370.8649  1.100000e+01  2.700000e+01
ntheta       2.055917e+01 4.160716e+00 2.223933e-02   2.160530e-01       370.8649  1.200000e+01  2.800000e+01
root.theta   2.167186e-01 5.011742e-02 2.678812e-04   3.902376e-03       164.9374  1.181041e-01  3.128729e-01
all theta    4.816399e-01 2.772717e-01           NA             NA             NA            NA            NA


Branches with posterior probabilities higher than 0.1:
           pp magnitude.of.theta2 naive.SE.of.theta2 rel.location
105 0.4889435           0.7148205        0.001327034    0.3937397
7   0.4208331           0.7078562        0.001742704    0.2698228
124 0.3822639           0.7505428        0.001478796    0.2770057
75  0.3674647           0.6101155        0.001298598    0.4340670
205 0.3638078           0.4198842        0.001380652    0.4947676
174 0.2860408           0.6918421        0.002126212    0.3341549
77  0.2444432           0.6043097        0.001716163    0.4078330
38  0.2187018           0.3167810        0.002742139    0.2570815
158 0.2125593           0.7169394        0.002674720    0.2217479
73  0.2017313           0.6425357        0.001902677    0.4154734
10  0.2003600           0.6669375        0.003080085    0.1862990
123 0.1998172           0.1652771        0.001900481    0.2310065
39  0.1804183           0.3209233        0.003367055    0.2573276
78  0.1670762           0.2270772        0.002694049    0.3106394
182 0.1567053           0.6411136        0.003492767    0.2086860
148 0.1562482           0.5862709        0.003605366    0.2593180
68  0.1482487           0.3929635        0.003503418    0.3566572
126 0.1445346           0.5955128        0.002954976    0.3717546
208 0.1441346           0.1991051        0.002669017    0.3865585
116 0.1431347           0.6056858        0.003415053    0.3773646
111 0.1424204           0.6110578        0.003508116    0.3197693
162 0.1415919           0.6604117        0.003401140    0.2465372
97  0.1403920           0.7391596        0.003221358    0.2624942
167 0.1393920           0.6207144        0.003852175    0.3040400
55  0.1326496           0.4480910        0.004257501    0.3718383
92  0.1303068           0.4053709        0.003995424    0.3620068
29  0.1289069           0.5425962        0.003815883    0.3704750
103 0.1265356           0.7291450        0.002714020    0.2271323
165 0.1215073           0.4965859        0.004131324    0.3599820
57  0.1209931           0.3516587        0.003621236    0.2827822
157 0.1191075           0.3849116        0.003893155    0.2982321
44  0.1187646           0.6710881        0.003770289    0.2639313
51  0.1176219           0.4584457        0.004052137    0.3341962
106 0.1173362           0.3097750        0.004013390    0.3680138
49  0.1170219           0.6303266        0.003718234    0.3757329
80  0.1168505           0.5655263        0.003969134    0.2905248
101 0.1165933           0.5447341        0.003986113    0.3939158
172 0.1153648           0.4949332        0.004319770    0.4098902
120 0.1141935           0.4312917        0.004754308    0.4400578
56  0.1138792           0.6105672        0.004524600    0.3917847
```

40	0.1109365	0.6549762	0.004127483	0.2380328
114	0.1108222	0.5885925	0.004489973	0.3647037
96	0.1105651	0.4354266	0.004222927	0.3045888
110	0.1100509	0.5405334	0.004712267	0.3230098
16	0.1079938	0.4682017	0.004279181	0.3318592
207	0.1074224	0.3652693	0.002811614	0.3652672
82	0.1070510	0.4522838	0.004267803	0.4039586
53	0.1063654	0.5337292	0.004432474	0.3568596
183	0.1057940	0.5222926	0.004492648	0.3146739
128	0.1057368	0.5897774	0.004509557	0.2235756
112	0.1048512	0.4775415	0.004542319	0.4089215
152	0.1047083	0.5313464	0.004480523	0.3684023
91	0.1041940	0.5288102	0.004516411	0.3815984
137	0.1037369	0.5159712	0.004495332	0.3090665
161	0.1037369	0.2808682	0.003816694	0.3035419
94	0.1031370	0.5810051	0.004700815	0.3349869
99	0.1031370	0.7512981	0.003164982	0.2558129
13	0.1026798	0.5305533	0.004396875	0.2879374
163	0.1022513	0.5422723	0.004499369	0.2448315
11	0.1021656	0.5396840	0.004512198	0.3374546
66	0.1015371	0.5893669	0.004034781	0.3833692
113	0.1014228	0.4919806	0.004595871	0.3915539
25	0.1011942	0.4914312	0.004449119	0.2439849
139	0.1008228	0.4298159	0.004660073	0.2756623
42	0.1001943	0.4988943	0.004805215	0.3363007
154	0.1001943	0.4702764	0.004679118	0.4279287

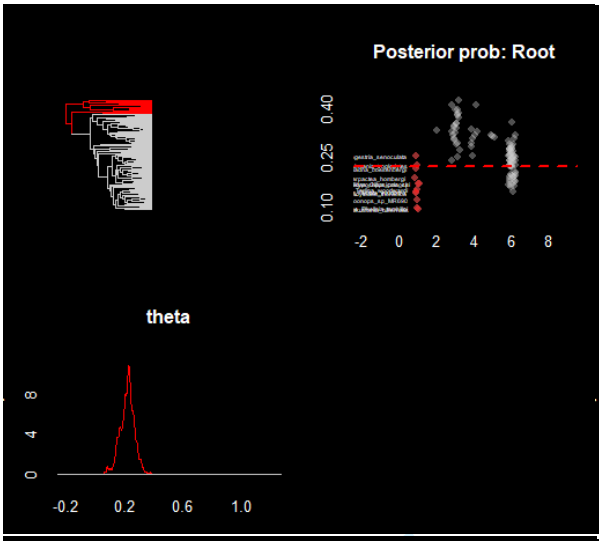
Posterior prob: Root
theta

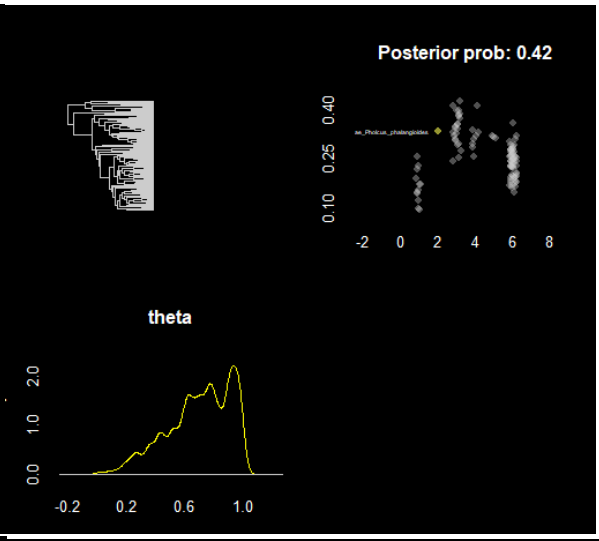
Posterior prob: 0.42
theta

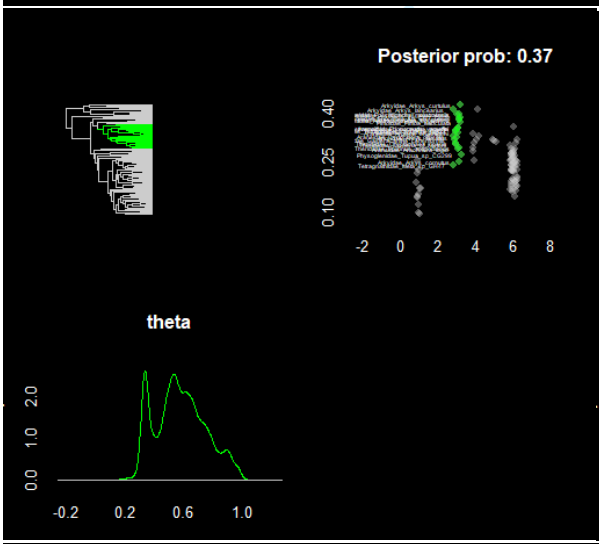
Posterior prob: 0.37
theta

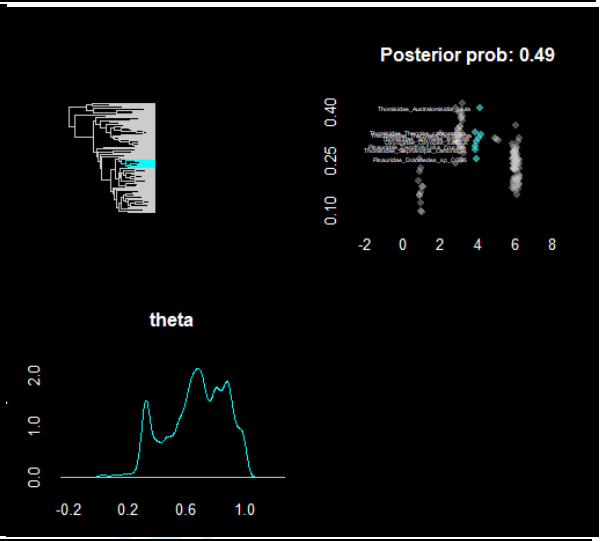
Posterior prob: 0.49
theta

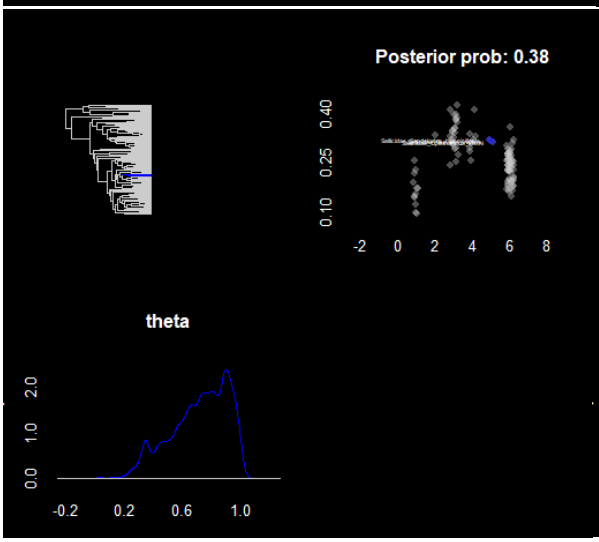
Posterior prob: 0.38
theta

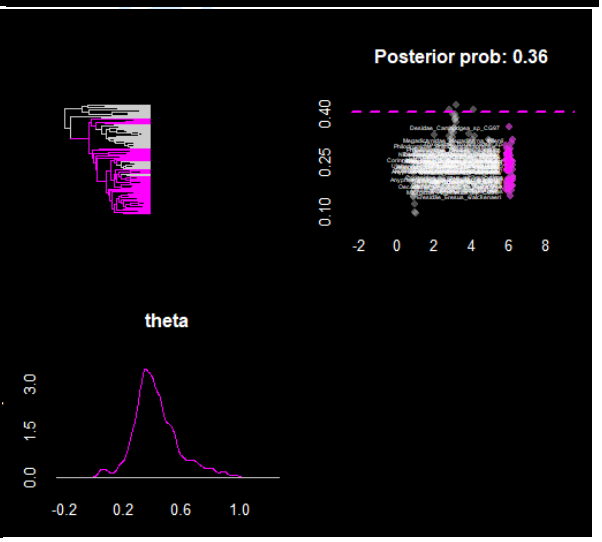
Posterior prob: 0.36
theta

1st run

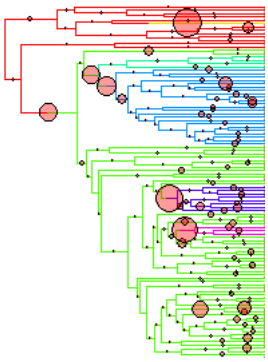

2nd run

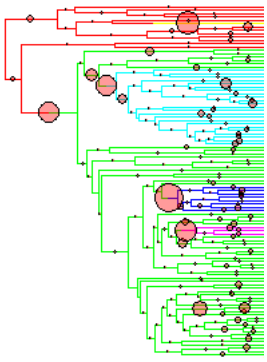

dk=25

1st run

```
bayou MCMC chain: 5e+05 generations
50001 samples, first 15000 samples discarded as burnin


Summary statistics for parameters:
                      Mean            SD     Naive SE Time-series SE Effective Size    HPD95Lower    HPD95Upper
lnL          1.620600e+02 1.026816e+01 5.488405e-02   1.090602e+00       88.64469  1.435812e+02  1.815969e+02
prior       -6.762982e+01 1.004997e+01 5.371782e-02   5.770774e-01      303.29243 -8.817559e+01 -5.025839e+01
alpha        1.617064e-03 9.890788e-04 5.286698e-06   1.094971e-04       81.59363  6.079167e-07  3.356591e-03
sig2         1.859885e-05 4.838978e-06 2.586469e-08   2.475538e-07      382.09210  9.654033e-06  2.826025e-05
k            2.361748e+01 5.038452e+00 2.693089e-02   2.895977e-01      302.69409  1.400000e+01  3.300000e+01
ntheta       2.461748e+01 5.038452e+00 2.693089e-02   2.895977e-01      302.69409  1.500000e+01  3.400000e+01
root.theta   2.125136e-01 5.131029e-02 2.742572e-04   3.744528e-03      187.76512  1.175074e-01  3.149041e-01
all theta    4.777083e-01 2.781078e-01           NA              NA             NA            NA            NA


Branches with posterior probabilities higher than 0.1:
           pp magnitude.of.theta2 naive.SE.of.theta2 rel.location
7   0.5563111           0.6680434        0.001530146    0.2769606
105 0.4827438           0.6891115        0.001191024    0.3767509
124 0.4220045           0.7376938        0.001411143    0.3043483
205 0.3987201           0.4270102        0.001312564    0.5041703
174 0.3411234           0.7114294        0.001807027    0.3317912
75  0.3230673           0.5888159        0.001412253    0.4251572
10  0.2842409           0.6862178        0.002650777    0.1556206
77  0.2778698           0.5601918        0.001549598    0.4131916
38  0.2550711           0.2687579        0.002288423    0.2150873
158 0.2373864           0.7411883        0.002400327    0.1697242
78  0.2270727           0.2209586        0.002351072    0.3093765
182 0.2179018           0.6675436        0.003109899    0.1994184
73  0.2122450           0.6163938        0.001670357    0.4265756
167 0.1957317           0.6484186        0.003083253    0.1735731
162 0.1953031           0.6337291        0.003016316    0.2635930
39  0.1916462           0.2959787        0.003046990    0.2418081
40  0.1857037           0.6274942        0.003591982    0.3007751
123 0.1788755           0.1603494        0.002004224    0.2639141
126 0.1786755           0.5948786        0.002616703    0.3230482
208 0.1727616           0.2205144        0.002443034    0.3643075
68  0.1685618           0.4005831        0.003145531    0.3236899
106 0.1625907           0.2834389        0.003091784    0.2958930
99  0.1625336           0.7900321        0.002263854    0.2479597
57  0.1602480           0.3799685        0.003506528    0.2934548
92  0.1596766           0.4147729        0.003689815    0.3052698
111 0.1579624           0.5831466        0.003439248    0.2758343
56  0.1528484           0.6036378        0.003919020    0.3118629
83  0.1472202           0.5528300        0.003835691    0.2959340
157 0.1470202           0.3863350        0.003639278    0.2504670
98  0.1461916           0.5264878        0.003732152    0.3563590
97  0.1455345           0.7564607        0.003133527    0.2627512
161 0.1424490           0.2563524        0.003276131    0.2141711
29  0.1422204           0.5350107        0.003610109    0.3673081
96  0.1405348           0.3900503        0.003757047    0.2926030
136 0.1400206           0.5095069        0.004118765    0.2352852
114 0.1395635           0.6064220        0.003750088    0.2719858
91  0.1380493           0.5048935        0.004021937    0.4143582
160 0.1377350           0.5782780        0.004226693    0.2449168
44  0.1367636           0.7045576        0.003423262    0.2665758
```

155	0.1357922	0.3926231	0.004108482	0.3710042
94	0.1350780	0.6196605	0.004170998	0.3166965
112	0.1342495	0.4741537	0.003827648	0.3871287
116	0.1342209	0.6737829	0.003591094	0.3206298
48	0.1337638	0.6005426	0.003815911	0.3669597
62	0.1335067	0.6399160	0.003108121	0.3016364
36	0.1332781	0.5833752	0.003601098	0.4445077
52	0.1324496	0.5759936	0.004093329	0.3069080
110	0.1306497	0.5070130	0.004134777	0.2643017
13	0.1297069	0.4380490	0.003651326	0.2569460
150	0.1295926	0.5180394	0.004083748	0.2668810
43	0.1295640	0.3848729	0.003518768	0.3010105
198	0.1283927	0.4859418	0.003654625	0.2963087
95	0.1273642	0.6100894	0.003946494	0.3575415
101	0.1270213	0.5766043	0.004277405	0.3252218
121	0.1270213	0.2599112	0.003608580	0.3201898
109	0.1266213	0.4790530	0.004148227	0.2451182
183	0.1263356	0.4871408	0.003765439	0.3591317
190	0.1259928	0.4047752	0.003646990	0.4077490
113	0.1253357	0.4888740	0.004161339	0.3475860
148	0.1243072	0.5579232	0.004096399	0.2438004
35	0.1238501	0.5749840	0.004087299	0.3501340
34	0.1225073	0.4204500	0.003829332	0.3687094
42	0.1221644	0.5222558	0.004100409	0.3418793
31	0.1219645	0.4789958	0.003943465	0.3721641
55	0.1213359	0.4628059	0.004214878	0.3383352
207	0.1213359	0.3836046	0.002483258	0.2757729
129	0.1209359	0.5179833	0.004198872	0.3368462
195	0.1209359	0.3595897	0.003254766	0.3863139
103	0.1205931	0.6711577	0.003307970	0.1408690
168	0.1198789	0.3771936	0.004559546	0.2498770
128	0.1194503	0.5492808	0.004290549	0.2164297
177	0.1189361	0.4857981	0.004455268	0.3551755
152	0.1188218	0.5025446	0.004041474	0.3665567
51	0.1184218	0.4443897	0.004377384	0.3513076
53	0.1183361	0.5072981	0.004099659	0.3272815
32	0.1163933	0.5094623	0.004073574	0.3543867
16	0.1160791	0.4322218	0.003533797	0.3064376
66	0.1158505	0.5861752	0.003734515	0.4176436
159	0.1148220	0.5120930	0.004303579	0.3032798
11	0.1146792	0.4932896	0.004174248	0.3162960
28	0.1145935	0.4258304	0.004181395	0.3469959
165	0.1141363	0.4593744	0.003931080	0.3622995
117	0.1126507	0.3406718	0.003999032	0.3544694
140	0.1123650	0.4215392	0.004216537	0.3112937
134	0.1123079	0.3629622	0.003850328	0.4361983
163	0.1118793	0.5488797	0.004566789	0.2501011
154	0.1101366	0.4609950	0.004269854	0.3723673
132	0.1099651	0.5050428	0.004206702	0.2403134
151	0.1099080	0.3340345	0.003894702	0.4322650
181	0.1094223	0.3827422	0.004355823	0.2383470
12	0.1088509	0.4638843	0.004184326	0.3369227
80	0.1071082	0.5233224	0.004360499	0.1860581
82	0.1066796	0.3719267	0.004183257	0.3437831
169	0.1060797	0.4178391	0.004282820	0.3213128
172	0.1054511	0.4888173	0.004150925	0.3866152
6	0.1050226	0.3539427	0.004015418	0.4072360
49	0.1035655	0.5655415	0.003990964	0.2961656
137	0.1032227	0.5247240	0.004604020	0.3458440
41	0.1031084	0.3896751	0.004431111	0.1612293
8	0.1028513	0.3316059	0.004160493	0.3364030
21	0.1023941	0.4143459	0.004441542	0.3073425
120	0.1021656	0.3957039	0.004898601	0.2720682
64	0.1020227	0.4997273	0.004471826	0.3722481
1	0.1015656	0.4405879	0.004645691	0.3160924
25	0.1013656	0.4874177	0.004384080	0.2701514
166	0.1009371	0.3759077	0.004375837	0.3018032
17	0.1006800	0.3816836	0.004690777	0.4632552
30	0.1004514	0.3932465	0.004024663	0.3188067
22	0.1003086	0.3362562	0.004705424	0.3163404

2nd run

```
bayou MCMC chain: 5e+05 generations
50001 samples, first 15000 samples discarded as burnin


Summary statistics for parameters:
                    Mean           SD     Naive SE Time-series SE Effective Size    HPD95Lower    HPD95Upper
lnL         1.609708e+02 10.154744193 5.427784e-02   1.2070537152       70.77580  1.421309e+02  1.794518e+02
```

prior	-6.755269e+01	11.645323078	6.224509e-02	0.7710839499	228.08659	-8.817727e+01	-4.138871e+01
alpha	7.185753e-02	0.445494380	2.381200e-03	0.0542235591	67.50072	1.714661e-06	1.713886e-01
sig2	2.324342e-04	0.001292547	6.908759e-06	0.0001346806	92.10493	6.092358e-06	5.420867e-04
k	2.347663e+01	6.040342700	3.228607e-02	0.4140747250	212.79710	8.000000e+00	3.300000e+01
ntheta	2.447663e+01	6.040342700	3.228607e-02	0.4140747250	212.79710	9.000000e+00	3.400000e+01
root.theta	2.191349e-01	0.051958027	2.777194e-04	0.0037904137	187.90229	1.281132e-01	3.274578e-01
all theta	4.800263e-01	0.276285742	NA	NA	NA	NA	NA

Branches with posterior probabilities higher than 0.1:

	pp	magnitude.of.theta2	naive.SE.of.theta2	rel.location
7	0.5379693	0.6728440	0.001684991	0.2482273
105	0.4796869	0.6877709	0.001492680	0.3258008
205	0.4117193	0.4205556	0.001126223	0.4986664
124	0.3907491	0.7219437	0.001716342	0.2581462
77	0.3326953	0.5567731	0.001560391	0.3617395
174	0.3160962	0.6934694	0.001976921	0.3176735
75	0.3153534	0.5989550	0.001655819	0.4044738
38	0.2578995	0.3257259	0.002467962	0.2930141
123	0.2378436	0.1724161	0.001747356	0.2697950
10	0.2192446	0.6455496	0.003084228	0.1721002
78	0.2119879	0.2181959	0.002162260	0.3303883
158	0.2105880	0.7010896	0.002900213	0.2299441
167	0.2045597	0.6521437	0.003071350	0.2000368
39	0.1980458	0.3670993	0.003263519	0.2831004
73	0.1973030	0.6384755	0.001998486	0.3200711
162	0.1779898	0.6308160	0.003316489	0.2913496
57	0.1690475	0.3605164	0.003318410	0.3434635
68	0.1656762	0.4268325	0.003366081	0.2839411
126	0.1611908	0.6445181	0.003068227	0.2749702
96	0.1584481	0.4418977	0.003646518	0.2805094
62	0.1541055	0.6709290	0.003324242	0.3201953
157	0.1527341	0.3902574	0.003829534	0.2781681
40	0.1522199	0.6063383	0.003596592	0.2916278
44	0.1474773	0.6941339	0.003400866	0.2689567
106	0.1473916	0.3039231	0.003465225	0.3185658
116	0.1471916	0.5670378	0.003450904	0.3571755
182	0.1461059	0.6354240	0.003781243	0.1901078
161	0.1441918	0.3074608	0.003671089	0.2690948
148	0.1441061	0.5980783	0.003778345	0.2810911
111	0.1419633	0.6217625	0.003429438	0.2972469
152	0.1413919	0.5098582	0.003860316	0.3135562
203	0.1392206	0.3697792	0.002066867	0.4199097
134	0.1366208	0.4144541	0.003865165	0.4360904
92	0.1365922	0.4376629	0.004033767	0.3761197
51	0.1355923	0.4979896	0.004353935	0.3675132
172	0.1344780	0.4560875	0.003638340	0.3858416
35	0.1330210	0.5603700	0.003684649	0.3257267
110	0.1315353	0.5340182	0.004026919	0.2938372
64	0.1299926	0.5434953	0.004031527	0.3503023
112	0.1296212	0.4816965	0.004070715	0.3269420
29	0.1295926	0.5628605	0.003813273	0.3234790
97	0.1283641	0.6672147	0.003859936	0.3185287
31	0.1273642	0.5422885	0.004207695	0.3498458
138	0.1271356	0.3208249	0.003691562	0.2854967
56	0.1267356	0.5814426	0.003854919	0.3150948
34	0.1265356	0.5174057	0.003840905	0.3452017
190	0.1261642	0.4577814	0.003680379	0.3597732
160	0.1251643	0.5896881	0.004252952	0.2634649
128	0.1247072	0.5940560	0.003882466	0.2205351
192	0.1235358	0.4799686	0.003738646	0.4068681
183	0.1234215	0.5381284	0.004079883	0.3615677
120	0.1233644	0.4364860	0.004370921	0.3386017
137	0.1232501	0.5440119	0.004003804	0.3034611
165	0.1229073	0.4952663	0.004148994	0.3848459
163	0.1227073	0.5686821	0.003983108	0.1730333
208	0.1226501	0.2115100	0.003108844	0.2849253
27	0.1225930	0.5125437	0.004197711	0.3661169
28	0.1223644	0.3929464	0.003661485	0.2788662
103	0.1216216	0.6913857	0.003153698	0.1829403
42	0.1211074	0.4900680	0.004347180	0.3239864
177	0.1199931	0.4517498	0.004116685	0.3257084
66	0.1193646	0.6034739	0.003986071	0.3536665
5	0.1184218	0.1768870	0.003362543	0.2805527
52	0.1179361	0.5641241	0.004189742	0.3187767
32	0.1178504	0.4773940	0.003952302	0.3025652
140	0.1177361	0.4047696	0.004609753	0.3248262
101	0.1175647	0.5436653	0.004008820	0.3592629
151	0.1174504	0.4364212	0.004329088	0.3646107
99	0.1168790	0.6861831	0.003735416	0.2726284
30	0.1168505	0.3764003	0.003491542	0.3958663
188	0.1164791	0.3612572	0.004005101	0.3905071

49	0.1161934	0.6133740	0.003945352	0.3311671
147	0.1159648	0.3034309	0.004134314	0.2931000
195	0.1155934	0.3832567	0.002690192	0.3311892
13	0.1154791	0.4623140	0.004351257	0.2578258
98	0.1153363	0.5295883	0.004524546	0.2831749
36	0.1150506	0.6027607	0.004233817	0.3929938
43	0.1150220	0.3983061	0.004312623	0.2423020
83	0.1146792	0.5989218	0.004174438	0.2512612
11	0.1141078	0.4848821	0.004319019	0.2820286
113	0.1140221	0.5187963	0.004457584	0.3716666
184	0.1138792	0.4635461	0.004328294	0.3307320
125	0.1138221	0.3985133	0.004669810	0.2138056
94	0.1137364	0.5603916	0.004313339	0.3281488
25	0.1133078	0.4994442	0.004299619	0.2689805
169	0.1130507	0.4503854	0.004202399	0.3419697
12	0.1122222	0.4867335	0.004253866	0.3268328
121	0.1121079	0.3170730	0.003942927	0.3036274
159	0.1119650	0.4904775	0.004493353	0.2729166
108	0.1113651	0.3987533	0.004095140	0.3996927
89	0.1111079	0.4742150	0.004458237	0.3127601
85	0.1099080	0.4721316	0.004126869	0.2380919
114	0.1093366	0.6254573	0.004063633	0.2785796
55	0.1090223	0.4393004	0.003968138	0.3097440
82	0.1086224	0.4609635	0.004048983	0.3567832
26	0.1081938	0.4430445	0.004584399	0.2624576
16	0.1077081	0.5213762	0.004062958	0.3702078
87	0.1071653	0.5156972	0.004269092	0.2971345
168	0.1069653	0.3912643	0.004645875	0.3706453
118	0.1069082	0.4436255	0.004369031	0.3231953
86	0.1066225	0.4996549	0.004057269	0.3603994
178	0.1066225	0.3927014	0.004291465	0.3559857
91	0.1064511	0.5448278	0.004204350	0.3527375
181	0.1062796	0.3164545	0.004278226	0.2375975
132	0.1059082	0.5437934	0.003718649	0.2054071
164	0.1056797	0.4802214	0.004534605	0.2982139
196	0.1056511	0.5175621	0.003584717	0.3720853
139	0.1049083	0.4529922	0.005006002	0.3200179
135	0.1039655	0.4475589	0.004597571	0.2952106
95	0.1039083	0.5728403	0.004680920	0.3605988
129	0.1027370	0.4944368	0.004575388	0.2740582
109	0.1026513	0.4742755	0.004487263	0.2850422
155	0.1026513	0.4178657	0.004336229	0.3326206
22	0.1024227	0.3344575	0.004426546	0.3257971
102	0.1018513	0.6815339	0.003648067	0.2001155
198	0.1016228	0.4665732	0.004355220	0.3492943
53	0.1009657	0.5046364	0.004443505	0.2823244
154	0.1007657	0.4559194	0.004783038	0.3133020
9	0.1001086	0.3683035	0.004390741	0.2712295

1st run

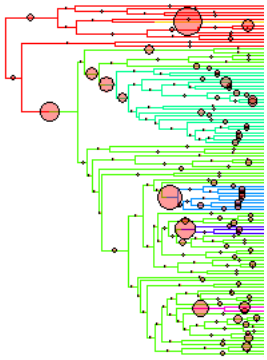

2nd run

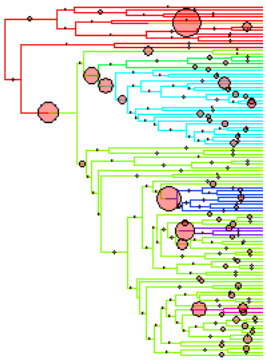

Graphical Overview

dk=10

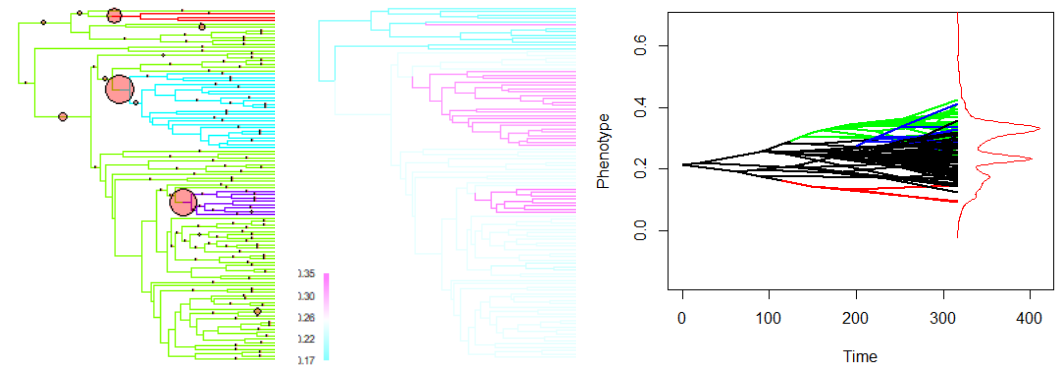

dk=15

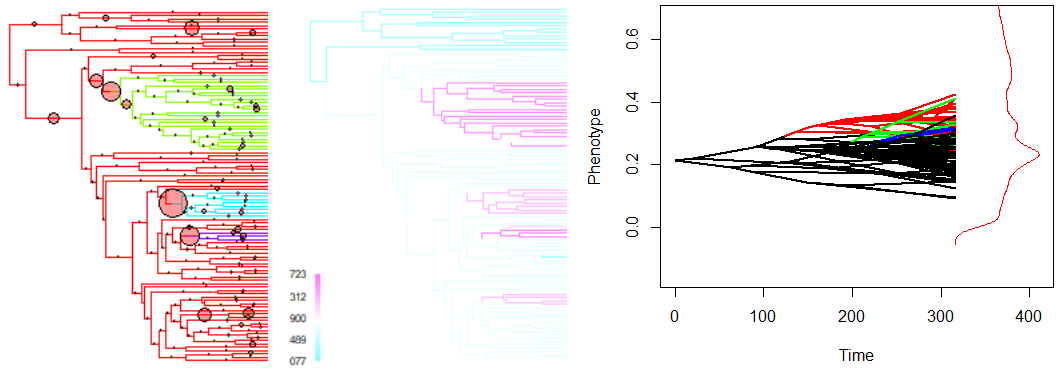

dk=20

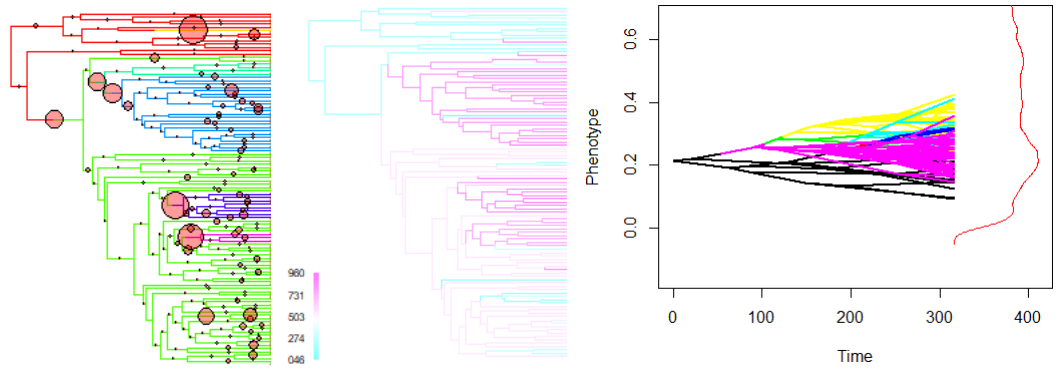

dk=25

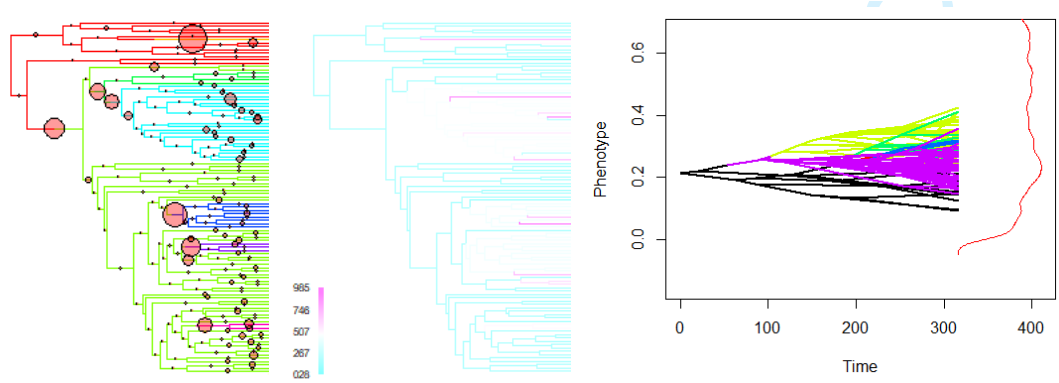

dk=10

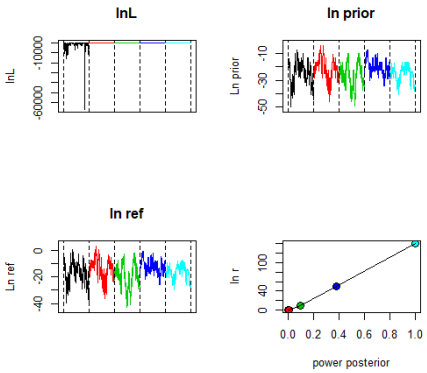

dk=15

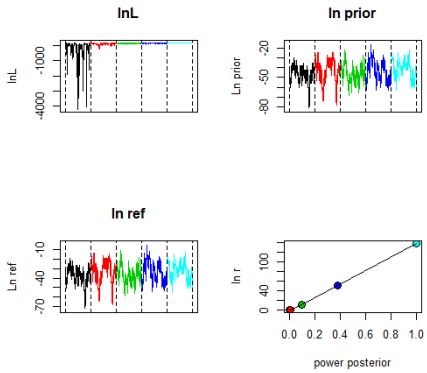

dk=20

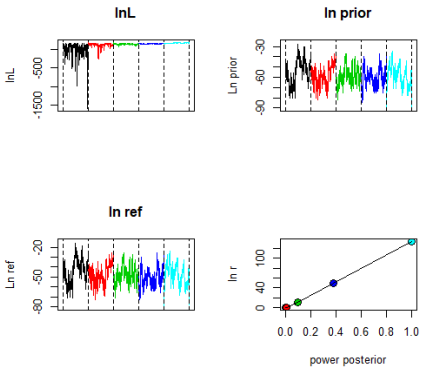

dk=25

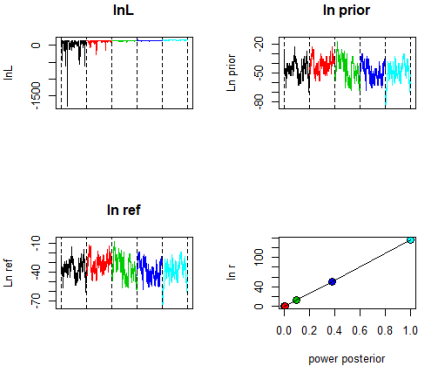

Track proportions

Analyses on the spinning track proportions h_r indicated five shifts in the evolutionary regime: *shift 1* within Desidae (*Cambridgea*) (*pp* = 0.507); *shift 2* at the basis of Hersiliidae (*pp* = 0.584); *shift 3* at the basis of Araneoidea (*pp* = 0.579); *shift 4* in the grate-shaped tapetum clade (excl. Zoropsidae) (*pp* = 0.590); and shift 5 in Pholcidae (*pp* = 0.470) (Fig. 2).

dk=10

1st run

```
bayou MCMC chain: 5e+05 generations
50001 samples, first 15000 samples discarded as burnin


Summary statistics for parameters:
                    Mean          SD     Naive SE Time-series SE Effective Size    HPD95Lower   HPD95Upper
lnL         16.681624596 6.601972613 0.0352880198   0.5525162014       142.7767  5.859888e+00  30.25038071
prior      -33.363181902 9.062078896 0.0484374653   0.4248462248       454.9798 -4.998691e+01 -16.52965475
alpha        0.078579780 0.134841578 0.0007207380   0.0104065303       167.8942  5.380774e-07   0.32512359
sig2         0.004314983 0.007172589 0.0000383380   0.0005414266       175.4982  1.455283e-04   0.01771922
k            9.359465173 3.110413544 0.0166253847   0.1496178914       432.1845  4.000000e+00  15.00000000
ntheta      10.359465173 3.110413544 0.0166253847   0.1496178914       432.1845  5.000000e+00  16.00000000
root.theta   0.645805952 0.080940900 0.0004326349   0.0040178417       405.8359  4.634329e-01   0.79537226
all theta    0.795465704 0.353744866           NA             NA             NA            NA           NA


Branches with posterior probabilities higher than 0.1:
           pp magnitude.of.theta2 naive.SE.of.theta2 rel.location
41  0.5475401           1.0073017        0.001149294    0.4455449
63  0.4721444           1.0165306        0.001169757    0.4082685
51  0.4208331           1.1157983        0.001482974    0.3970738
110 0.2992115           1.0885257        0.002458634    0.3241738
3   0.2596137           1.0542901        0.002340689    0.3410308
12  0.1526199           0.3524285        0.002227587    0.3071139
49  0.1470202           1.1651524        0.003472182    0.3952328
134 0.1337066           0.3821136        0.003163619    0.4181395
44  0.1290498           0.3717356        0.003482380    0.3549203
43  0.1199931           0.9230671        0.003065408    0.4053066
40  0.1198217           1.0602204        0.004460484    0.3722172
72  0.1115651           0.9570654        0.004540468    0.3528037
19  0.1097080           0.4976294        0.005211915    0.3650219
34  0.1088509           1.0355903        0.004688640    0.4139093
9   0.1067939           0.8703929        0.004273563    0.4443110
126 0.1023084           0.8580633        0.005234225    0.4137820
2   0.1014228           0.3755528        0.004100532    0.3536857
39  0.1009942           0.9801605        0.002859536    0.4044059
```

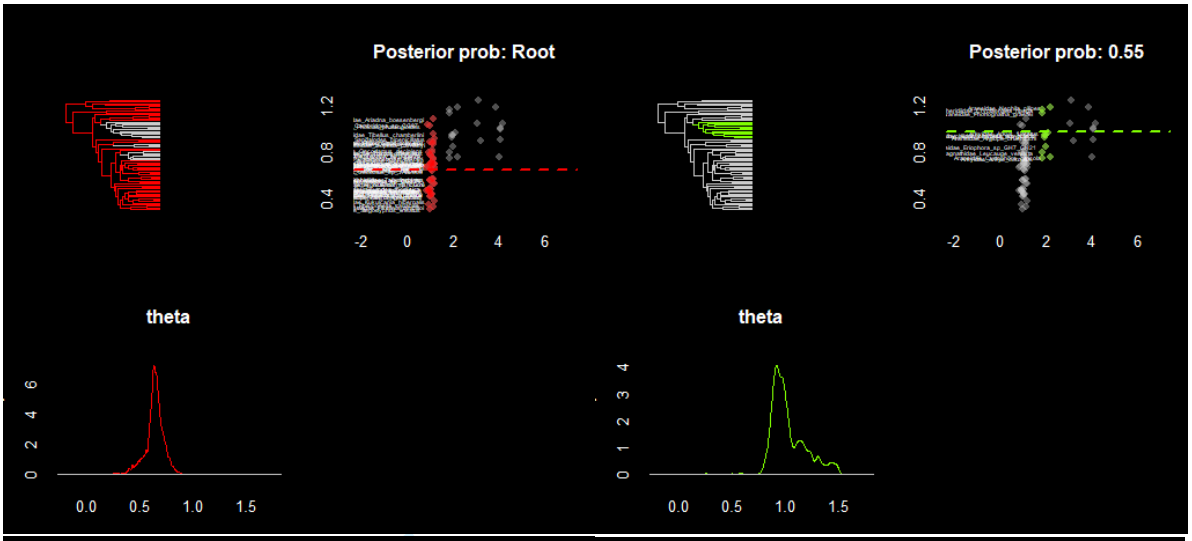

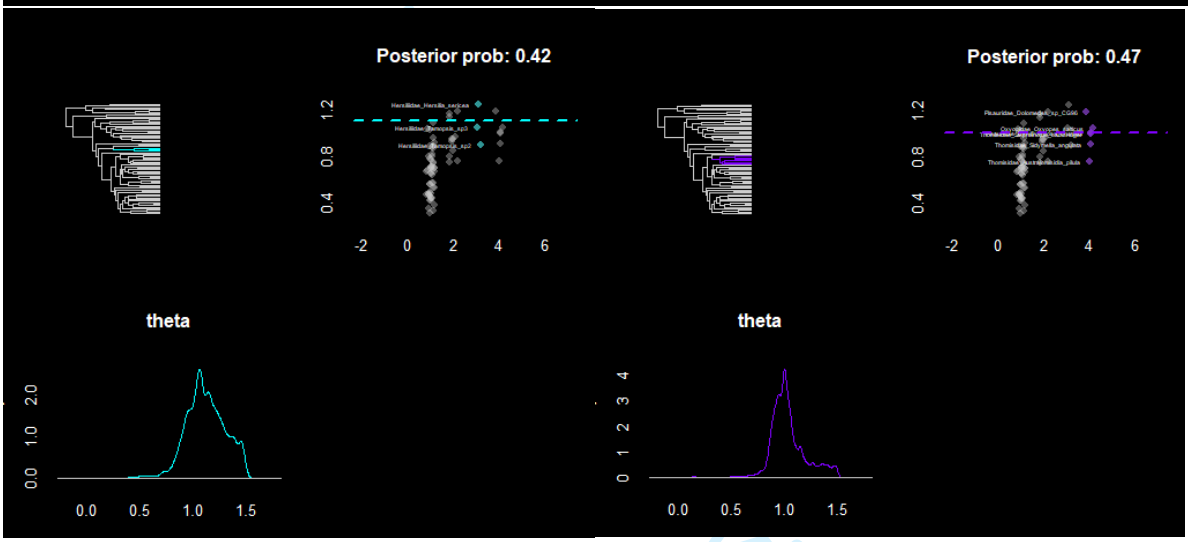

2nd run

```
bayou MCMC chain: 5e+05 generations
50001 samples, first 15000 samples discarded as burnin


Summary statistics for parameters:
                     Mean          SD     Naive SE Time-series SE Effective Size    HPD95Lower   HPD95Upper
lnL          14.698774278 5.687091980 3.039792e-02    0.381869146       221.7948  6.305569e+00  27.28139191
prior       -33.378533156 9.081412033 4.854080e-02    0.409498957       491.8143 -5.225351e+01 -17.38799317
alpha         0.045737151 0.108059932 5.775881e-04    0.009159913       139.1703  1.043710e-06   0.24794374
sig2          0.002629133 0.005739366 3.067733e-05    0.000482247       141.6409  1.336972e-04   0.01362111
k             9.479401177 3.111058477 1.662883e-02    0.143416694       470.5621  3.000000e+00  15.00000000
ntheta       10.479401177 3.111058477 1.662883e-02    0.143416694       470.5621  4.000000e+00  16.00000000
root.theta    0.650315421 0.089714798 4.795321e-04    0.003330487       725.6256  4.776579e-01   0.83827510
all theta     0.790432329 0.379337346           NA             NA             NA            NA           NA


Branches with posterior probabilities higher than 0.1:
           pp magnitude.of.theta2 naive.SE.of.theta2 rel.location
41  0.4594309           1.0415541        0.001394564    0.4011567
51  0.3481801           1.1240615        0.002057146    0.3929486
63  0.3390949           1.0465629        0.001745553    0.4078270
110 0.2236729           1.0924944        0.003470282    0.3302937
3   0.1933318           1.0479631        0.003216379    0.3234796
40  0.1358208           0.9958672        0.005354402    0.3980805
12  0.1342495           0.3601418        0.002827135    0.2849830
44  0.1229930           0.3435547        0.004125672    0.3479225
49  0.1226787           1.1048981        0.004965567    0.3439703
134 0.1127364           0.4244799        0.004843818    0.3631194
39  0.1080510           1.0226561        0.004054350    0.3471310
72  0.1023370           0.9580933        0.005776195    0.3622634
43  0.1015085           0.9536951        0.004810113    0.3009776
```

1st run

2nd run

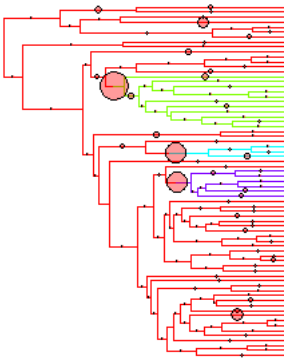

dk=15

1st run

```
bayou MCMC chain: 5e+05 generations
50001 samples, first 15000 samples discarded as burnin


Summary statistics for parameters:
                    Mean          SD     Naive SE Time-series SE Effective Size    HPD95Lower   HPD95Upper
lnL          20.255655777 7.576097479 4.049479e-02   0.7155134816       112.1129  7.225489e+00  35.13446333
prior       -43.285420771 9.627044660 5.145725e-02   0.4834496722       396.5367 -6.077064e+01 -25.12733226
alpha         0.079589449 0.170737955 9.126067e-04   0.0122834950       193.2041  1.156697e-05   0.32722933
sig2          0.003743783 0.007564302 4.043174e-05   0.0005950132       161.6161  1.273295e-04   0.01553405
k            12.804382607 3.908599788 2.089175e-02   0.2033033910       369.6180  6.000000e+00  20.00000000
ntheta       13.804382607 3.908599788 2.089175e-02   0.2033033910       369.6180  7.000000e+00  21.00000000
root.theta    0.622352747 0.087446318 4.674069e-04   0.0056002190       243.8221  4.035289e-01   0.76621962
all theta     0.792936825 0.355189121           NA             NA             NA            NA           NA


Branches with posterior probabilities higher than 0.1:
           pp magnitude.of.theta2 naive.SE.of.theta2 rel.location
41  0.5886806           0.9971223        0.001044284    0.4202270
63  0.5584538           1.0222383        0.001051700    0.4519040
51  0.5031998           1.1149188        0.001296206    0.4073298
110 0.4055483           1.0879452        0.002156508    0.3256313
3   0.3801783           1.0765080        0.001866051    0.3454226
134 0.1964459           0.3868898        0.002931403    0.3604780
44  0.1954174           0.3466767        0.002877214    0.3571495
12  0.1946746           0.3571313        0.002224896    0.2725981
72  0.1879607           0.9360756        0.003525786    0.3489090
9   0.1757328           0.8728126        0.002854000    0.4324756
49  0.1753900           1.1869823        0.003065595    0.3159247
43  0.1559625           0.9364711        0.002422014    0.4100932
19  0.1554197           0.4240041        0.003318687    0.3239184
74  0.1431918           0.9534157        0.003146058    0.3107047
94  0.1329353           0.9816680        0.003229827    0.2578055
40  0.1293355           1.0873242        0.004576470    0.3598164
2   0.1275356           0.4079306        0.004055380    0.3817936
7   0.1237644           0.9386245        0.005763951    0.3402069
126 0.1236501           0.8524262        0.005298251    0.3885757
66  0.1205360           0.9454446        0.004416382    0.3284540
132 0.1187646           0.9615592        0.003991921    0.3100871
83  0.1177076           0.9467981        0.005401136    0.2788282
57  0.1173933           0.7259482        0.005144585    0.3468255
113 0.1140506           0.4806350        0.004624144    0.3884664
28  0.1131935           0.6512505        0.005327441    0.2915586
32  0.1100794           1.1087588        0.004844296    0.3701471
39  0.1098794           1.0170359        0.003281804    0.3676239
65  0.1090795           0.8677072        0.005833216    0.3454261
1   0.1087081           0.4035368        0.004167809    0.3512137
59  0.1081652           0.9786345        0.005077155    0.4090986
34  0.1069367           1.0383221        0.005490101    0.3778471
36  0.1066796           0.9370553        0.005371359    0.3773861
64  0.1039369           0.6744857        0.005125071    0.3962822
62  0.1001943           1.0727247        0.004339842    0.3590331
```

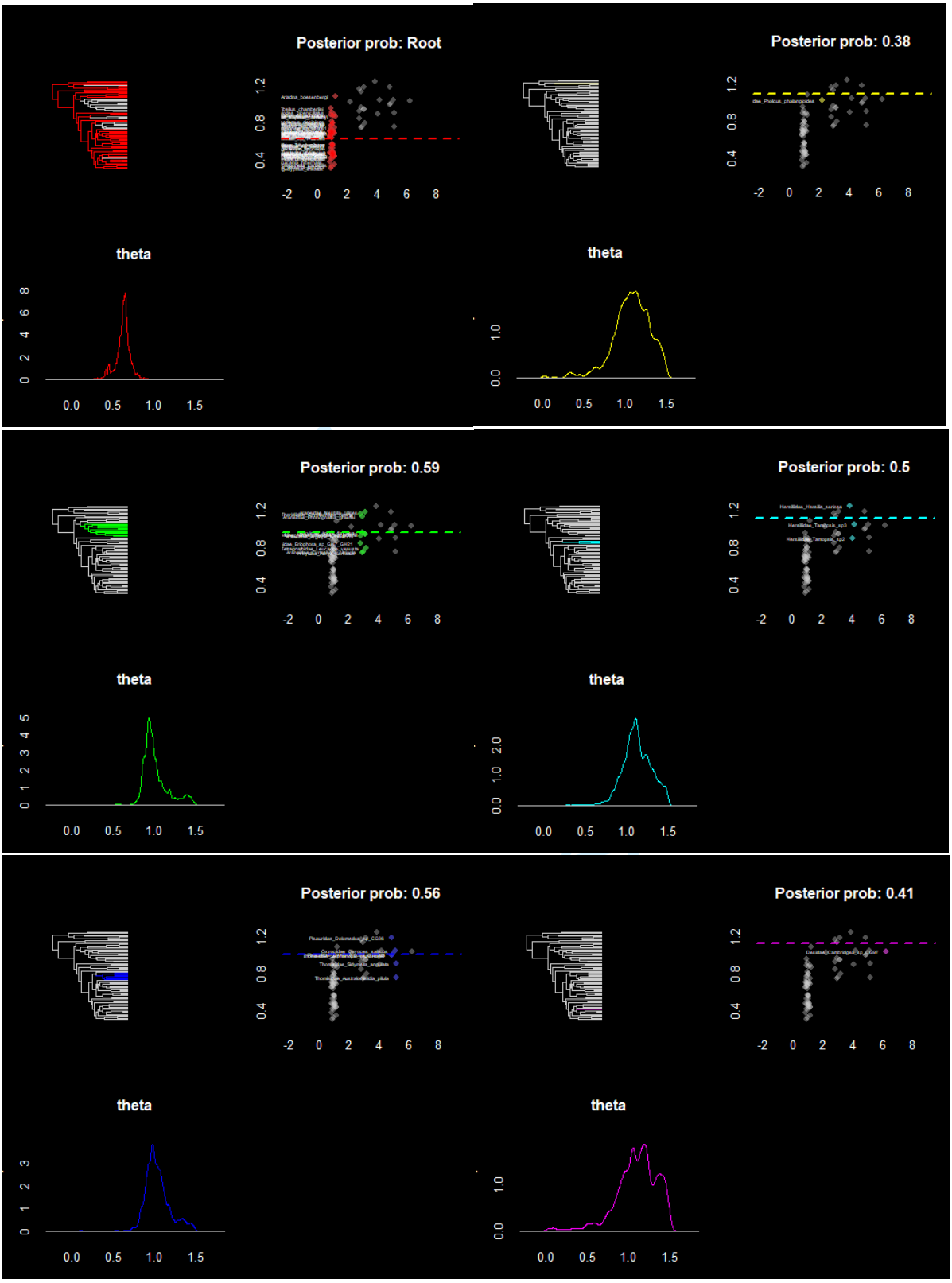

2nd run

```
bayou MCMC chain: 5e+05 generations
50001 samples, first 15000 samples discarded as burnin


Summary statistics for parameters:
                    Mean          SD     Naive SE Time-series SE Effective Size    HPD95Lower   HPD95Upper
lnL          19.772231608 7.175051683 0.0383511687   0.5934161722       146.1946  7.455764e+00  33.48931003
prior       -43.172493144 9.409622273 0.0502951097   0.4554680086       426.8041 -6.080857e+01 -25.58433051
alpha         0.077611415 0.158419496 0.0008467636   0.0113465342       194.9354  2.596583e-05   0.33191152
sig2          0.003757215 0.007922586 0.0000423468   0.0005305335       223.0018  1.394867e-04   0.01464511
k            12.758870922 3.828905886 0.0204657781   0.1926357538       395.0714  6.000000e+00  20.00000000
ntheta       13.758870922 3.828905886 0.0204657781   0.1926357538       395.0714  7.000000e+00  21.00000000
```

```
root.theta   0.633753545 0.087696847 0.0004687460   0.0045145904       377.3386  4.554713e-01   0.81377519
all theta    0.789481976 0.360133261           NA             NA              NA            NA           NA


Branches with posterior probabilities higher than 0.1:
           pp magnitude.of.theta2 naive.SE.of.theta2 rel.location
41  0.5956517           0.9958904        0.001061164    0.4403410
63  0.5618250           1.0385576        0.001131009    0.3948063
51  0.5535684           1.1218228        0.001196671    0.3817303
110 0.4110051           1.0957930        0.002089388    0.3382450
3   0.3479515           1.0956487        0.002070425    0.3615407
134 0.2137021           0.3851953        0.002246171    0.3349299
44  0.2115308           0.3574978        0.002654434    0.3338210
12  0.2009314           0.3402019        0.001972542    0.3269733
49  0.1653334           1.1174518        0.004078118    0.3122992
19  0.1570196           0.4896617        0.003999369    0.3645752
43  0.1550197           0.9067334        0.002709349    0.3424464
72  0.1429633           0.9517843        0.004057225    0.3457380
9   0.1411919           0.8470595        0.003772625    0.3910225
66  0.1323353           0.9639623        0.004337092    0.3289439
74  0.1281641           0.9692939        0.003994440    0.3137050
40  0.1274784           1.1145788        0.003992362    0.3468670
83  0.1255643           0.9579362        0.005409913    0.2198379
2   0.1237358           0.3905095        0.004221943    0.3404363
107 0.1222502           0.4855960        0.004631842    0.3202966
62  0.1194503           1.0812441        0.004411797    0.3417225
126 0.1177361           0.8045765        0.005689631    0.3661818
113 0.1158505           0.5243556        0.005505217    0.3803106
132 0.1132221           0.9646885        0.004056956    0.3612333
98  0.1127936           0.4975761        0.005254734    0.3757164
124 0.1124221           0.4332693        0.003948222    0.3941055
1   0.1091652           0.4874581        0.005530417    0.3462338
69  0.1082510           0.5393984        0.005097745    0.3528629
34  0.1081938           1.1133653        0.004445500    0.4022393
7   0.1073082           0.9210447        0.005799781    0.2493566
39  0.1058511           1.0223865        0.003404385    0.3956717
28  0.1047940           0.6721789        0.005747642    0.3106713
97  0.1026227           0.8825749        0.005894299    0.3753341
94  0.1022513           0.9661145        0.003182192    0.2633653
4   0.1013371           0.4714718        0.004841163    0.3949465
57  0.1009657           0.7037050        0.005245261    0.3408707
```

1st run

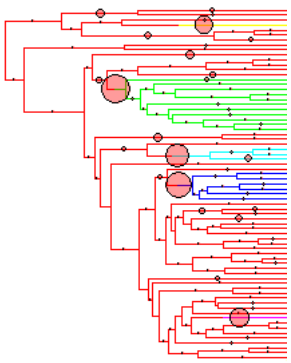

2nd run

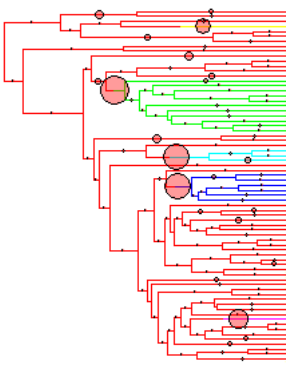

dk=20

1st run

```
bayou MCMC chain: 5e+05 generations
50001 samples, first 15000 samples discarded as burnin


Summary statistics for parameters:
                     Mean          SD     Naive SE Time-series SE Effective Size    HPD95Lower  HPD95Upper
lnL          26.957593235 8.39122459 0.0448517007    0.757505950      122.70961  1.064374e+01  44.0657668
prior       -49.540129245 8.34464277 0.0446027175    0.407740028      418.84063 -6.669935e+01 -34.6338282
alpha         0.279076954 1.05244037 0.0056253697    0.108922413       93.35992  6.083675e-05   0.8130411
sig2          0.009858556 0.03072429 0.0001642235    0.002869677      114.62980  1.362489e-04   0.0295632
k            14.534683732 3.77448633 0.0201749017    0.189682439      395.96925  8.000000e+00  22.0000000
```

```
ntheta      15.534683732 3.77448633 0.0201749017    0.189682439      395.96925  9.000000e+00  23.0000000
root.theta   0.576335987 0.10418704 0.0005568873    0.010418457      100.00474  3.653701e-01   0.7246926
all theta    0.795506805 0.30951907           NA             NA             NA            NA          NA


Branches with posterior probabilities higher than 0.1:
           pp magnitude.of.theta2 naive.SE.of.theta2 rel.location
63  0.7488144           0.9909847       0.0006563528    0.4652187
51  0.7152734           1.0986312       0.0009486732    0.4598527
41  0.6144792           0.9539915       0.0007832727    0.4681117
3   0.6054797           1.0527847       0.0010849604    0.4345480
110 0.5887664           1.0614312       0.0012346697    0.3911497
9   0.2830695           0.8312668       0.0016794758    0.4272712
43  0.2802697           0.8816038       0.0013737031    0.4231132
19  0.2281298           0.4267251       0.0021231754    0.3823937
44  0.2268442           0.3126079       0.0017876175    0.3933866
134 0.2227873           0.3772025       0.0015868514    0.3862618
72  0.2212445           0.9571558       0.0023864627    0.3363543
49  0.2017313           1.1763092       0.0024316725    0.3497429
12  0.1992172           0.3660376       0.0020875905    0.3135564
74  0.1971316           0.9444076       0.0021649227    0.3005935
40  0.1559625           1.1755367       0.0026802716    0.3661535
32  0.1544769           1.1228561       0.0031818628    0.3827089
34  0.1543626           1.1289100       0.0025072048    0.3574528
66  0.1519913           0.9888665       0.0029889019    0.3500921
20  0.1467345           0.7734519       0.0020435506    0.4195830
57  0.1463345           0.7448846       0.0037593623    0.3371173
83  0.1415348           0.9601932       0.0042054720    0.2679541
2   0.1396206           0.3304970       0.0025223868    0.2936509
126 0.1384492           0.8800932       0.0034697751    0.3190261
4   0.1346494           0.4730120       0.0025990846    0.3563608
129 0.1275927           0.6937397       0.0013816058    0.3958146
7   0.1268213           0.9894102       0.0049258626    0.2886246
94  0.1266499           0.9184966       0.0025792877    0.3220062
133 0.1210502           0.6525401       0.0009346781    0.4171101
28  0.1202217           0.7116712       0.0043737576    0.3410562
50  0.1177076           0.9687375       0.0032823348    0.3768626
11  0.1145363           0.7981780       0.0026089401    0.2346989
62  0.1142792           1.0961657       0.0032981065    0.3322574
132 0.1139363           0.9409728       0.0037995803    0.2658711
54  0.1135649           1.1564768       0.0036374838    0.3258694
130 0.1090509           0.4405846       0.0036681941    0.3145309
113 0.1065653           0.4773092       0.0035112671    0.3327002
46  0.1037655           0.3804813       0.0035497002    0.2178653
115 0.1032798           0.7681859       0.0051039181    0.2875690
```

2nd run

```
bayou MCMC chain: 5e+05 generations
50001 samples, first 15000 samples discarded as burnin


Summary statistics for parameters:
                     Mean           SD     Naive SE Time-series SE Effective Size    HPD95Lower   HPD95Upper
lnL          22.780884308  8.929739245 4.773010e-02   0.8450213073       111.6715  7.656321e+00  39.38643146
prior       -54.434665982 10.000195105 5.345176e-02   0.5071027020       388.8885 -7.522545e+01 -37.58610317
alpha         0.072128043  0.176226339 9.419425e-04   0.0135286498       169.6808  5.852822e-06   0.36029753
sig2          0.002968855  0.007371046 3.939877e-05   0.0005605417       172.9189  7.058359e-05   0.01430239
k            17.250214273  4.667543978 2.494836e-02   0.2457465694       360.7463  8.000000e+00  26.00000000
ntheta       18.250214273  4.667543978 2.494836e-02   0.2457465694       360.7463  9.000000e+00  27.00000000
root.theta    0.609123737  0.099845120 5.336794e-04   0.0060510296       272.2671  3.794539e-01   0.80069739
all theta     0.790710409  0.365996757            NA             NA             NA            NA          NA


Branches with posterior probabilities higher than 0.1:
           pp magnitude.of.theta2 naive.SE.of.theta2 rel.location
51  0.5744529           1.1532516        0.001349387    0.4030849
110 0.5468545           1.1526842        0.001659571    0.3135882
41  0.5409119           1.0134430        0.001057634    0.4050465
63  0.5236272           1.0433278        0.001324539    0.4049555
3   0.4740586           1.1012901        0.001762025    0.3455047
72  0.2331010           0.9654896        0.003055691    0.3104587
9   0.2300154           0.8653376        0.002737653    0.4144565
44  0.2276727           0.3423093        0.002708162    0.3170111
43  0.2227301           0.9170377        0.002227455    0.3685989
134 0.2211302           0.3757431        0.002233798    0.3459541
12  0.1915033           0.3298594        0.002515344    0.2745200
40  0.1904463           1.1153373        0.003406403    0.3164990
19  0.1893320           0.4428669        0.003190342    0.3354367
```

74	0.1854751	0.9861699	0.003285686	0.2743635
4	0.1755900	0.4802295	0.003180615	0.3028012
49	0.1744472	1.1445242	0.003625183	0.3399754
66	0.1729901	0.9653293	0.004254147	0.3256616
132	0.1717330	0.9765451	0.003403517	0.3221104
11	0.1704188	0.8896821	0.002853938	0.2823252
59	0.1651049	1.0406874	0.004014371	0.3298253
2	0.1585052	0.3870671	0.004162771	0.3179738
97	0.1582195	0.8408836	0.004667746	0.3183055
57	0.1575624	0.6745561	0.004529710	0.3352519
62	0.1545912	1.0743827	0.003660781	0.2936640
126	0.1536484	0.9461534	0.004205412	0.3072418
83	0.1520770	0.9621872	0.005056823	0.1762011
7	0.1492200	0.9112078	0.005204460	0.2385554
94	0.1476487	0.9790392	0.003176155	0.3038358
113	0.1461345	0.4338545	0.004049911	0.3117988
67	0.1456774	0.8075670	0.004887932	0.3629097
84	0.1432490	0.4418748	0.004623906	0.2147486
129	0.1413919	0.7106219	0.002375321	0.4715078
32	0.1403634	1.0634785	0.004205004	0.3500584
5	0.1395349	0.9029870	0.005028365	0.2527838
20	0.1392778	0.8070035	0.003728049	0.3595709
68	0.1379350	0.4904419	0.004773954	0.2913318
28	0.1361636	0.6170452	0.005158611	0.2497333
34	0.1356494	1.1169811	0.003635953	0.2765136
65	0.1355923	0.8541353	0.005386562	0.2958571
98	0.1345352	0.4720290	0.004483504	0.3369289
39	0.1337066	0.9870407	0.002858649	0.3480691
128	0.1329067	0.8120434	0.002689865	0.3221460
52	0.1326210	0.6605847	0.004423742	0.3507842
64	0.1310782	0.6641664	0.004979936	0.3059681
21	0.1298212	0.6259043	0.005479324	0.1592698
17	0.1289926	0.8389313	0.005001676	0.2980263
88	0.1281070	0.7375323	0.005462603	0.2973677
50	0.1272499	0.9428767	0.004757814	0.2963063
105	0.1263071	0.7888992	0.005628463	0.3417667
82	0.1230501	0.7277373	0.005131939	0.3736197
69	0.1216502	0.5841947	0.005487479	0.3344744
54	0.1207074	1.0399121	0.005008767	0.3088188
116	0.1202217	0.7741119	0.006172764	0.2864039
18	0.1189075	0.7368990	0.004934934	0.2970545
56	0.1174790	0.8873613	0.005552845	0.2990090
118	0.1173362	0.8396956	0.004623673	0.3146698
107	0.1170790	0.5181743	0.005491249	0.3750780
106	0.1164791	0.7304198	0.005734429	0.3758514
117	0.1143649	0.8551640	0.005668632	0.3418606
101	0.1126507	0.6569013	0.005769443	0.3906936
1	0.1118508	0.4262397	0.004423219	0.2791199
124	0.1107651	0.4642934	0.004743083	0.3150546
76	0.1087652	0.7289157	0.006133836	0.2602937
55	0.1085081	0.8250769	0.006336219	0.3126560
53	0.1083081	0.8500664	0.006208685	0.2817961
130	0.1077367	0.4877895	0.004583497	0.2778809
100	0.1070796	0.6389949	0.005849882	0.3523520
8	0.1064225	0.7930243	0.005472947	0.3641544
6	0.1054225	0.6590967	0.006107212	0.1916006
95	0.1053083	0.7814183	0.006435376	0.2681420
48	0.1051940	0.9549858	0.006002344	0.2994112
77	0.1048512	0.5850658	0.006167252	0.2650239
30	0.1047083	0.7921238	0.005880447	0.3448318
24	0.1044512	0.7604119	0.005416313	0.3214297
140	0.1043940	0.5806450	0.004285017	0.3487910
45	0.1033084	0.4874438	0.005156262	0.2292081
23	0.1012228	0.8035930	0.005775422	0.3750312
85	0.1003086	0.6612622	0.006531082	0.3052343

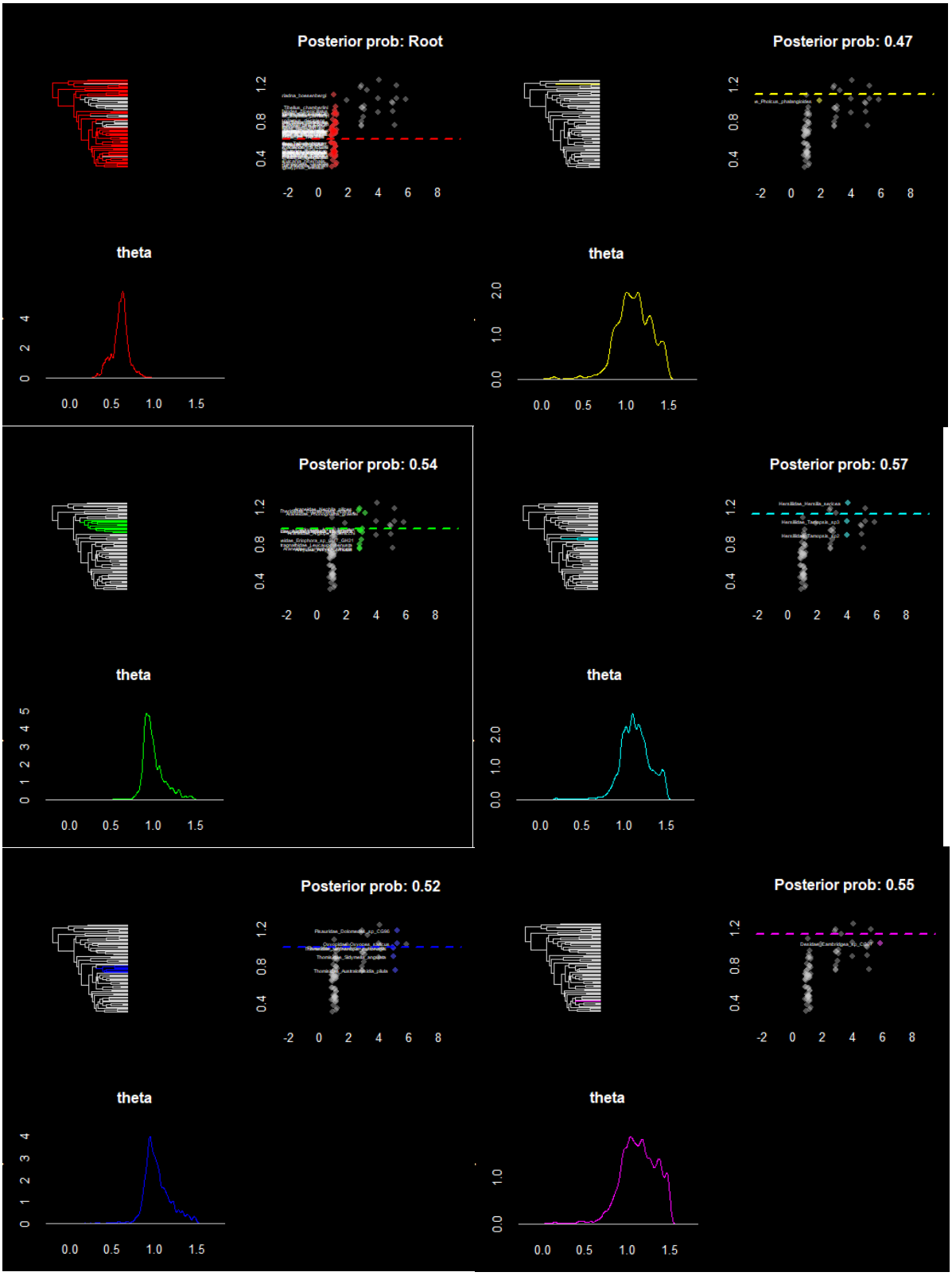

1st run 2nd run

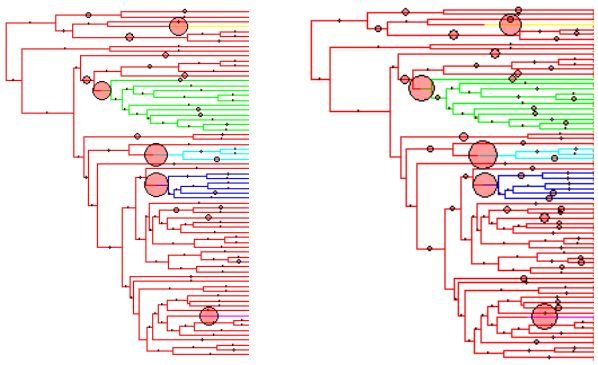

dk=25

1st run

```
bayou MCMC chain: 5e+05 generations
50001 samples, first 15000 samples discarded as burnin


Summary statistics for parameters:
                     Mean           SD     Naive SE Time-series SE Effective Size    HPD95Lower   HPD95Upper
lnL          28.239218567 9.783089703 0.0522913201   0.9801144494       99.63192  9.806589e+00  46.65144383
prior       -60.493554651 9.304996033 0.0497358749   0.5023686082      343.07368 -7.804273e+01 -42.75716874
alpha         0.099425350 0.194635206 0.0010403392   0.0144211751      182.15517  2.767301e-05   0.41865613
sig2          0.003483747 0.006167719 0.0000329669   0.0005064919      148.28736  9.966576e-05   0.01425765
k            19.608365236 4.924623898 0.0263224699   0.3173742476      240.77022  1.100000e+01  29.00000000
ntheta       20.608365236 4.924623898 0.0263224699   0.3173742476      240.77022  1.200000e+01  30.00000000
root.theta    0.573170165 0.102568265 0.0005482348   0.0087200089      138.35414  3.490522e-01   0.74616409
all theta     0.797243076 0.343977522            NA              NA             NA            NA           NA


Branches with posterior probabilities higher than 0.1:
            pp magnitude.of.theta2 naive.SE.of.theta2 rel.location
110 0.6922462           1.1354755       0.0013112650    0.3272785
51  0.6674190           1.1358909       0.0011858983    0.3749562
63  0.6411348           1.0313195       0.0010019363    0.4520868
3   0.6188218           1.0892701       0.0013128394    0.3368557
41  0.5711102           0.9999914       0.0009512704    0.4587492
72  0.3238672           0.9928569       0.0022176434    0.3172103
9   0.3223816           0.8781380       0.0020496453    0.4290945
19  0.2789841           0.4327917       0.0022647851    0.3397455
43  0.2628993           0.8881511       0.0016650055    0.3637087
44  0.2612136           0.3075226       0.0019046786    0.3068275
74  0.2461574           0.9986344       0.0023222096    0.2769526
134 0.2461002           0.3802536       0.0018654209    0.3632603
40  0.2228444           1.1345745       0.0028276341    0.3449532
66  0.2158734           0.9758605       0.0029331234    0.3064689
49  0.2143020           1.1727529       0.0031317162    0.2724195
20  0.2142163           0.7885130       0.0019782636    0.3711688
57  0.2093309           0.7302362       0.0030974387    0.3083957
12  0.2078738           0.3574824       0.0021560524    0.3209389
83  0.2062739           0.9864635       0.0036495313    0.1961427
4   0.2012456           0.4875371       0.0024505564    0.2726282
34  0.1921890           1.1344332       0.0028756148    0.3047169
32  0.1910748           1.1377110       0.0030573938    0.3355554
126 0.1869893           0.9415806       0.0031823914    0.2739931
132 0.1781898           0.9221515       0.0033835319    0.3511706
2   0.1760185           0.3532469       0.0029688757    0.2727519
129 0.1731615           0.6816823       0.0014176328    0.4375743
7   0.1652477           1.0161808       0.0041575367    0.2331426
21  0.1604480           0.6706439       0.0047843991    0.1947835
59  0.1598766           1.0945721       0.0035568695    0.3345347
84  0.1587624           0.4269376       0.0044080327    0.1795563
28  0.1571339           0.6772479       0.0044588493    0.2804082
97  0.1570196           0.8724681       0.0042394895    0.3052102
98  0.1561911           0.4657563       0.0036213619    0.3224094
116 0.1556768           0.8418586       0.0046959577    0.2286812
107 0.1547054           0.4777477       0.0033750819    0.2843145
54  0.1515628           1.0759945       0.0039653288    0.2503094
65  0.1482772           0.9085513       0.0041697201    0.2997742
11  0.1473059           0.8457654       0.0033091085    0.2195648
52  0.1471630           0.6399303       0.0035809639    0.3747103
16  0.1451346           0.8324107       0.0050344169    0.2231471
50  0.1441632           0.9494327       0.0039131073    0.3319825
5   0.1429633           0.8739284       0.0051518796    0.2243006
62  0.1422204           1.1076351       0.0034394249    0.3290266
94  0.1420776           0.9297863       0.0030960242    0.2721789
```

39	0.1418776	0.9692762	0.0023245213	0.3824043
8	0.1408491	0.7955375	0.0044791759	0.2613668
118	0.1401634	0.8841132	0.0041798165	0.3225309
113	0.1383921	0.4396925	0.0036346029	0.2763762
1	0.1355923	0.4018847	0.0031104160	0.2781093
47	0.1351066	0.7608190	0.0054710702	0.2285766
133	0.1341352	0.6744650	0.0021092101	0.3527202
53	0.1334495	0.9139682	0.0050987645	0.2833130
67	0.1326781	0.7861372	0.0048122571	0.3451885
48	0.1307354	0.9591599	0.0050208843	0.2784762
6	0.1288212	0.6501783	0.0050266653	0.2125457
124	0.1285641	0.4788944	0.0035929789	0.2790427
115	0.1282212	0.8420611	0.0051397559	0.2869962
128	0.1279641	0.8214020	0.0034219189	0.2952285
68	0.1271070	0.4799097	0.0041957731	0.2516544
76	0.1246500	0.7151858	0.0054796456	0.2115092
117	0.1241358	0.7604407	0.0043637482	0.3235640
82	0.1240215	0.8015647	0.0044427501	0.4073867
69	0.1237358	0.5263500	0.0043150400	0.3297356
130	0.1230501	0.4614638	0.0032835930	0.3299366
105	0.1207931	0.6835806	0.0046061110	0.3267574
140	0.1204503	0.6077233	0.0035711297	0.2922312
106	0.1191360	0.7274355	0.0048684455	0.3161684
56	0.1174504	0.9342250	0.0052214938	0.3510651
30	0.1155934	0.8271046	0.0050200996	0.2870492
96	0.1150791	0.4633365	0.0050016461	0.2828169
17	0.1150220	0.8707254	0.0045539213	0.2353843
23	0.1145935	0.7836549	0.0044991515	0.3985640
15	0.1141649	0.7418010	0.0059001339	0.2222750
88	0.1129364	0.7978463	0.0051499118	0.2848228
26	0.1109079	0.9486884	0.0042595786	0.3338021
24	0.1107651	0.7925087	0.0043370423	0.3428841
18	0.1103651	0.7805744	0.0050598174	0.2992731
104	0.1102223	0.6770781	0.0062538690	0.2373302
36	0.1099080	1.0005596	0.0047380689	0.3373520
86	0.1096223	0.6811590	0.0053290099	0.3016315
95	0.1085367	0.7815904	0.0055956777	0.1820287
100	0.1073939	0.6407340	0.0048031988	0.3144480
55	0.1061082	0.8704982	0.0056924487	0.2475925
101	0.1047083	0.6439893	0.0056765656	0.3785500
103	0.1041369	0.7903493	0.0061731226	0.1995276
75	0.1039941	0.7305992	0.0060835654	0.2548916
14	0.1031941	0.5010191	0.0049636989	0.2723702
136	0.1031655	0.7114087	0.0052446819	0.1866803
64	0.1024227	0.6883080	0.0043643889	0.3648971
46	0.1002514	0.4694807	0.0049950185	0.2041057
85	0.1000229	0.6343282	0.0054677421	0.2496815

2nd run

```
bayou MCMC chain: 5e+05 generations
50001 samples, first 15000 samples discarded as burnin


Summary statistics for parameters:
                     Mean           SD     Naive SE Time-series SE Effective Size    HPD95Lower   HPD95Upper
lnL          19.172619676  7.396599018 3.953536e-02   0.5753844776       165.2524  7.071677e+00  33.81314863
prior       -44.257782833 10.023845192 5.357818e-02   0.5116136348       383.8703 -6.325892e+01 -26.25314402
alpha         0.055010807  0.147954145 7.908256e-04   0.0121348092       148.6580  5.267573e-06   0.25157146
sig2          0.002684074  0.006805077 3.637363e-05   0.0006238984       118.9703  1.079101e-04   0.01130531
k            13.279841152  4.052433250 2.166055e-02   0.2132432321       361.1447  5.000000e+00  20.00000000
ntheta       14.279841152  4.052433250 2.166055e-02   0.2132432321       361.1447  6.000000e+00  21.00000000
root.theta    0.627351843  0.096528021 5.159492e-04   0.0053162008       329.6887  3.784701e-01   0.79440732
all theta     0.797277074  0.373128277           NA             NA             NA            NA           NA


Branches with posterior probabilities higher than 0.1:
           pp magnitude.of.theta2 naive.SE.of.theta2 rel.location
41  0.5617965           1.0459006        0.001174444    0.4228581
63  0.5068568           1.0744641        0.001307533    0.3989462
51  0.4912291           1.1684278        0.001531174    0.3601213
110 0.3954060           1.1180455        0.002279182    0.2858580
3   0.3950346           1.1195662        0.001999134    0.3239847
12  0.1817325           0.3365725        0.002686392    0.2695209
134 0.1816468           0.4001534        0.003086782    0.3536554
44  0.1719902           0.3702340        0.003269534    0.3080018
72  0.1702474           0.9718064        0.004131067    0.3242892
9   0.1657620           0.8836744        0.003711176    0.3753858
43  0.1642763           0.9618822        0.002811196    0.3574905
57  0.1519913           0.6738214        0.004666776    0.3381812
```

40	0.1478773	1.0926337	0.004180143	0.3522941
49	0.1437918	1.0956389	0.004514393	0.3420789
74	0.1387921	0.9810007	0.004194530	0.2925560
132	0.1372779	0.9921636	0.003619990	0.3287242
19	0.1357637	0.4666282	0.004269376	0.3114188
113	0.1336781	0.4768966	0.004929626	0.3258180
59	0.1273927	0.9908135	0.005093165	0.3519610
66	0.1216502	0.8887008	0.005302200	0.3386586
62	0.1196217	1.1311541	0.004429433	0.3429080
2	0.1193360	0.4622584	0.005352005	0.3506073
28	0.1193075	0.6415916	0.005579999	0.2929973
83	0.1177933	0.9593805	0.006001183	0.2583691
97	0.1152506	0.8422999	0.005975840	0.3593261
39	0.1148220	1.0261031	0.002894846	0.3813469
69	0.1127936	0.5076815	0.005289734	0.3901888
20	0.1116222	0.8713123	0.004368238	0.3719576
54	0.1116222	0.9977495	0.006209198	0.3497977
106	0.1087366	0.7475156	0.005955479	0.3912190
65	0.1085081	0.8333138	0.005863428	0.3497176
130	0.1073939	0.4877670	0.005466364	0.3390670
68	0.1067653	0.5698094	0.005596636	0.3573892
4	0.1061368	0.5098455	0.004957704	0.3111052
84	0.1057940	0.4687646	0.006087000	0.2353628
82	0.1049083	0.7548147	0.005694539	0.4024407
21	0.1045083	0.7129973	0.006436879	0.1914542
101	0.1037941	0.5691597	0.005213802	0.3921160
126	0.1037655	0.8975999	0.005419755	0.3020558
32	0.1035369	1.0675306	0.004869544	0.3413620
64	0.1033655	0.7019593	0.005810423	0.4071812

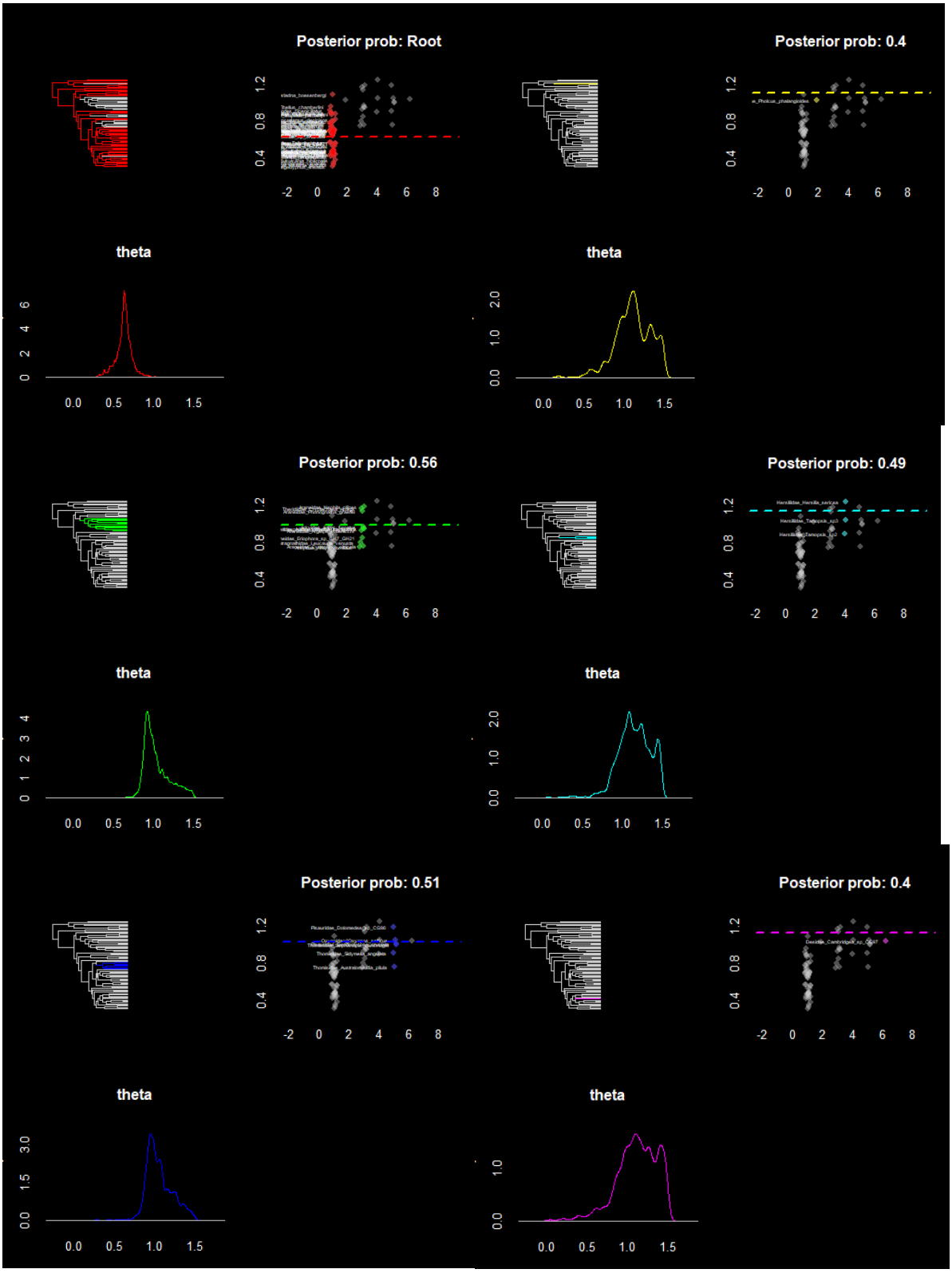
Posterior prob: Root
theta
Posterior prob: 0.4
theta
Posterior prob: 0.56
theta
Posterior prob: 0.49
theta
Posterior prob: 0.51
theta
Posterior prob: 0.4
theta

1st run

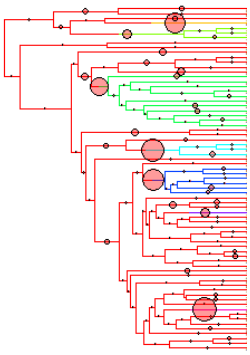

2nd run

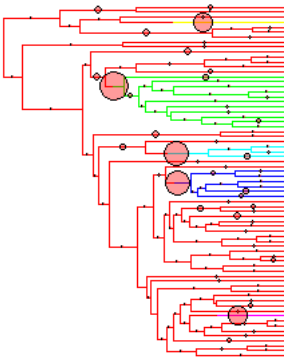

Graphical Overview

dk=10

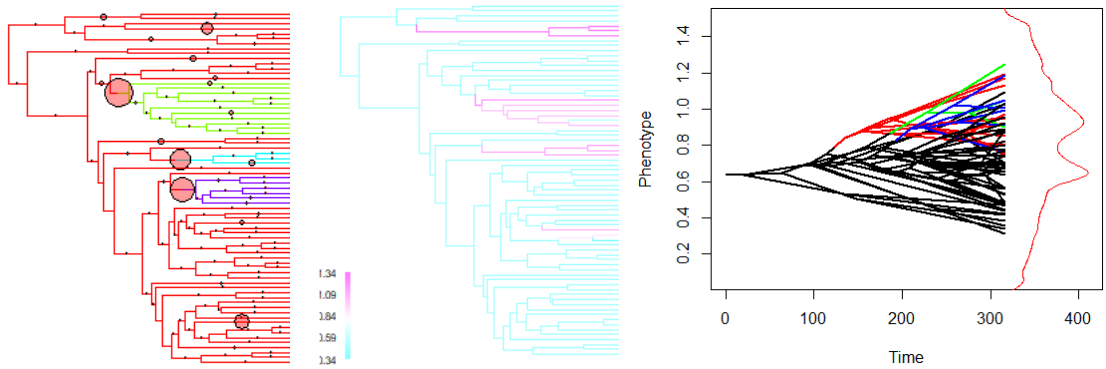

dk=15

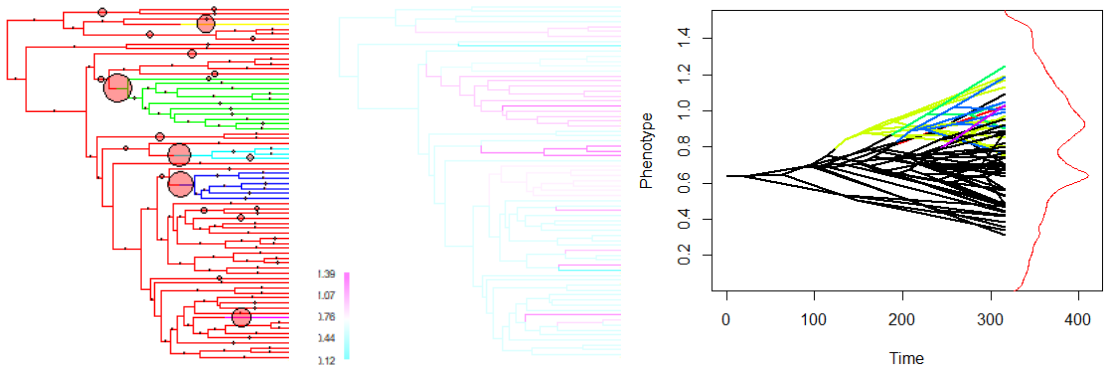

dk=20

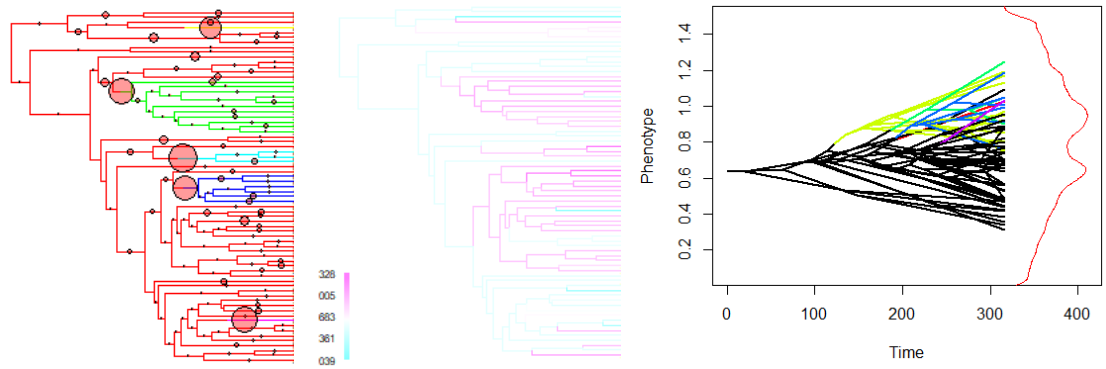

dk=25

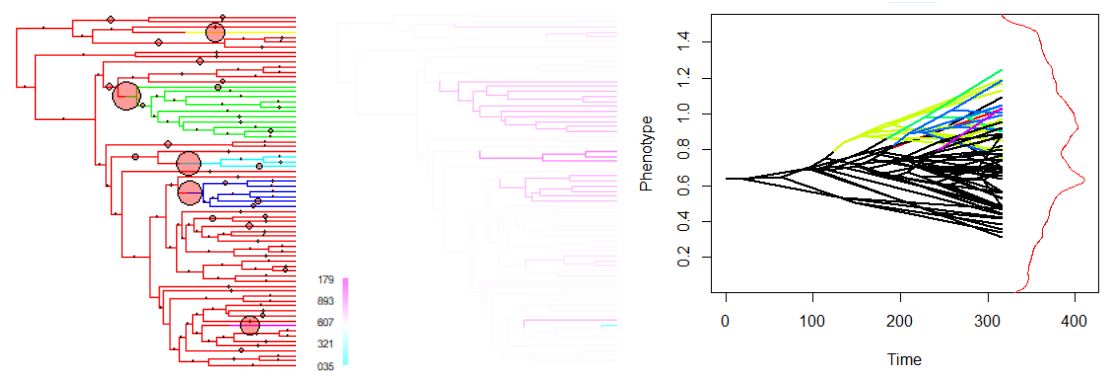

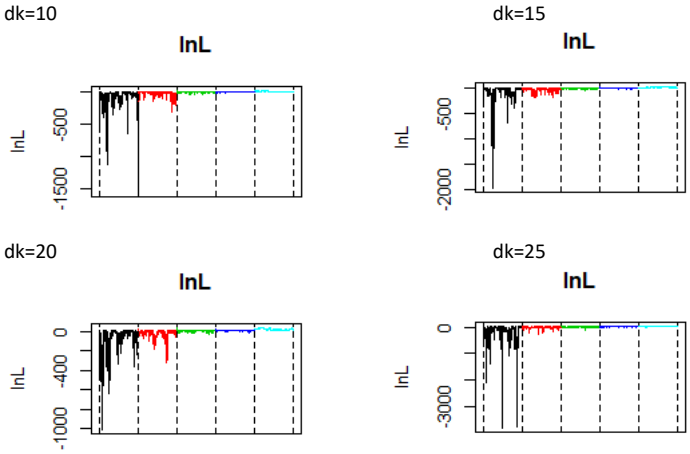

ESM.7. Phylogenetic Generalized Linear Squares analysis

Results from PGLS models demonstrate that spinning apparatus and web type correlate with silk anchor characteristics. For spinning apparatus, we found that cribellar species build anchors with lower dragline insertion location c_d (P = 0.0046) and track proportion h_r (P < 0.0001) in comparison to species without cribellum (Fig. S6.1a,d, Tab. S6.1). Results were less consistent for web type. Aerial web builders show a higher c_d than species that build substrate webs or no webs (Fig. S6.1d, Tab. S6.2). Besides the tendency of aerial web builders to show higher h_r, this effect was not statistically significant (Fig. S6.1a, Tab. S6.2). Results from phylogenetic regressions demonstrate a clear positive relationship between c_d and h_r (B = 0.113, P < 0.00001) (Fig. S6.1b, Tab. S6.3). All results from PGLS models were highly robust to phylogenetic uncertainty (see below).

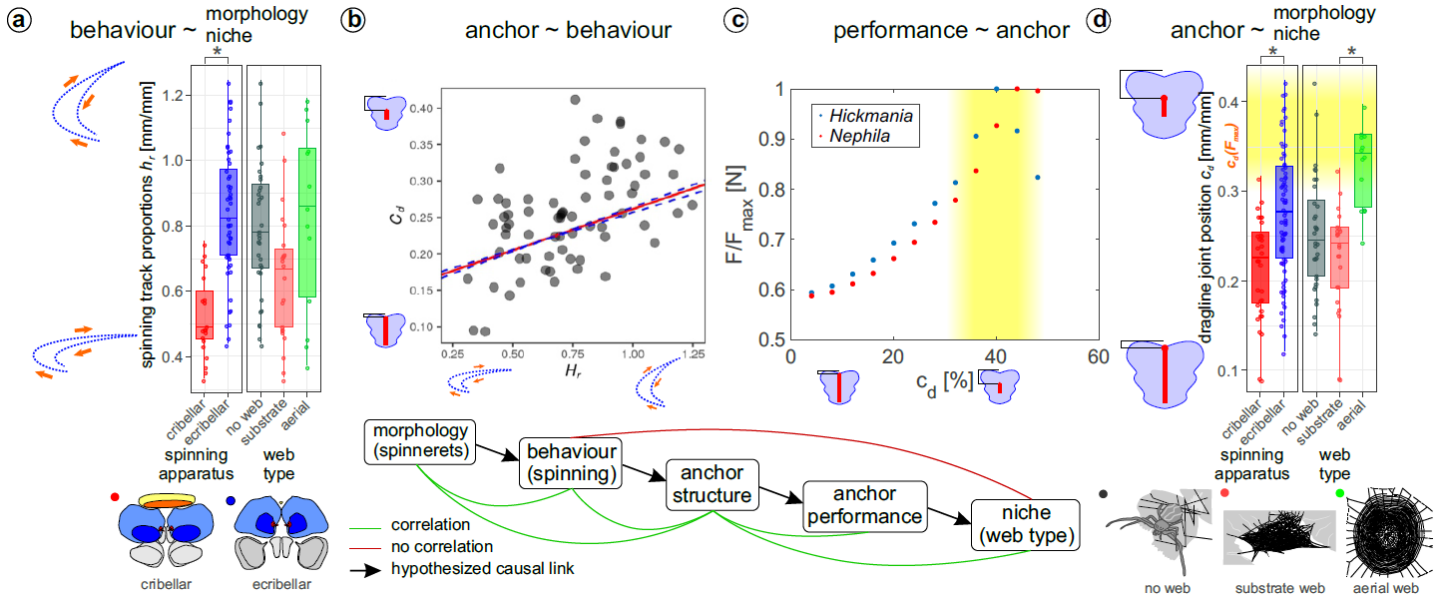

Fig. S6.1. Correlation of morphology, behaviour, biomechanics and ecology. ***(a)*** Data representation of spinning track proportions h_r. Asterisks above boxplots indicate significant difference between groups. Schematics left of the plot indicate a single movement unit of an anterior lateral spinneret during anchor production, with the arrows indicating the direction of movement (abducting to the right). Below plots a schematic illustration of the spinning apparatus in an exemplary cribellar (*Deinopis*) and ecribellar (*Argiope*) spider, with the cribellum (or the its inactive remnant, called colulus) in yellow (spinning field orange), the anterior lateral spinnerets in blue (darker hue for spinning fields) and the dragline spigot(s) in red. ***(b)*** Phylogenetic least square regression of web anchor structure (C_d) against geometric spinning trajectory proportions (H_r). The solid red line shows the average PGLS regression line (mean intercept and slope across 100 phylogenetic trees). Dashed blue lines represent phylogenetic uncertainty for the slope and intercept (minimum and maximum intercept and slope across 100 phylogenetic trees). See Tab. S6.3 for details. ***(c)*** Relationship between anchor resistance and web anchor structure, studied by numerical modeling (see main manuscript). ***(d)*** Data representation of web anchor structure c_d. Asterisks above boxplots indicate significant difference between groups. The yellow hue indicates the range of optimal c_d. Left of the plot a schematic illustration of anchor structure with the blue shape indicating the piriform silk film, the red line the fused dragline and the red pie the loading point (where the upstream dragline is inserted into the anchor). Schematic drawings under the plot illustrate exemplary silk uses in web type groups. Below plots (b) and (c) a summary of tested correlations and hypothesized causal links.

Tab. S6.1. Results from phylogenetic least square models (PGLS) for web anchor structure (c_d) and geometric spinning trajectory proportions (h_r) against spinning apparatus (cribellum). Estimates accounting for phylogenetic uncertainty are provided (average Beta, minimum, maximum and 95% confidence intervals of each parameter across 100 phylogenetic trees). Numbers in bold indicate significant effects (average $P < 0.05$).

c_d								
Variable	**Beta**	**min**	**max**	SD_{tree}	CI_{low}	CI_{high}	P	SD_P
Spinning apparatus	-0.045	-0.049	-0.041	0.002	-0.045	-0.044	**0.00461**	0.00158
h_r								
Spinning apparatus	-0.276	-0.299	-0.254	0.001	-0.278	-0.274	**0.00000**	0.00000

Tab. S6.2. Results from phylogenetic least square models (PGLS) for web anchor structure (c_d) and geometric spinning trajectory proportions (h_r) against web type (absent, substrate, aerial). Estimates accounting for phylogenetic uncertainty are provided (average Beta, minimum, maximum and 95% confidence intervals of each parameter across 100 phylogenetic trees). Numbers in bold indicate significant effects (average $P < 0.05$).

c_d								
Variable	**Beta**	**min**	**max**	SD_{tree}	CI_{low}	CI_{high}	P	SD_P
Intercept (Absent)	0.217	0.210	0.224	0.003	0.216	0.217	**0.00000**	0.00000
Substrate	-0.017	-0.021	-0.011	0.002	-0.017	-0.016	0.30053	0.05447
Aerial	0.041	0.036	0.049	0.002	0.041	0.042	**0.03553**	0.00921
h_r								
Intercept (Absent)	0.701	0.667	0.728	0.012	0.699	0.704	**0.00000**	0.00000
Substrate	-0.120	-0.144	-0.091	0.012	-0.123	-0.118	0.09858	0.03796
Aerial	0.020	-0.040	0.059	0.017	0.016	0.023	0.80425	0.11855

Tab. S6.3. Results from phylogenetic least square regressions for web anchor structure (c_d) against geometric spinning trajectory proportions (h_r). Regression estimates accounting for phylogenetic uncertainty are provided (average estimate, minimum, maximum and 95% confidence intervals for each parameter across 100 phylogenetic trees). SD_{tree} represents the standard deviation of estimates across trees. P represents the average P-value across all trees. SD_P is the standard deviation in P-values across trees. Numbers in bold indicate significant effects (average $P < 0.05$).

$c_d \sim h_r$								
Parameter	**Estimate**	**min**	**max**	SD_{tree}	CI_{low}	CI_{high}	P	SD_P
Intercept	0.148	0.142	0.155	0.003	0.148	0.149	**0.00000**	0.00000
Slope	0.113	0.102	0.122	0.004	0.112	0.114	**0.00034**	0.00017

Sensitivity Analysis

c_d ~ Spinning apparatus

Plots below illustrate variation in PGLS model estimates due to phylogenetic uncertainty (across 100 trees) for c_d against spinning apparatus (see Tab. S6.1 for details). Histograms show the distribution of estimates (left) and P values (right), the red vertical line indicates average values across models. These results demonstrate that cribellar species have a significant lower c_d in comparison with ecribellar species across all PGLS models. Therefore, results are highly robust to phylogenetic uncertainty.

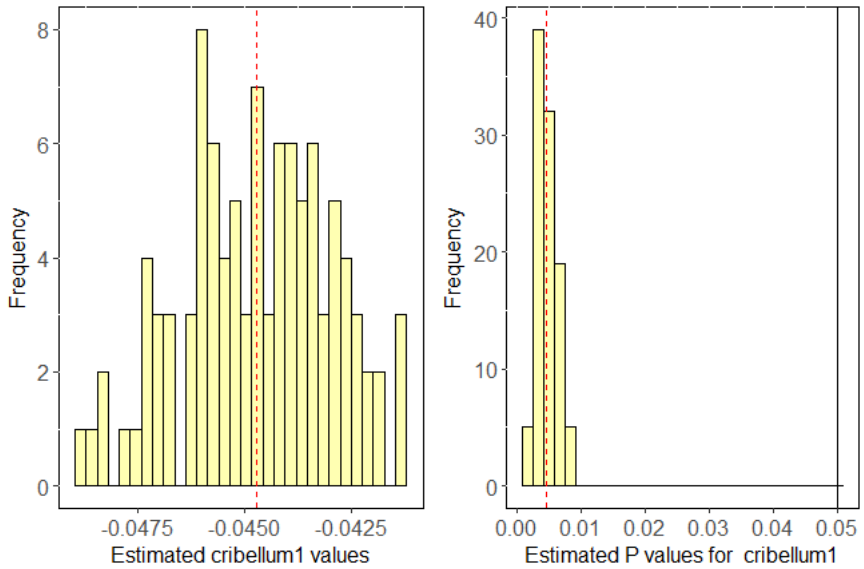

h_r ~ Spinning apparatus

Plots below illustrate variation in PGLS model estimates due to phylogenetic uncertainty (across 100 trees) for h_r against spinning apparatus (see Tab. S6.1 for details). Histograms show the distribution of estimates (left) and P values (right), the red vertical line indicates average values across models. These results demonstrate that cribellar species have a significant lower h_r in comparison with ecribellar species across all PGLS models. Therefore, results are highly robust to phylogenetic uncertainty.

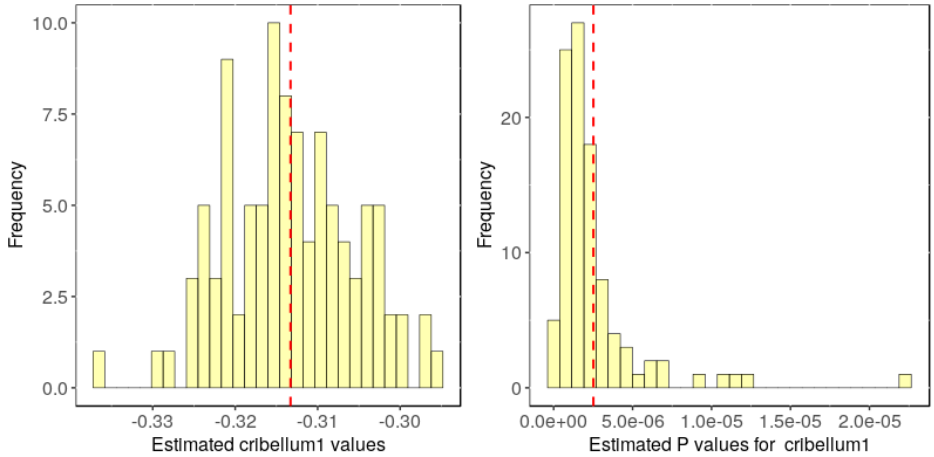

c_d ~ Web Type

Plots below illustrate variation in PGLS model estimates due to phylogenetic uncertainty (across 100 trees) for c_d against *Web Type* (see Tab. S6.2 for details). Histograms show the distribution of estimates (left) and P values (right), the red vertical line indicates average values across models. Results below demonstrate that c_d of substrate builders is not different to the intercept (= web absent) ($P > 0.05$) across all PGLS models while c_d of aerial web builders (web_type_2) is significantly different to the intercept (= web absent) for nearly all PGLS

models (across 100 trees). Therefore, results are robust to phylogenetic uncertainty, reinforcing that aerial webs show higher c_d.

Web_type_1 (substrate web)

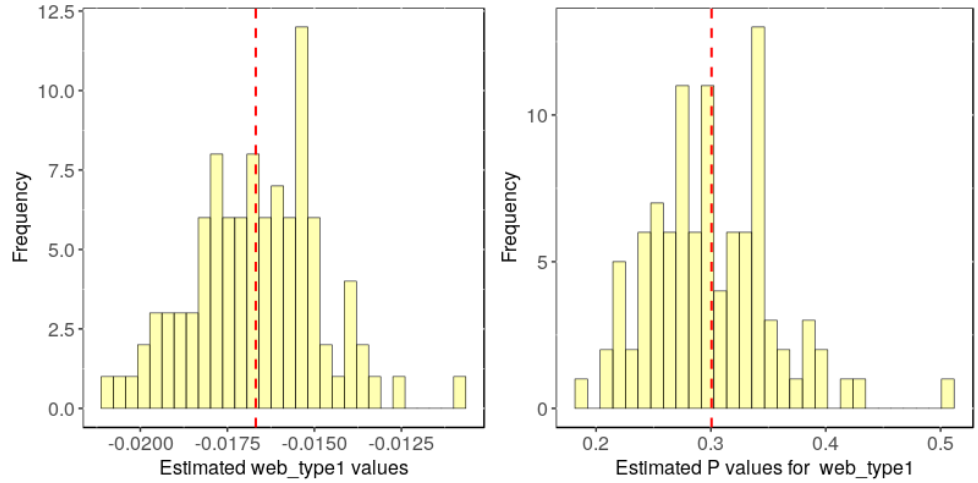

Web_type_2 (aerial web)

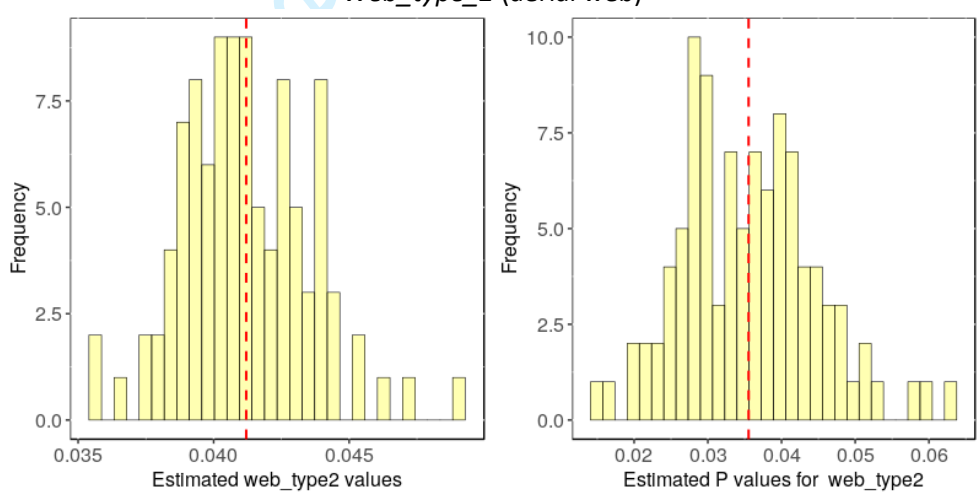

h_r ~ Web Type

Plots below illustrate variation in PGLS model estimates due to phylogenetic uncertainty (across 100 trees) for h_r against *Web Type* (see Tab. S6.2 for details). Histograms show the distribution of estimates (left) and P values (right), the red vertical line indicates average values across models. Results below demonstrate that h_r of substrate and aerial builders are not different to the intercept (= web absent) ($P > 0.05$) across all PGLS models. Therefore, results are robust to phylogenetic uncertainty, reinforcing that h_r did not correlate with web type.

Web_type_1 (substrate web)

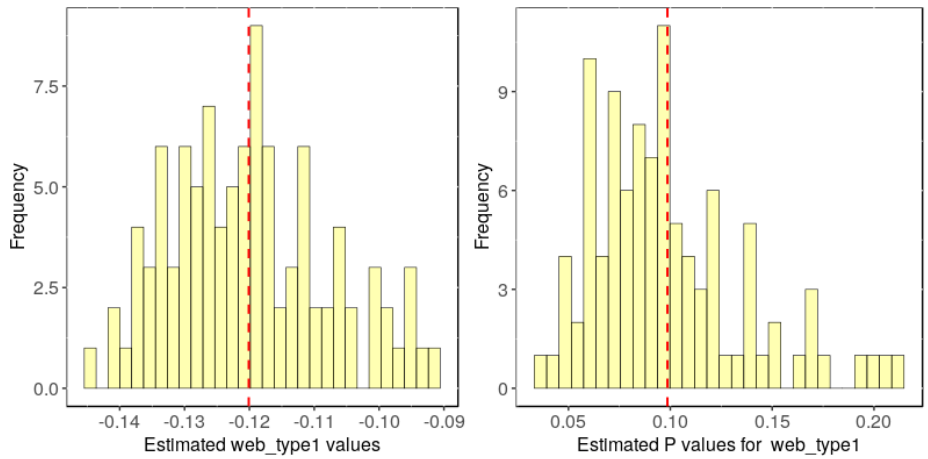

Web_type_2 (aerial web)

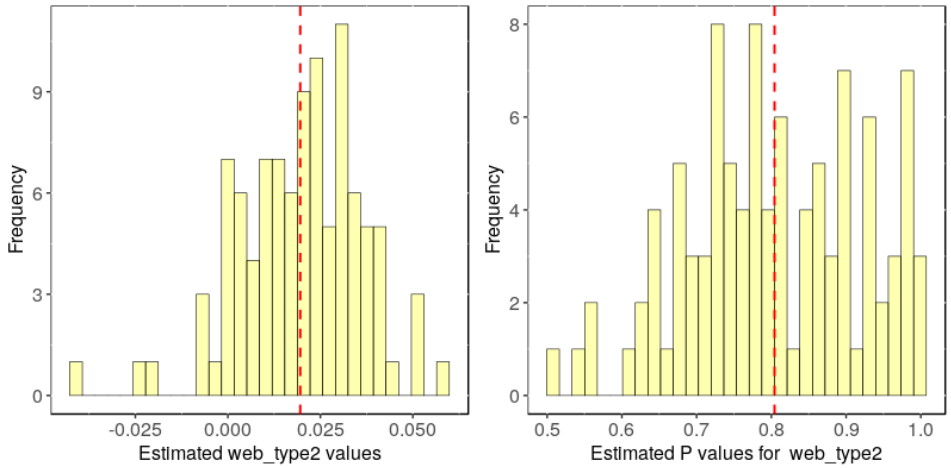

c_d ~ h_r

Plots below illustrate variation in PGLS model estimates due to phylogenetic uncertainty (across 100 trees) for c_d against h_r (see Tab. S6.3 for details). Histograms show the distribution of estimated slopes (left) and P values (right), the red vertical line indicates average across models. Results below demonstrate that the regression between c_d and h_r was significant ($P < 0.05$) for all PGLS models (across 100 trees). Therefore, results are robust to phylogenetic uncertainty, reinforcing that with c_d correlates with h_r .

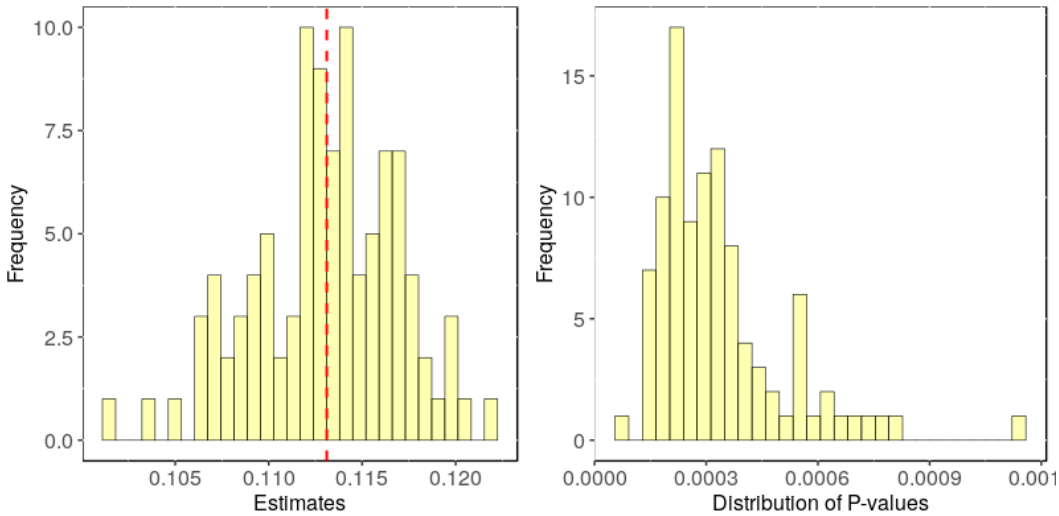

ESM.8. Geometric Morphometric PCMs on spinneret trajectory data with *geomorph*

GPA-Alignment

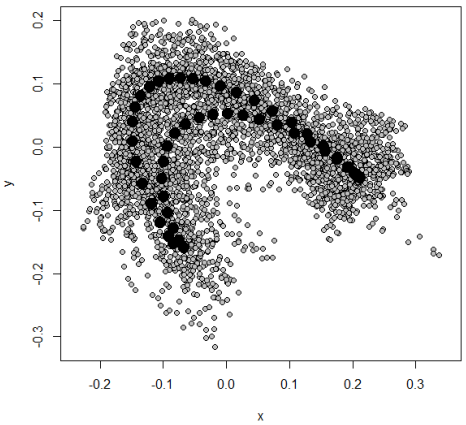

Phylogenetic signal

Spinneret-aligned:

```
Observed Phylogenetic Signal (K): 0.6847
P-value: 0.001
Based on 1000 random permutations
```

GPA-aligned:

```
Observed Phylogenetic Signal (K): 0.8007
P-value: 0.001
Based on 1000 random permutations
```

Phylo-Morphospace

Spinneret-aligned:

GPA-aligned:

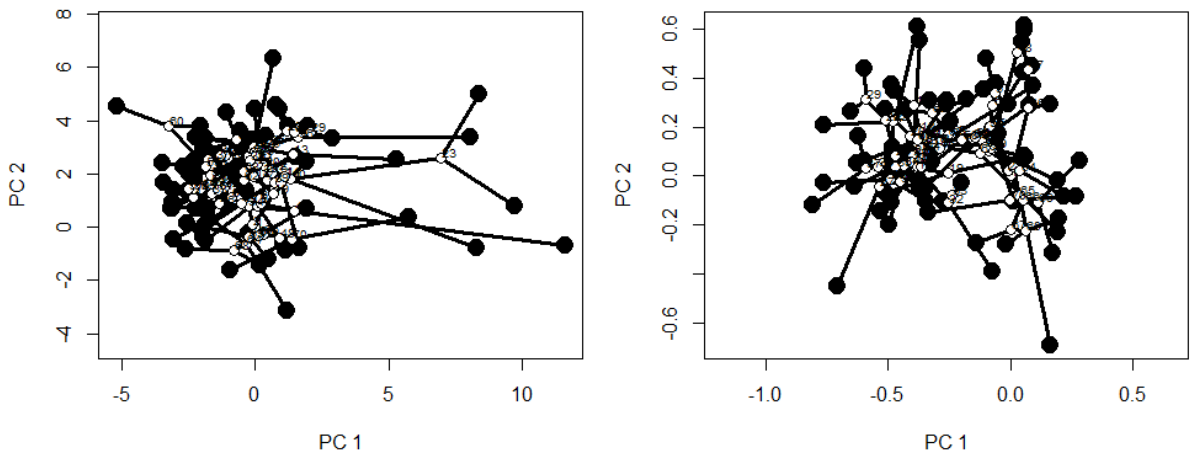

Comparing track shapes between groups

Cribellar vs. ecribellar

Spinneret-aligned:

```
procD.pgls(f1 = A ~ cribx, phy = treex, iter = 999)

Type I (Sequential) Sums of Squares and Cross-products
Randomized Residual Permutation Procedure Used
1000 Permutations
ANOVA effect sizes and P-values based on empirical F distributions


          Df     SS       MS     Rsq      F       Z Pr(>F)
cribx      1 0.0770 0.076955 0.00918 0.6394 -0.22243  0.585
Residuals 69 8.3049 0.120361 0.99082
Total     70 8.3819
```

GPA-aligned:

```
          Df       SS        MS     Rsq      F       Z Pr(>F)
cribx      1 0.001554 0.0015539 0.01643 1.1525 0.53222  0.316
Residuals 69 0.093034 0.0013483 0.98357
Total     70 0.094588
```

Web types*

Spinneret-aligned(*):

```
procD.pgls(f1 = A ~ webx, phy = treex, iter = 999)

Type I (Sequential) Sums of Squares and Cross-products
Randomized Residual Permutation Procedure Used
1000 Permutations
ANOVA effect sizes and P-values based on empirical F distributions

          Df     SS      MS     Rsq     F      Z Pr(>F)
webx       2 0.5109 0.25546 0.06096 2.207 1.5808  0.059 .
Residuals 68 7.8710 0.11575 0.93904
Total     70 8.3819
```

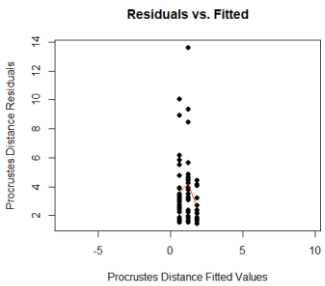

GPA-aligned**:

```
          Df        SS         MS    Rsq       F       Z Pr(>F)
webx       2 0.011057 0.0055287 0.1169 4.5008 3.2716  0.002 **
Residuals 68 0.083530 0.0012284 0.8831
Total     70 0.094588
```

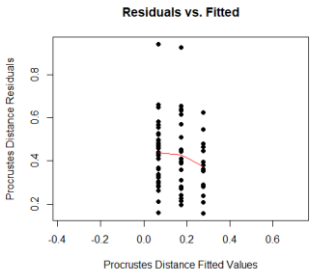

Centrality(*)

Spinneret-aligned*:

```
procD.pgls(f1 = A ~ centrx, phy = treex, iter = 999)

Type I (Sequential) Sums of Squares and Cross-products
Randomized Residual Permutation Procedure Used
1000 Permutations
ANOVA effect sizes and P-values based on empirical F distributions

          Df     SS      MS     Rsq      F      Z Pr(>F)
centrx     1 0.9031 0.90308 0.10774 8.3319 3.2017  0.001 **
Residuals 69 7.4788 0.10839 0.89226
Total     70 8.3819
---
Signif. codes:  0 ‘***’ 0.001 ‘**’ 0.01 ‘*’ 0.05 ‘.’ 0.1 ‘ ’ 1
```

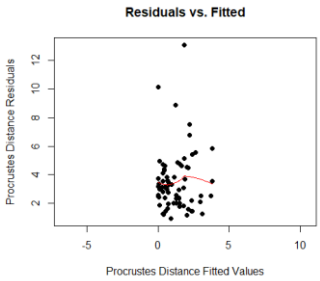

GPA-aligned:

```
          Df        SS         MS     Rsq       F       Z Pr(>F)
centrx     1 0.001512 0.0015122 0.01599 1.1211 0.51745  0.301
Residuals 69 0.093075 0.0013489 0.98401
Total     70 0.094588                                      ---
Signif. codes:  0 ‘***’ 0.001 ‘**’ 0.01 ‘*’ 0.05 ‘.’ 0.1 ‘ ’ 1
```

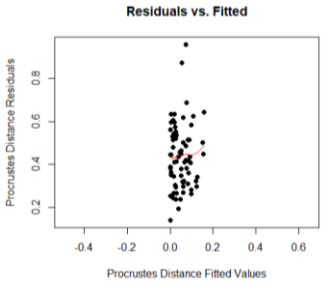

Comparing evolutionary rates

*Cribellar vs. ecribellar**

Spinneret-aligned*:

```
Observed Rate Ratio: 1.9277
P-value: 0.014
Based on 1000 random permutations
The rate for group no is 0.000945749418143697
The rate for group yes is 0.00182315706480094
```

GPA-aligned*:

```
Observed Rate Ratio: 1.5286
P-value: 0.135
Based on 1000 random permutations
The rate for group no is 1.1671141266508e-05
The rate for group yes is 1.78408875444222e-05
```

Web types(*)

Spinneret-aligned*:

```
Observed Rate Ratio: 3.0715
P-value: 0.001
Based on 1000 random permutations
The rate for group aerial is 0.000497090342255345
The rate for group basic is 0.00152680602048892
The rate for group none is 0.00121867711186004
```

GPA-aligned:

```
Observed Rate Ratio: 1.1937
P-value: 0.521
Based on 1000 random permutations
The rate for group aerial is 1.16577994359458e-05
The rate for group basic is 1.34765955897021e-05
The rate for group none is 1.3916021907465e-05
```

ESM.9. List of study material and sample sizes

Taxonomy (after World Spider Catalog V.19.5)

family	species	description	individual	vouch	REG#	status
Agelenidae	*Tegenaria ferruginea*	(Panzer, 1804)	BEU012	UG	ZIMG-I	f
			BEU013	UG	ZIMG-I	juv
			BEU014	UG	ZIMG-I	juv
			BEU015	UG	ZIMG-I	juv
Amaurobiidae	*Amaurobius fenestralis*	(Ström, 1768)	BEU019	UG	ZIMG-I	m sub
			BEU020	UG	ZIMG-I	f
			BEU021	UG	ZIMG-I	f
(to Cycloctenidae)	*Storenosoma* sp.		BLM033	AM	KS.128	m sub
			BLM038	AM	KS.128	f
(to Cycloctenidae)	*Storenosoma terraneum*	Davies, 1986	BLM061	AM	KS.128	juv
			BLM063	AM	KS.128	m
			BLM064	AM	KS.128	f
			BLM069	MQ		f
Anyphaenidae	*Amaurobioides litoralis*	Hickman, 1949	TAS011	AM	KS.128	f
			TAS012	AM	KS.128	juv
			TAS013	AM	KS.128	juv
			TAS014	AM	KS.128	m
			TAS015	UG	ZIMG-I	f
			TAS016	AM	KS.128	m
			TAS029	AM	KS.128	juv
	Anyphaena accentuata	(Walckenaer, 1802)	BEU001	UG	ZIMG-I	f
			BEU002	UG	ZIMG-I	juv
			BEU003	UG	ZIMG-I	juv
Araneidae	*Arachnura higginsi*	(L. Koch, 1872)	WGP001	AM	KS.128	f
	Poecilopachys australasia	(Griffith & Pidgeon, 1833	KWG005	MQ		f
	Eriophora sp.		WGP002	MQ		juv
	Eriophora transmarina	(Keyserling, 1865)	BKL002	AM	KS.128	f
			BKL009	MQ		f
	Eriophora sp.		HOP031	MQ		f
			HOP029	MQ		juv
			HOP035	MQ		
			HOP056	AM	KS.128	juv
	Argiope keyserlingi	Karsch, 1878	HOP016	UG	ZIMG-I	f
			HOP018	MQ		juv
			HOP019	AM	KS.128	f
	Nephila plumipes	(Latreille, 1804)	BKL006	MQ		f
			BKL008	MQ		f
			BKL011	MQ		f
			BKL012	AM	KS.128	f
			SON003	MQ		f
			SON004	AM	KS.128	f
			SON007	MQ		f
			WPP012	MQ		juv

			WPP014	MQ		juv
			WPP015	MQ		juv
			WPP016	AM	KS.128	juv
			WPP017	AM	KS.128	f
			HOP007	MQ		f
			HOP008	MQ		f
			SYD003	UG	ZIMG-I	f
	Austracantha minax	(Thorell, 1859)	HFW001	MQ		juv
			HFW002	AM	KS.128	f
			HFW003	AM	KS.128	f
	Phonognatha graeffei	(Keyserling, 1865)	HOP060	AM	KS.128	f
			HOP061	AM	KS.128	f
			MQC069	AM	KS.128	f
	Cyrtophora hirta	L. Koch, 1872	BRB004	AM	KS.128	juv
			BRB005	AM	KS.128	f
			BRB023	AM	KS.128	f
	Cyrtophora moluccensis	(Doleschall, 1857)	BRB029	MQ		f
Arkyidae	*Arkys lancearius*	Walckenaer, 1837	KWG003	UG	ZIMG-I	f
	Arkys curtulus	(Simon, 1903)	SON001	AM	KS.128	f
	Arkys furcatus	(Balogh, 1978)	SONX10	AM	KS.128	m
	Arkys cornutus	L. Koch, 1872	BRB022	AM	KS.128	f
Austrochilidae	*Hickmania troglodytes*	(Higgins & Petterd, 1883)	TAS002	UNSW		f
			TAS004	MQ		juv
			TAS005	MQ		m
			TAS006	AM	KS.128	f
			TAS007	UNSW		f
			TAS008	UG	ZIMG-I	f
Clubionidae	*Clubiona* sp. 3		MQC038	AM	KS.128	f
	Clubiona sp. 2		MQC046	AM	KS.128	f
	Clubiona sp. 1		HOP039	AM	KS.128	m
Corinnidae	*Nyssus coloripes*	Walckenaer, 1805	TAS043	AM	KS.128	f
			BLM006	AM	KS.128	m
	Nyssus albopunctatus	(Hogg, 1896)	SONX06	AM	KS.128	m sub
			BRB016	MQ		f
	Leichhardteus albofasciatu	Baehr & Raven, 2013	SONX08	MQ		juv
			SONX09	AM	KS.128	juv (n
			MGL019	AM	KS.128	f
Cycloctenidae	*Cycloctenus* sp.		NZ020	CM		m
			NZ021	CM		f
			NZ029	CM		m
Deinopidae	*Deinopis subrufa*	L. Koch, 1879	BKL001	AM	KS.128	m
			SON019	AM	KS.128	f
			SON020	UG	ZIMG-I	f
			SON021	AM	KS.128	m
			SON022	MQ		f
	Menneus nemesio	Coddington, Kuntner & O	MGL012	AM	KS.128	m

Desidae	*Badumna insignis*	(L. Koch, 1872)	KWG001	AM	KS.128	f
			MQC023	MQ		juv
			MQC013	AM	KS.128	f
			PPD003	AM	KS.128	f
			MQC064	UG	ZIMG-I	juv
			MQC065	AM	KS.128	juv
	Badumna longinqua	(L. Koch, 1867)	MQC056	AM	KS.128	juv
	Paramatachia sp. 1		BRB009	AM	KS.128	f
	Paramatachia sp. 2		MGL014	AM	KS.128	f
	Austmusia wilsoni	Gray, 1983	BLM049	AM	KS.128	juv
			BLM036	AM	KS.128	juv
			BLM037	AM	KS.128	juv
	spec. Namandia group		BLM044	AM	KS.128	m
			BLM034	AM	KS.128	juv
			BLM035	AM	KS.128	f
(to Stiphidiidae)	*Taurongia* sp.		TAS023	MQ		f
			TAS024	AM	KS.128	f
			TAS025	MQ		f
			TAS026	MQ		f
			TAS027	AM	KS.128	f
			TAS028	AM	KS.128	m
	Forsterina sp.		TAS022	AM	KS.128	m sub
	Cambridgea foliata	(L. Koch, 1872)	NZ010	CM		f
			NZ011	CM		f
			NZ012	CM		f
			NZ013	CM		juv
	Cambridgea plagiata	Forster & Wilton, 1973	NZ025	CM		f
			NZ026	CM		f
			NZ028	CM		f
	Metaltella simoni	(Keyserling, 1878)		MA	AMR-0	f
Dictynidae	*Brigittea civica*	(Lucas, 1850)	GRW012	UG	ZIMG-I	f
			GRW015	UG	ZIMG-I	f
			GRW016	UG	ZIMG-I	f
	Paradictyna rufoflava	(Chamberlain, 1946)	NZ031	CM		f
			NZ032	UA		f
			NZ033	UA		f
Dysderidae	*Harpactea rubicunda*	(C. L. Koch, 1838)	GRW009	UG	ZIMG-I	f
			GRW019	UG	ZIMG-I	f
Eresidae	*Stygodyphus dumicola*	Pocock, 1898	GRW001	UG	ZIMG-I	juv
			GRW002	UG	ZIMG-I	f
			GRW003	UG	ZIMG-I	juv
			GRW004	UG	ZIMG-I	juv
	Eresus sp.		GRW005	SH		f
Eutichuridae	*Calamoneta* sp.		MGL004	AM	KS.128	juv
			MGL009	AM	KS.128	juv
			MGL016	AM	KS.128	juv

Filistatidae	*Filistata insidiatrix*	(Forsskål, 1775)	1 ad f	AG		f
	Wandella orana	Gray, 1994	MQC023	MQ		juv
			MQC025	MQ		f
			MQC026	UG	ZIMG-I	f
			MQC037	MQ		f
	Kulkulcania hibernalis	(Hentz, 1842)	GRW006	UG	ZIMG-I	juv
			GRW007	UG	ZIMG-I	juv
			GRW008	UG	ZIMG-I	juv
			GRW	UG	ZIMG-I	juv
			Kh01	UA		f
			Kh02	UA		f
			Kh03	UA		f
Gradungulidae	*Kaiya terama*	Gray, 1987	BLM040	MQ		juv
			BLM045	MQ		f
			BLM046	UG	ZIMG-I	juv
			BLM048	MQ		juv
			BLM030	MQ		f
Hersiliidae	*Tamopsis brisbanensis*	Baehr & Baehr, 1987	PPD010	AM	KS.128	f
			HOP062	MQ		m
	Tamopsis sp. 2		SONX01	AM	KS.128	m sub
			SONX12	AM	KS.128	juv
	Tamopsis sp. 3		BRB015	UG	ZIMG-I	juv
			BRB020	AM	KS.128	m sub
Hypochilidae	*Hypochilus kastoni*	Platnick, 1987	ind. 1	MA	MJR-2:	f
			ind. 2	MA	MJR-lo	juv
Linyphiidae	*Linyphia triangularis*	(Clerck, 1757)	BEU022	UG	ZIMG-I	f
			BEU023	UG	ZIMG-I	m sub
			BEU024	UG	ZIMG-I	m
Megadictynidae	*Megadictyna thilenii*	Dahl, 1906	NZ001	CM		f
			NZ002	UA		f
			NZ004	CM		m
			NZ005	CM		juv
			NZ006	CM		m sub
Mimetidae	*Australomimetus* sp.		BLM009	UG	ZIMG-I	f
			BLM010	AM	KS.128	f
			BLM011	AM	KS.128	f
			BLM055	AM	KS.128	m
Miturgidae	*Mituliodon tarantulinus*	(L. Koch, 1873)	TAS041	UG	ZIMG-I	f
			TAS042	AM	KS.128	m
			SYD002	MQ		juv
			FRF005	AM	KS.128	juv
	Nuliodon sp.		BLM018	AM	KS.128	f
			BLM019	AM	KS.128	f
			BLM020	AM	KS.128	f
	Argoctenus sp.		SONX13	AM	KS.128	m

	Miturga sp. 1		BLM041	AM	KS.128	m
			BLM042	AM	KS.128	f
	Miturga sp. 2		BLM053	MQ		
			TAS039	AM	KS.128406	
Nicodamidae	*Oncodamus bidens*	(Karsch, 1878)	SON016	UG	ZIMG-I	f
			SON017	AM	KS.128	f
			BLM005	AM	KS.128	m sub
	Litodamus olga	Harvey, 1995	TAS009	AM	KS.128	f
	Dimidamus dimidiatus	(Simon, 1897)	BLM080	MQ		m
			BLM081	MQ		f
			BLM082	AM	KS.128	m
Oecobiidae	*Oecobius navus*	Blackwall, 1859	MQC048	UG	ZIMG-II-283	
			MQC051	AM	KS.128	f
			MQC054	AM	KS.128	f
			MQC066	AM	KS.128	f
			MQC067	AM	KS.128	f
Orsolobidae	*Tasmanoonops sp.*		BLM012	AM	KS.128	juv
			BLM056	AM	KS.128	juv
			BLM059	lost		juv
Oxyopidae	*Oxyopes molarius*	L. Koch, 1878	HFW005	AM	KS.128	f
			HFW006	UG	ZIMG-I	f
			HFW007	AM	KS.128	m
Philodromidae	*Tibellus tenellus*	(L. Koch, 1876)	HFW004	AM	KS.128	f
	Tibellus oblongus	(Walckenaer, 1802)	BEU008	UG	ZIMG-I	juv
			BEU009	UG	ZIMG-I	f
			BEU011	UG	ZIMG-I	f
	Philodromus aureolus	(Clerck, 1757)	BEU004	UG	ZIMG-I	m
			BEU005	UG	ZIMG-I	f
			BEU006	UG	ZIMG-I	f
			BEU007	UG	ZIMG-I	f
Pholcidae	*Pholcus phalangioides*	(Fuesslin, 1775)	MQC016	MQ		f
			MQC061	AM	KS.128	f
			MQC062	AM	KS.128	f
			MQC063	*lost*		
Physoglenidae	*Paratupua* sp.		BLM041	AM	KS.128	m
			BLM066	AM	KS.128	f
Pimoidae	*Pimoa rupicola*	(Simon, 1884)	1 ad f	UK		f
Pisauridae	*Dolomedes wollemi*	Raven & Hebron, 2018	BLM001	QM		f
			BLM002	QM		m
			BLM003	QM		juv
			BLM029	AM	KS.128	juv
			BLM031	AM	KS.128	juv
			BLM032	AM	KS.128	juv

	Dendrolycosa icadia	(L. Koch, 1876)	BRB025	AM	KS.128	m
			BRB026	AM	KS.128	f suba
			BRB027	AM	KS.128	m
Salticidae	*Sandalodes superbus*	(Karsch, 1878)	MQC001	MQ		f
			MQC011	AM	KS.128	f
			MQC018	AM	KS.128	f
			HOP015	MQ		f
			HOP055	UG	ZIMG-I	juv
	Servaea incana	(Karsch, 1878)	MQC021	AM	KS.128	f
			MQC043	AM	KS.128	f
	Servaea villosa	(Keyserling, 1881)	HOP045	AM	KS.128	f
	Opisthoncus sp.		HOP043	AM	KS.128	m
			HOP047	AM	KS.128	f
Scytodidae	*Scytodes thoracica*	(Latreille, 1802)	GRW010	UG	ZIMG-I	juv
			GRW016	UG	ZIMG-I	juv
			GRW017	UG	ZIMG-I	juv
			BRB012	AM	KS.128	f
Segestriidae	*Ariadna* sp. 1		BLM008	AM	KS.128	f suba
	Ariadna sp. 2		SONX03	AM	KS.128	juv
	Gippsicola sp.		BLM014	AM	KS.128	f
	Segestria florentina	(Rossi, 1790)	GRW020	UG	ZIMG-I	f
			GRW021	UG	ZIMG-I	f
			GRW022	UG	ZIMG-I	f
			GRW0X1	UG	ZIMG-I	f
Sparassidae	*Isopeda villosa*	L. Koch, 1875	MQC002	MQ		juv
			MQC003	MQ		f
			MQC3 offspri	MQ		juv
			MQC004	AM	KS.128	m
			MQC005	MQ		f
			MQC006	MQ		juv
			MQC008	MQ		f
			MQC010	MQ		juv
			BLM054	MQ		juv
Stiphidiidae	*Stiphidion facetum*	Simon, 1902	HOP009	AM	KS.128	f
			HOP010	AM	KS.128	m
			HOP051	AM	KS.128	f
			KWG002	MQ		f
			KWG007	MQ		f
	Stiphidion sp.		TAS038 (22)	AM	KS.128	f
	Barahna booloumba	Davies, 2003	MGL023	AM	KS.128	f
	Therlinya vexillum	Gray & Smith, 2002	MGL003	MQ		f
			MGL006	AM	KS.128	m
			MGL010	AM	KS.128	f
			MGL013	AM	KS.128	f
	Neolana dalmasi	(Marples, 1959)	NZ022	CM		f
			NZ023	CM		f
			NZ035	CM		f

Tetragnathidae	*Leucauge dromedaria*	(Thorell, 1881)	WGP003	MQ		f
			PPD006	UG	ZIMG-I	f
			PPD007	AM	KS.128	f
			PPD008	AM	KS.128	f
	Tetragnatha valida	Keyserling, 1887	BWN003	AM	KS.128	juv
			BWN004	AM	KS.128	f
			BWN005	AM	KS.128	f
	Meta sp.		BLM056	AM	KS.128	f
			BLM067	MQ		m
			BLM068	AM	KS.128	f
Thomisidae	*Australomisidia pilula*	(L. Koch, 1867)	PPD009	UG	ZIMG-I	f
			HOP037	MQ		
			HOP044	AM	KS.128	f
	Sidymella sp.		WPP005	MQ		f
			WPP008	MQ		
	Sidymella longipes	(L. Koch, 1874)	BRB008	AM	KS.128	f
	Tharpyna sp.		MQC039	AM	KS.128	f
	Stephanopis sp. 1		BRB002	AM	KS.128	f
			BRB003	MQ		juv
			BRB021	AM	KS.128	m
	Stephanopis sp. 2		MGL008	AM	KS.128	juv
Theridiidae	*Cryptachaea gigantipes*	(Keyserling, 1890)	MQC033	AM	KS.128	f
			MQC034	UG	ZIMG-I	f
			MQC035	AM	KS.128	f
	Episinus sp.		SONX11	AM	KS.128	f
	Hadrotarsinae spec. aff. Dipoena		BLM058	AM	KS.128	m
Titanoecidae	*Goeldia* sp.			MA	AMR-0	juv / f
Toxopidae	*Toxopsoides* sp.		TAS019	AM	KS.128	m
			TAS021	AM	KS.128	m
			TAS036	AM	KS.128	m
	Toxopsoides macleayi	Smith, 2013	BLM013	AM	KS.128	m
			BLM015	AM	KS.128	m
			BLM016	AM	KS.128	juv
Trechaleidae	*Paratrechalea ornata*	(Mello-Leitão, 1943)		MA	AMR-0	f / m
Uloboridae	*Philoponella congregabilis*	(Rainbow, 1916)	HOP020	AM	KS.128	f
			HOP057	AM	KS.128	f
			HOP058	AM	KS.128	f
	Philoponella variabilis	(Keyserling, 1887)	MQC040	AM	KS.128	f
			MQC041	UG	ZIMG-I	f
			MQC042	AM	KS.128	f
			MQC047	AM	KS.128	f
			MQC049	AM	KS.128	m sub
	Waitkera waitakerensis	(Chamberlain, 1946)	NZ030	UA		f
Zoropsidae	*Zoropsis spinimana*	(Dufour, 1820)	f1	UK		f

		f2	UK		f
*Kilyana*cf. *hendersoni*	Raven & Stumkat, 2005	MGL017	AM	KS.128	f
		MGL020	MQ		juv
		MGL021	MQ		m

Collection Data sample location	year	collector	identified b	***Analyses (number of obse*** **silk anchors** character analysis	morpho-metry
Kronsberg, MV, Germany; 54°19'50.4"N 12	Jul 2017	J. Wolff	J. Wolff	15	15
Kronsberg, MV, Germany; 54°19'50.4"N 12	Jul 2017	J. Wolff	J. Wolff	13	13
Kronsberg, MV, Germany; 54°19'50.4"N 12	Jul 2017	J. Wolff	J. Wolff	17	15
Kronsberg, MV, Germany; 54°19'50.4"N 12	Jul 2017	J. Wolff	J. Wolff		
Barther Stadtwald, Barth, MV, Germany; 5	Jul 2017	J. Wolff	J. Wolff	15	15
Barther Stadtwald, Barth, MV, Germany; 5	Jul 2017	J. Wolff	J. Wolff		
Barther Stadtwald, Barth, MV, Germany; 5	Jul 2017	J. Wolff	J. Wolff	15	15
Newnes Plateau, NSW, Australia; 33°15'20	Mar 2017	A. Grabolle	G. Milledge		
Newnes Plateau, NSW, Australia; 33°15'20	Mar 2017	A. Grabolle	H. Smith /		
Megalong Road, Blackheath, NSW, Australi	Mar 2018	J. Wolff	H. Smith /	15	15
Megalong Road, Blackheath, NSW, Australi	Mar 2018	J. Wolff	H. Smith /		
Megalong Road, Blackheath, NSW, Australi	Mar 2018	J. Wolff	H. Smith /		
Megalong Road, Blackheath, NSW, Australi	Mar 2018	J. Wolff	J. Wolff/ H	2	
Pirate Bay, Eaglehawk Neck, TAS, Australia	Jan 2017	J. Wolff	J. Wolff / H	15	15
Pirate Bay, Eaglehawk Neck, TAS, Australia	Jan 2017	J. Wolff	J. Wolff / H	15	15
Pirate Bay, Eaglehawk Neck, TAS, Australia	Jan 2017	J. Wolff	J. Wolff / H		
Pirate Bay, Eaglehawk Neck, TAS, Australia	Jan 2017	J. Wolff	J. Wolff / H		
Pirate Bay, Eaglehawk Neck, TAS, Australia	Jan 2017	J. Wolff	J. Wolff / H		
Pirate Bay, Eaglehawk Neck, TAS, Australia	Jan 2017	J. Wolff	J. Wolff / H		
Pirate Bay, Eaglehawk Neck, TAS, Australia	Jan 2017	J. Wolff	J. Wolff / H		
Barther Stadtwald, Barth, MV, Germany; 5	Jul 2017	J. Wolff	J. Wolff	15	15
Barther Stadtwald, Barth, MV, Germany; 5	Jul 2017	J. Wolff	J. Wolff	19	15
Barther Stadtwald, Barth, MV, Germany; 5	Jul 2017	J. Wolff	J. Wolff	21	15
Wilga Park, North Ryde, NSW, Australia; 33	Jan 2016	J. Wolff	J. Wolff / H	13	13
Ku-ring-gai Wildflower Garden, St. Ives, NS	Jan 2016	H. Smith /	H. Smith	15	15
Wilga Park, North Ryde, NSW, Australia; 33	Jan 2016	J. Wolff	J. Wolff	16	16
McKell Park, Brooklyn, NSW, Australia; 33°	Jan 2016	J. Wolff	H. Smith	13	13
McKell Park, Brooklyn, NSW, Australia; 33°	Apr 2016	J. Wolff	J. Wolff	13	12
Blue Gum Track, Hornsby, NSW, Australia;	Dec 2016	J. Wolff	J. Wolff		
Blue Gum Track, Hornsby, NSW, Australia;	Dec 2016	J. Wolff	J. Wolff		
Blue Gum Track, Hornsby, NSW, Australia;	Dec 2016	J. Wolff	J. Wolff		
Florence Cotton Park, Hornsby, NSW, Aust	Jan 2017	J. Wolff	H. Smith		
Reddy Park, Hornsby, NSW, Australia; 33°4	Nov 2016	J. Wolff	J. Wolff	15	15
Reddy Park, Hornsby, NSW, Australia; 33°4	Nov 2016	J. Wolff	J. Wolff	15	15
Reddy Park, Hornsby, NSW, Australia; 33°4	Nov 2016	J. Wolff	J. Wolff / H	15	15
McKell Park, Brooklyn, NSW, Australia; 33°	Apr 2016	J. Wolff	J. Wolff	9	9
McKell Park, Brooklyn, NSW, Australia; 33°	Apr 2016	J. Wolff	J. Wolff	9	9
McKell Park, Brooklyn, NSW, Australia; 33°	Apr 2016	J. Wolff	J. Wolff		
McKell Park, Brooklyn, NSW, Australia; 33°	May 2016	J. Wolff	J. Wolff / H		
Wahroonga Park, Wahroonga, NSW, Austr	May 2016	J. Wolff	J. Wolff		
Wahroonga Park, Wahroonga, NSW, Austr	May 2016	J. Wolff	J. Wolff / H		
Wahroonga Park, Wahroonga, NSW, Austr	May 2016	J. Wolff	J. Wolff		
Bicentennial Park, West Pymble, NSW, Aus	Jan 2016	J. Wolff	J. Wolff	15	15

Bicentennial Park, West Pymble, NSW, Aus	Jan 2016	J. Wolff	J. Wolff	16	15
Bicentennial Park, West Pymble, NSW, Aus	May 2016	J. Wolff	J. Wolff		
Bicentennial Park, West Pymble, NSW, Aus	May 2016	J. Wolff	J. Wolff / H		
Bicentennial Park, West Pymble, NSW, Aus	May 2016	J. Wolff	J. Wolff / H		
Florence Cotton Reserve, Hornsby, NSW, A	Apr 2016	J. Wolff	J. Wolff		
Florence Cotton Reserve, Hornsby, NSW, A	Apr 2016	J. Wolff	J. Wolff		
Mosman shoreline, Sydney, NSW, Australia	May 2017	J. Wolff	J. Wolff		
Grasstree Rest Area, Mangalore, VIC, Austr	Jan 2017	J. Wolff	J. Wolff / H	15	15
Grasstree Rest Area, Mangalore, VIC, Austr	Jan 2017	J. Wolff	J. Wolff / H	13	13
Grasstree Rest Area, Mangalore, VIC, Austr	Jan 2017	J. Wolff	J. Wolff / H	15	15
Reddy Park, Hornsby, NSW, Australia; 33°4	Mar 2017	J. Wolff	J. Wolff / H	15	15
Reddy Park, Hornsby, NSW, Australia; 33°4	Mar 2017	J. Wolff	J. Wolff / H	15	15
Macquarie University Campus, Sydney, NS	May 2017	J. Wolff	J. Wolff / H	15	15
Lota Creek Park, Brisbane, QLD, Australia;	May 2017	J. Wolff	H. Smith /	15	15
Lota Creek Park, Brisbane, QLD, Australia;	May 2017	J. Wolff	H. Smith /	15	15
Lota Creek Park, Brisbane, QLD, Australia;	May 2017	J. Wolff	H. Smith /	15	15
Brisbane, QLD, Australia; hand coll. at day	Mar 2018	M. Kelly	J. Wolff	14	14
Ku-ring-gai Wildflower Garden, St. Ives, NS	Jan 2016	H. Smith /	H. Smith	15	15
Sydney, NSW, Australia; hand coll. from su	Apr 2016	M. Herber	H. Smith	26	25
Binna Burra Rd, Beechmont, QLD, Australia	Mar 2017	A. Grabolle	H. Smith	16	15
Lota Creek Park, Brisbane, QLD, Australia;	Apr 2017	R. Raven /	H. Smith	15	15
Bates Creek, Dover, TAS, Australia; 43°18'1	Jan 2017	N. Doran /	N. Doran	18	15
Bates Creek, Dover, TAS, Australia; 43°18'1	Jan 2017	N. Doran /	N. Doran		
Bates Creek, Dover, TAS, Australia; 43°18'1	Jan 2017	N. Doran /	N. Doran		
Bates Creek, Dover, TAS, Australia; 43°18'1	Jan 2017	N. Doran /	N. Doran /	19	15
Bates Creek, Dover, TAS, Australia; 43°18'1	Jan 2017	N. Doran /	N. Doran	14	13
Bates Creek, Dover, TAS, Australia; 43°18'1	Jan 2017	N. Doran /	N. Doran		
Macquarie University Campus, Sydney, NS	Nov 2016	J. Wolff	J. Wolff / H	14	14
Macquarie University Campus, Sydney, NS	Dec 2016	J. Wolff	J. Wolff / H	21	15
Normanhurst Park, Normanhurst, NSW, Au	Dec 2016	J. Wolff	J. Wolff / H	14	14
Friendly Beach, TAS, Australia; 42°01'35.1"	Jan 2017	J. Wolff	H. Smith	15	15
Hassans Walls Lookout, Lithgow, NSW, Aus	Feb 2017	J. Wolff	H. Smith /	17	15
Binna Burra Rd, Beechmont, QLD, Australia	Mar 2017	A. Grabolle	H. Smith	15	15
Lota Creek Park, Brisbane, QLD, Australia;	Mar 2017	R. Raven	J. Wolff	17	15
Binna Burra Rd, Beechmont, QLD, Australia	Mar 2017	A. Grabolle	J. Wolff	14	14
Binna Burra Rd, Beechmont, QLD, Australia	Mar 2017	A. Grabolle	H. Smith	17	15
Rainforest Getaways, Mt. Glorious, QLD, A	Apr 2017	R. Raven /	H. Smith	15	15
Lake Tikitapu, Rotorua, Bay of Plenty, New	Mar 2018	B. McQuill	J. Wolff	16	15
Lake Tikitapu, Rotorua, Bay of Plenty, New	Mar 2018	B. McQuill	J. Wolff	5	
Lake Tikitapu, Rotorua, Bay of Plenty, New	Mar 2018	B. McQuill	J. Wolff	12	12
McKell Park, Brooklyn, NSW, Australia; 33°	Jan 2016	J. Wolff	H. Smith /	16	16
Grangewood Pl, West Pennant Hills, NSW,	Oct 2016	B. Jones	H. Smith /	15	15
Grangewood Pl, West Pennant Hills, NSW,	Oct 2016	B. Jones	H. Smith /		
Grangewood Pl, West Pennant Hills, NSW,	Oct 2016	B. Jones	H. Smith /		
Grangewood Pl, West Pennant Hills, NSW,	Oct 2016	B. Jones	H. Smith /	13	13
Greene's Falls Track, Mt. Glorious, QLD, Au	Apr 2017	R. Raven	H. Smith	12	12

Ku-ring-gai Wildflower Garden, St. Ives, NS	Jan 2016	J. Wolff	H. Smith	14	14
Macquarie University Campus, Sydney, NS	Sep 2016	J. Wolff	J. Wolff		
Macquarie University Campus, Sydney, NS	Apr 2016	J. Wolff	H. Smith	29	15
Pretoria Parade, Hornsby, NSW, Australia;	Feb 2016	J. Wolff	H. Smith	15	15
Macquarie University Campus, Sydney, NS	May 2017	J. Wolff	J. Wolff		
Macquarie University Campus, Sydney, NS	May 2017	J. Wolff	H. Smith		
Macquarie University Campus, Sydney, NS	Mar 2017	J. Wolff	J. Wolff / H	15	15
Nudgee Beach Reserve, Brisbane, QLD, Aus	May 2017	J. Wolff	H. Smith		
Greene's Falls Track, Mt. Glorious, QLD, Au	Apr 2017	R. Raven	H. Smith	15	15
Mt Wilson Rd, Mt Wilson, NSW, Australia;	Feb 2017	A. Graboll	H. Smith	14	14
Megalong Road, Blackheath, NSW, Australi	Feb 2017	A. Graboll	H. Smith	15	15
Megalong Road, Blackheath, NSW, Australi	Feb 2017	A. Graboll	H. Smith	15	15
Mt Wilson Rd, Mt Wilson, NSW, Australia;	Feb 2017	A. Graboll	H. Smith	27	15
Megalong Road, Blackheath, NSW, Australi	Feb 2017	A. Graboll	H. Smith		
Megalong Road, Blackheath, NSW, Australi	Feb 2017	A. Graboll	H. Smith	3	
Jacksons Bend Track, Fern Tree, TAS, Austr	Jan 2017	J. Wolff	J. Wolff / H	14	14
Jacksons Bend Track, Fern Tree, TAS, Austr	Jan 2017	J. Wolff	H. Smith		
Jacksons Bend Track, Fern Tree, TAS, Austr	Jan 2017	J. Wolff	J. Wolff / H	4	
Jacksons Bend Track, Fern Tree, TAS, Austr	Jan 2017	J. Wolff	J. Wolff / H	15	15
Jacksons Bend Track, Fern Tree, TAS, Austr	Jan 2017	J. Wolff	H. Smith	15	15
Jacksons Bend Track, Fern Tree, TAS, Austr	Jan 2017	J. Wolff	H. Smith		
Jacksons Bend Track, Fern Tree, TAS, Austr	Jan 2017	J. Wolff	H. Smith	19	15
Lake Tikitapu, Whakarewarewa, Bay of Ple	Mar 2018	B. McQuill	J. Wolff	17	15
Lake Tikitapu, Whakarewarewa, Bay of Ple	Mar 2018	B. McQuill	J. Wolff	18	15
Lake Tikitapu, Whakarewarewa, Bay of Ple	Mar 2018	B. McQuill	J. Wolff	16	15
Lake Tikitapu, Whakarewarewa, Bay of Ple	Mar 2018	B. McQuill	J. Wolff		
Lake Tikitapu, Whakarewarewa, Bay of Ple	Mar 2018	B. McQuill	J. Wolff	16	15
Lake Tikitapu, Whakarewarewa, Bay of Ple	Mar 2018	B. McQuill	J. Wolff	13	13
Lake Tikitapu, Whakarewarewa, Bay of Ple	Mar 2018	B. McQuill	J. Wolff	15	15
Parque Nacional El Palmar, Entre Rios, Arg	Aug 2003	A. Ojangu	C. Grismad	13	13
Waiblingen, BW, Germany; 48°50'00.3"N 9	Jul 2017	W. Schleg	W. Schlege	12	11
Waiblingen, BW, Germany; 48°50'00.3"N 9	Jul 2017	W. Schleg	W. Schlege	23	15
Waiblingen, BW, Germany; 48°50'00.3"N 9	Jul 2017	W. Schleg	W. Schlege	21	15
Redwoods, Whakarewarewa, Bay of Plenty	Mar 2018	A.-C. Joel	A.-C. Joel	13	13
Redwoods, Whakarewarewa, Bay of Plenty	Mar 2018	A.-C. Joel	A.-C. Joel	6	
Redwoods, Whakarewarewa, Bay of Plenty	Mar 2018	A.-C. Joel	A.-C. Joel	2	
Rotenberg, Stuttgart, BW, Germany; 48°47	Jul 2017	W. Schleg	W. Schlege	17	8
Rotenberg, Stuttgart, BW, Germany; 48°47	Jul 2017	W. Schleg	W. Schlege	15	15
lab stock of the University of Konstanz	Jul 2017	A. Jordan	A. Jordan	15	15
lab stock of the University of Konstanz	Jul 2017	A. Jordan	A. Jordan	14	14
lab stock of the University of Greifswald	Jul 2017	G. Uhl	G. Uhl		
lab stock of the University of Greifswald	Jul 2017	G. Uhl	G. Uhl	15	15
Ait Baha, Anti-Atlas, Morocco; 30°03'33"N	Nov 2016	S. Huber	S. Huber	15	15
Greene's Falls Track, Mt. Glorious, QLD, Au	Apr 2017	R. Raven	H. Smith	16	15
Greene's Falls Track, Mt. Glorious, QLD, Au	Apr 2017	R. Raven	H. Smith	25	15
Greene's Falls Track, Mt. Glorious, QLD, Au	Apr 2017	R. Raven	H. Smith	24	15

Gola di Gorropu, Sardinia, Italy; 40°11'08.4	May 2013	A. Grabolı	J. Wolff / A	9	8
Macquarie University Campus, Sydney, NS'	Sept 2016	J. Wolff	J. Wolff	9	9
Macquarie University Campus, Sydney, NS'	Oct 2016	J. Wolff	J. Wolff	9	9
Macquarie University Campus, Sydney, NS'	Oct 2016	J. Wolff	J. Wolff	9	9
Macquarie University Campus, Sydney, NS'	Nov 2016	J. Wolff	J. Wolff	15	15
from lab stock of University of Aachen	2017	A.-C. Joel	A.-C. Joel	10	10
from lab stock of University of Aachen	2017	A.-C. Joel	A.-C. Joel		
from lab stock of University of Aachen	2017	A.-C. Joel	A.-C. Joel	3	
from lab stock of University of Aachen	2017	A.-C. Joel	A.-C. Joel		
from lab stock of University of Aachen	2017	A.-C. Joel	A.-C. Joel		
from lab stock of University of Aachen	2017	A.-C. Joel	A.-C. Joel		
from lab stock of University of Aachen	2017	A.-C. Joel	A.-C. Joel		
Mt Wilson Rd, Mt Wilson, NSW, Australia;	Feb 2017	A. Grabolı	J. Wolff	2	
Mt Wilson Rd, Mt Wilson, NSW, Australia;	Feb 2017	A. Grabolı	J. Wolff	15	15
Mt Wilson Rd, Mt Wilson, NSW, Australia;	Feb 2017	A. Grabolı	J. Wolff	8	8
Mt Wilson Rd, Mt Wilson, NSW, Australia;	Feb 2017	A. Grabolı	J. Wolff		
Megalong Road, Blackheath, NSW, Australi	Feb 2017	A. Grabolı	J. Wolff	13	13
Pretoria Parade, Hornsby, NSW, Australia;	Dec 2016	J. Wolff	H. Smith	22	15
Reddy Park, Hornsby, NSW, Australia; 33°4	Sep 2017	J. Wolff	J. Wolff / H	17	15
Emmaville Rd, Ashford, NSW, Australia; 29	Mar 2017	A. Grabolı	H. Smith	19	15
Emmaville Rd, Ashford, NSW, Australia; 29	Mar 2017	A. Grabolı	H. Smith	27	15
Lota Creek Park, Brisbane, QLD, Australia; :	Apr 2017	R. Raven	J. Wolff / H	17	15
Lota Creek Park, Brisbane, QLD, Australia; :	Apr 2017	R. Raven	H. Smith	35	15
USA: California: Siskiyou Co.: Six Rivers Nat	Jun 2017	M. Ramíre	M. Ramíre	12	12
USA: California: Siskiyou Co.: Six Rivers Nat	Jun 2017	M. Ramíre	M. Ramíre	19	15
Barther Stadtwald, Barth, MV, Germany; 5	Jul 2017	J. Wolff	J. Wolff	8	8
Barther Stadtwald, Barth, MV, Germany; 5	Jul 2017	J. Wolff	J. Wolff	16	15
Barther Stadtwald, Barth, MV, Germany; 5	Jul 2017	J. Wolff	J. Wolff	5	
Okere Falls Reserve, Okere Falls, Bay of Ple	Mar 2018	J. Wolff / E	J. Wolff / B	27	15
Okere Falls Reserve, Okere Falls, Bay of Ple	Mar 2018	J. Wolff / E	J. Wolff / B	9	
Okere Falls Reserve, Okere Falls, Bay of Ple	Mar 2018	J. Wolff / E	J. Wolff / B	16	15
Okere Falls Reserve, Okere Falls, Bay of Ple	Mar 2018	J. Wolff / E	J. Wolff / B	4	15
Okere Falls Reserve, Okere Falls, Bay of Ple	Mar 2018	J. Wolff / E	J. Wolff / B	17	
Cathedral Reserve, Mount Wilson, NSW, A	Mar 2017	J. Wolff	J. Wolff / H	15	15
Cathedral Reserve, Mount Wilson, NSW, A	Mar 2017	J. Wolff	H. Smith	19	15
Cathedral Reserve, Mount Wilson, NSW, A	Mar 2017	J. Wolff	H. Smith	17	15
Cathedral Reserve, Mount Wilson, NSW, A	Mar 2017	J. Wolff	H. Smith		
Pirate Bay, Eaglehawk Neck, TAS, Australia	Jan 2017	J. Wolff	H. Smith /	5	
Pirate Bay, Eaglehawk Neck, TAS, Australia	Jan 2017	J. Wolff	H. Smith /		
Royal Botanic Gardens, Sydney, NSW, Aust	Feb 2017	A. Grabolı	H. Smith /	14	14
Brentwood Pl, Frenchs Forest, NSW, Austra	Feb 2017	A. Grabolı	H. Smith /	14	14
Blackheath Glen Reserve, Blackheath, NSW	Mar 2017	A. Grabolı	H. Smith	5	
Blackheath Glen Reserve, Blackheath, NSW	Mar 2017	A. Grabolı	H. Smith	14	14
Blackheath Glen Reserve, Blackheath, NSW	Mar 2017	A. Grabolı	H. Smith	4	
Arcadia Valley Rd, Baffle West, QLD, Austra	Mar 2017	A. Grabolı	H. Smith	10	10

Glowworm Tunnel Rd, Newnes Plateau, NS	Mar 2017	A. Grabolle	H. Smith		
Glowworm Tunnel Rd, Newnes Plateau, NS	Mar 2017	A. Grabolle	H. Smith	14	14
Tableland Rd, Wentworth Falls, NSW, Aust	Mar 2017	J. Wolff	J. Wolff		
Friendly Beach, TAS, Australia; 42°01'35.1"	Jan 2017	J. Wolff	H. Smith	24	15
Leura, NSW, Australia; hand coll. at day, ur	Oct 2016	L. Mannin	H. Smith	24	15
Leura, NSW, Australia; hand coll. at day, ur	Oct 2016	L. Mannin	H. Smith	15	15
Leura, NSW, Australia; hand coll. at day, ur	Dec 2016	L. Mannin	H. Smith	19	15
Tyenna, TAS; 42°41'50.2"S 146°39'58.6"E;	Jan 2017	J. Wolff	H. Smith	18	15
Megalong Road, Blackheath, NSW, Australi	Mar 2018	J. Garb	J. Wolff	15	15
Megalong Road, Blackheath, NSW, Australi	Mar 2018	J. Garb	J. Wolff	18	15
Megalong Road, Blackheath, NSW, Australi	Mar 2018	J. Garb	J. Wolff / H		
Macquarie University Campus, Sydney, NS	Dec 2016	J. Wolff	J. Wolff		
Macquarie University Campus, Sydney, NS	Dec 2016	J. Wolff	J. Wolff / H	17	15
Macquarie University Campus, Sydney, NS	Mar 2017	J. Wolff	J. Wolff / H	22	15
Macquarie University Campus, Sydney, NS	May 2017	J. Wolff	J. Wolff / H. Smith		
Macquarie University Campus, Sydney, NS	May 2017	J. Wolff	J. Wolff / H. Smith		
Cathedral Reserve, Mount Wilson, NSW, A	Mar 2017	A. Grabolle	H. Smith		
Mt Wilson Rd, Mt Wilson, NSW, Australia;	Mar 2018	J. Wolff	H. Smith	6	
Mt Wilson Rd, Mt Wilson, NSW, Australia;	Mar 2018	J. Wolff	J. Wolff	22	15
North Holbrook Rest Area, Hume Fwy, NSV	Jan 2017	J. Wolff	H. Smith	14	14
North Holbrook Rest Area, Hume Fwy, NSV	Jan 2017	J. Wolff	J. Wolff / H	15	15
North Holbrook Rest Area, Hume Fwy, NSV	Jan 2017	J. Wolff	H. Smith	15	15
North Holbrook Rest Area, Hume Fwy, NSV	Jan 2017	J. Wolff	J. Wolff / H	20	15
Barther Stadtwald, Barth, MV, Germany; 5	Jul 2017	J. Wolff	J. Wolff	22	15
Barther Stadtwald, Barth, MV, Germany; 5	Jul 2017	J. Wolff	J. Wolff	16	15
Barther Stadtwald, Barth, MV, Germany; 5	Jul 2017	J. Wolff	J. Wolff	23	15
Barther Stadtwald, Barth, MV, Germany; 5	Jul 2017	J. Wolff	J. Wolff		
Barther Stadtwald, Barth, MV, Germany; 5	Jul 2017	J. Wolff	J. Wolff	17	15
Barther Stadtwald, Barth, MV, Germany; 5	Jul 2017	J. Wolff	J. Wolff	19	15
Barther Stadtwald, Barth, MV, Germany; 5	Jul 2017	J. Wolff	J. Wolff	18	15
Macquarie University Campus, Sydney, NS	Apr 2016	J. Wolff	J. Wolff	8	
Macquarie University Campus, Sydney, NS	Mar 2017	J. Wolff	H. Smith	14	14
Macquarie University Campus, Sydney, NS	Mar 2017	J. Wolff	H. Smith	18	15
Macquarie University Campus, Sydney, NS	Mar 2017	J. Wolff	J. Wolff	12	12
Megalong Road, Blackheath, NSW, Australi	Mar 2017	J. Wolff	H. Smith	6	6
Megalong Road, Blackheath, NSW, Australi	Mar 2018	J. Wolff	H. Smith	17	15
San Pietro Val Lemina, Piedmont, Italy; 44°	Aug 2014	J. Wolff / A	A. Grabolle	20	14
Newnes, Wolgan Valley, NSW, Australia; 3	Dec 2016	J. Wolff	R. Raven	12	
Newnes, Wolgan Valley, NSW, Australia; 3	Dec 2016	J. Wolff	R. Raven		
Newnes, Wolgan Valley, NSW, Australia; 3	Dec 2016	J. Wolff	R. Raven	15	15
Megalong Road, Blackheath, NSW, Australi	Feb 2017	A. Grabolle	R. Raven	15	15
Megalong Road, Blackheath, NSW, Australi	Feb 2017	A. Grabolle	R. Raven		
Megalong Road, Blackheath, NSW, Australi	Feb 2017	A. Grabolle	R. Raven	15	15

Lota Park, Brisbane, QLD, Australia; 27°28':	Apr 2017	J. Wolff	J. Wolff / H	15	15
Lota Park, Brisbane, QLD, Australia; 27°28':	Apr 2017	J. Wolff	J. Wolff / H	15	15
Lota Park, Brisbane, QLD, Australia; 27°28':	Apr 2017	J. Wolff	J. Wolff / H	14	14
Macquarie University Campus, Sydney, NS	Mar 2016	J. Wolff	J. Wolff	15	15
Macquarie University Campus, Sydney, NS	Apr 2016	J. Wolff	J. Wolff / H	26	15
Macquarie University Campus, Sydney, NS	Sep 2016	J. Wolff	J. Wolff / H	16	15
Ginger Meggs Park, Hornsby, NSW, Austral	Nov 2016	J. Wolff	J. Wolff	23	15
Ginger Meggs Park, Hornsby, NSW, Austral	Dec 2016	J. Wolff	J. Wolff		
Macquarie University Campus, Sydney, NS	Sep 2016	J. Wolff	H. Smith	22	15
Macquarie University Campus, Sydney, NS	Dec 2016	J. Wolff	H. Smith	15	15
Normanhurst Park, Normanhurst, NSW, Au	Dec 2016	J. Wolff	H. Smith	18	15
Normanhurst Park, Normanhurst, NSW, Au	Dec 2016	J. Wolff	H. Smith	15	15
Normanhurst Park, Normanhurst, NSW, Au	Dec 2016	J. Wolff	H. Smith	15	15
Bad Cannstatt, Stuttgart, B-W, Germany; h	Jul 2017	W. Schleg	W. Schlege	25	15
Bad Cannstatt, Stuttgart, B-W, Germany; h	Jul 2017	W. Schleg	W. Schlege	17	15
Bad Cannstatt, Stuttgart, B-W, Germany; h	Jul 2017	W. Schleg	W. Schlege	18	15
Cameby, QLD, Australia; 26°37'17"S 150°2	Mar 2017	A. Crave	R. Raven /	15	15
Blackheath, NSW, Australia; 33°40'23.2"S 1	Mar 2017	J. Wolff	H. Smith	36	15
Dorrigo Mountain, NSW, Australia; 30°21'4	Mar 2017	A. Grabolle	H. Smith	23	15
Dry Canyon, Newnes Plateau, NSW, Austra	Mar 2017	J. Wolff	H. Smith	13	12
Stuttgart Harbour, Stuttgart, B-W; German	Jul 2017	W. Schleg	W. Schlegel		
Stuttgart Harbour, Stuttgart, B-W; German	Jul 2017	W. Schleg	W. Schlege	15	15
Stuttgart Harbour, Stuttgart, B-W; German	Jul 2017	W. Schleg	W. Schlege	14	14
Stuttgart Harbour, Stuttgart, B-W; German	Jul 2017	W. Schleg	W. Schlege	15	15
Macquarie University Campus, Sydney, NS	Mar 2016	J. Wolff	J. Wolff		
Macquarie University Campus, Sydney, NS	Mar 2016	J. Wolff	J. Wolff	15	15
Macquarie University Campus, Sydney, NS	Mar 2016	J. Wolff	J. Wolff	15	15
Macquarie University Campus, Sydney, NS	Mar 2016	J. Wolff	J. Wolff / H. Smith		
Macquarie University Campus, Sydney, NS	Mar 2016	J. Wolff	J. Wolff		
Macquarie University Campus, Sydney, NS	Mar 2016	J. Wolff	J. Wolff		
Macquarie University Campus, Sydney, NS	Apr 2016	J. Wolff	J. Wolff		
Macquarie University Campus, Sydney, NS	Apr 2016	J. Wolff	J. Wolff		
Cathedral Reserve, Mount Wilson, NSW, A	Mar 2017	J. Wolff	J. Wolff		
Hornsby Park, Hornsby, NSW, Australia; 33	Mar 2016	J. Wolff	J. Wolff / H	6	
Hornsby Park, Hornsby, NSW, Australia; 33	Mar 2016	J. Wolff	J. Wolff / H	5	
Normanhurst Park, Hornsby, NSW, Australi	Dec 2016	J. Wolff	J. Wolff / H	15	15
Ku-ring-gai Wildflower Garden, St. Ives, NS	Jan 2016	H. Smith /	H. Smith	3	
McCarrs Creek, Kuring-Gai Chase, NSW, Au	Oct 2016	J. Wolff	J. Wolff	4	
Jacksons Bend Track, Fern Tree, TAS, Austr	Jan 2017	J. Wolff	H. Smith	11	11
Rainforest Getaways, Mt. Glorious, QLD, A	Apr 2017	J. Wolff	H. Smith	22	15
Greene's Falls Track, Mt. Glorious, QLD, Au	Apr 2017	R. Raven /	J. Wolff	15	15
Greene's Falls Track, Mt. Glorious, QLD, Au	Apr 2018	R. Raven /	J. Wolff / H. Smith		
Greene's Falls Track, Mt. Glorious, QLD, Au	Apr 2019	R. Raven /	J. Wolff / H	14	14
Greene's Falls Track, Mt. Glorious, QLD, Au	Apr 2020	R. Raven /	J. Wolff / H	22	15
Lake Tikitapu, Whakarewarewa, Bay of Ple	Mar 2018	J. Wolff / A	J. Wolff / A	2	
Lake Tikitapu, Whakarewarewa, Bay of Ple	Mar 2018	J. Wolff / A	J. Wolff / A	8	8
Lake Tikitapu, Whakarewarewa, Bay of Ple	Mar 2018	J. Wolff / A	J. Wolff / A	9	9

Wilga Park, North Ryde, NSW, Australia; 33	Jan 2016	J. Wolff	J. Wolff	17	17
Pretoria Parade, Hornsby, NSW, Australia;	Dec 2016	J. Wolff	J. Wolff	26	15
Pretoria Parade, Hornsby, NSW, Australia;	Dec 2016	J. Wolff	H. Smith	26	15
Pretoria Parade, Hornsby, NSW, Australia;	Dec 2016	J. Wolff	H. Smith	15	15
Piles Creek Loop Track, Brisbane Water NP	Mar 2017	J. Wolff	H. Smith	14	14
Piles Creek Loop Track, Brisbane Water NP	Mar 2017	J. Wolff	H. Smith	14	14
Piles Creek Loop Track, Brisbane Water NP	Mar 2017	J. Wolff	H. Smith	14	14
Megalong Road, Blackheath, NSW, Australi	Mar 2018	J. Wolff	J. Wolff / H. Smith		
Megalong Road, Blackheath, NSW, Australi	Mar 2018	J. Wolff	J. Wolff	10	10
Megalong Road, Blackheath, NSW, Australi	Mar 2018	J. Wolff	J. Wolff / H	3	
Pretoria Parade, Hornsby, NSW, Australia;	Dec 2016	J. Wolff	J. Wolff	15	15
Normanhurst Park, Normanhurst, NSW, Au	Dec 2016	J. Wolff	J. Wolff		
Normanhurst Park, Normanhurst, NSW, Au	Dec 2016	J. Wolff	H. Smith	22	15
Bicentennial Park, West Pymble, NSW, Aus	Jan 2016	J. Wolff	J. Wolff	20	15
Bicentennial Park, West Pymble, NSW, Aus	Jan 2016	J. Wolff	J. Wolff	15	15
Lota Creek Park, Brisbane, QLD, Australia;	May 2017	J. Wolff	H. Smith	15	15
Macquarie University Campus, Sydney, NS	Nov 2016	J. Wolff	H. Smith	32	15
West Mount Cotton Rd, Mt. Cotton, QLD, A	Apr 2017	J. Wolff	H. Smith	15	15
West Mount Cotton Rd, Mt. Cotton, QLD, A	Apr 2017	J. Wolff	J. Wolff	16	15
Lota Creek Park, Brisbane, QLD, Australia;	Apr 2017	R. Raven	H. Smith	4	
Greene's Falls Track, Mt. Glorious, QLD, Au	Apr 2017	R. Raven	H. Smith	15	15
Macquarie University Campus, Sydney, NS	Nov 2016	J. Wolff	J. Wolff / H	15	15
Macquarie University Campus, Sydney, NS	Nov 2016	J. Wolff	J. Wolff	15	15
Macquarie University Campus, Sydney, NS	Nov 2016	J. Wolff	J. Wolff / H	15	15
Binna Burra Rd, Beechmont, QLD, Australia	Mar 2017	A. Grabolle	J. Wolff / H	20	15
Mt Wilson Rd, Mt Wilson, NSW, Australia;	Mar 2018	J. Wolff	H. Smith	18	15
Parque Nacional Lihué Calel, La Pampa, Arg	Aug 2003	M. Ramíre	M. Ramíre	25	15
Gordon River Rd, National Park, TAS, Austr	Jan 2017	J. Wolff	H. Smith	14	14
Gordon River Rd, National Park, TAS, Austr	Jan 2017	J. Wolff	H. Smith		
Jacksons Bend Track, Fern Tree, TAS, Austr	Jan 2017	J. Wolff	H. Smith	25	25
Dry Canyon, Newnes Plateau, NSW, Austra	Mar 2017	J. Wolff	J. Wolff / H	3	
Dry Canyon, Newnes Plateau, NSW, Austra	Mar 2017	J. Wolff	J. Wolff / H. Smith		
Dry Canyon, Newnes Plateau, NSW, Austra	Mar 2017	J. Wolff	J. Wolff / H	22	15
Parque Nacional El Palmar, Entre Rios, Arg	Aug 2003	A. Ojangu	C. Grismad	11	11
Reddy Park, Hornsby, NSW, Australia; 33°4	Nov 2016	J. Wolff	H. Smith		
Florence Cotton Reserve, Hornsby, NSW, A	Jan 2017	J. Wolff	H. Smith		
Florence Cotton Reserve, Hornsby, NSW, A	Jan 2017	J. Wolff	H. Smith	17	15
Macquarie University Campus, Sydney, NS	Dec 2016	J. Wolff	H. Smith	15	15
Macquarie University Campus, Sydney, NS	Dec 2016	J. Wolff	J. Wolff	15	15
Macquarie University Campus, Sydney, NS	Dec 2016	J. Wolff	H. Smith	15	15
Macquarie University Campus, Sydney, NS	Dec 2016	J. Wolff	H. Smith		
Macquarie University Campus, Sydney, NS	Dec 2016	J. Wolff	H. Smith		
Lake Tikitapu, Whakarewarewa, Bay of Ple	Mar 2018	A.-C. Joel	A.-C. Joel	12	12
lab stock from University of Bern	2015	B. Eggs	W. Nentwi	10	9

lab stock from University of Bern	2015	B. Eggs W. Nentwi	8	8
Rainforest Getaways, Mt. Glorious, QLD, A	Apr 2017	R. Raven / H. Smith	12	12
Rainforest Getaways, Mt. Glorious, QLD, A	Apr 2017	R. Raven / J. Wolff	7	
Rainforest Getaways, Mt. Glorious, QLD, A	Apr 2017	R. Raven / J. Wolff	14	14

rvations given)

spinneret kinematics		spinneret morphology
character analysis	tracking and metrics	microCT
		1
11	5	
6	5	
9	5	
5	5	
5	5	
5	5	1
6	5	
4	4	
8	5	
11	5	
15	5	
7	5	
9	5	
1		
8	5	
8	5	
7	5	
8	5	1
7	5	
6	5	
5	5	
5	5	
3	3	

2		
		1
7	5	
9	5	
12	5	
9	5	
8	5	
7	5	
		1
7	5	
9	5	
10	5	
15	5	
6	5	
		1
8	5	
5	5	
10	5	
7	5	
8	5	
10	5	
9	5	
11	5	
7	5	
14	5	
		1
10	5	
10	5	

6	5	
4		
9	5	
		1
14	5	
7	5	
10	5	
2		
7	5	
6	5	
6	5	
8	5	
7	5	
7	5	
7	5	
7	5	
8	5	
9	5	
8	5	
10	5	
8	5	
8	5	
7	5	
5		
10	5	
12	5	1
10	5	
9	5	
10	5	
13	5	

8	5	
6	5	
6	5	
11	5	
6	5	
7	5	
		1
6	5	
6	5	
6	5	1
8	5	
10	5	
10	5	
		1
8	5	
8	5	1
6	5	
8	5	
10	5	
8	5	
6	5	
5		
9	5	1
8	5	
9	5	
9	5	1
7	5	
9	5	
1		
9	5	
8	5	
6	5	

2		
2		
13	5	1
9	5	
11	5	
7	5	
8	5	
10	5	
		1
8	5	
7	5	
4		
11	5	
1		
7	5	
8	5	1
6	5	
9	5	
8	5	
8	5	
9	5	
9	5	
11	5	
7	5	
8	5	
4	4	
8	5	

6	5	
11	5	
6	5	
10	5	
10	5	
10	5	1
10	5	
8	5	
10	5	
8	5	
9	5	1
8	5	
10	5	
1		
2		1
1		
5	5	
8	5	
10	5	
9	5	
8	5	1
9	5	
9	5	
11	5	
10	5	

10	5	1
7	5	
11	5	
11	5	1
8	5	
7	5	
8	5	
8		
7	5	
8	5	
8	5	
5	5	1
9	5	
3		
8	5	
11	5	
6	5	
3	3	
11	5	
6	5	
6	5	
8	5	
9	5	
7	5	
1		1
3		
7	5	
10	5	
1		

6	5
8	5
6	5

ESM.10. Terminal mapping for the phyloge

family	studied species
Agelenidae	Tegenaria_ferruginea
Amaurobiidae	Amaurobius_fenestralis
Antrodiaetidae	(outgroup)
Anyphaenidae	Amaurobioides_litoralis
Anyphaenidae	Anyphaena_accentuata
Araneidae	Arachnura_higginsi
Araneidae	Argiope_keyserlingi
Araneidae	Austracantha_minax
Araneidae	Cyrtophora_hirta
Araneidae	Cyrtophora_moluccensis
Araneidae	Eriophora_sp
Araneidae	Nephila_plumipes
Araneidae	Phonognatha_graeffei
Araneidae	Poecilopachys_australasia
Arkyidae	Arkys_cornutus
Arkyidae	Arkys_curtulus
Arkyidae	Arkys_furcatus
Arkyidae	Arkys_lancearius
Austrochilidae	Hickmania_troglodytes
Clubionidae	Clubiona_sp1
Clubionidae	Clubiona_sp2
Clubionidae	Clubiona_sp3
Corinnidae	Leichhardteus_albofasciatus
Corinnidae	Nyssus_albopunctatus
Corinnidae	Nyssus_coloripes
Cycloctenidae	Cycloctenus_sp
Cycloctenidae	Storenosoma_terraneum
Deinopidae	Deinopis_subrufa
Deinopidae	Menneus_nemesio
Desidae	Austmusia_wilsoni
Desidae	Badumna_insignis
Desidae	Badumna_longinqua
Desidae	Barahna_booloumba
Desidae	Cambridgea_foliata
Desidae	Cambridgea_plagiata
Desidae	Forsterina_sp
Desidae	Matachiinae_spec
Desidae	Metaltella_simoni
Desidae	Paramatachia_sp
Dictynidae	Brigittea_civica
Dictynidae	Paradictyna_rufoflava
Dysderidae	Harpactea_rubicunda
Eresidae	Eresus_sp
Eresidae	Stygodyphus_dumicola
Eutichuridae	Calamoneta_sp
Filistatidae	Filistata_insidiatrix
Filistatidae	Kulkulcania_hibernalis

Filistatidae	Wandella_orana
Gradungulidae	Kaiya_terama
Hersiliidae	Tamopsis_brisbanensis
Hersiliidae	Tamopsis_sp2
Hersiliidae	Tamopsis_sp3
Hypochilidae	Hypochilus_kastoni
Linyphiidae	Linyphia_triangularis
Liphistiidae	(outgroup)
Megadictynidae	Megadictyna_thilenii
Mimetidae	Australomimetus_sp
Miturgidae	Argoctenus_sp
Miturgidae	Mituliodon_tarantulinus
Miturgidae	Miturga_sp
Miturgidae	Nuliodon_sp
Nicodamidae	Dimidamus_dimidiatus
Nicodamidae	Litodamus_olga
Nicodamidae	Oncodamus_bidens
Oecobiidae	Oecobius_navus
Orsolobidae	Tasmanoonops_sp
Oxyopidae	Oxyopes_molarius
Philodromidae	Philodromus_aureolus
Philodromidae	Tibellus_oblongus
Philodromidae	Tibellus_tenellus
Pholcidae	Pholcus_phalangioides
Physoglenidae	Paratupua_sp
Pimoidae	Pimoa_rupicola
Pisauridae	Dendrolycosa_icadia
Pisauridae	Dolomedes_wollemi
Salticidae	Opisthoncus_sp
Salticidae	Sandalodes_bipenicillatus
Salticidae	Servaea_incana
Scytodidae	Scytodes_thoracica
Segestriidae	Ariadna_sp
Segestriidae	Gippsicola_sp
Segestriidae	Segestria_florentina
Sparassidae	Isopeda_villosa
Stiphidiidae	Neolana_dalmasi
Stiphidiidae	Stiphidion_facetum
Stiphidiidae	Stiphidion_sp
Stiphidiidae	Taurongia_sp
Stiphidiidae	Therlinya_vexillum
Tetragnathidae	Leucauge_dromedaria
Tetragnathidae	Meta_sp
Tetragnathidae	Tetragnatha_valida
Theridiidae	Cryptachaea_gigantipes
Theridiidae	Episinus_sp
Theridiidae	spec_aff_Dipoena
Thomisidae	Australomisidia_pilula
Thomisidae	Sidymella_longipes
Thomisidae	Stephanopis_sp
Thomisidae	Tharpyna_sp
Titanoecidae	Goeldia_sp

Toxopidae	Toxopsoides_macleayi
Toxopidae	Toxopsoides_sp
Trechaleidae	Trechalea_ornata
Uloboridae	Philoponella_congregabilis
Uloboridae	Philoponella_variabilis
Uloboridae	Waitkera_waitakerensis
Zoropsidae	Kilyana_hendersoni
Zoropsidae	Zoropsis_spinimana

netic inference

sequence terminal	notes
Tegenaria_domestica	
=	
Antrodiaetus_unicolor	
Amaurobioides_maritima	
=	
Arachnura_logio	
Argiope_bruennichi	
Gasteracantha_cancriformis	close relatives, followir
Cyrtophora_citricola	
=	
Eriophora_sp_GH7_GH21	
Nephila_pilipes	
=	
=	
=	
none (taxonomy)	
none (taxonomy)	
=	
=	
none (taxonomy)	
none (taxonomy)	
Clubiona_huttoni	
none (taxonomy)	matched to subfamily (
none (taxonomy)	
Nyssus_cf_coloripes	
Cycloctenus_sp_CG98	
Pakeha_sp_CG169	close relative to Pakeh
Deinopis_spinosa	
Menneus_camelus	
none (taxonomy)	matched to subfamily I
=	
=	
Barahna_sp_CG293	
Cambridgea_sp_CG97	
none (taxonomy)	
none (taxonomy)	Matched to subfamily I
none (taxonomy)	
Metaltella_sp_CG60	
Paramatachia_sp_CG277	
Brigittea_latens	
none (taxonomy)	Matched to subfamily I
Harpactea_hombergi	
Eresus_walckenaeri	
Stegodyphus_lineatus	
Calamoneta_sp_MR661	
Filistata_insidiatrix	
=	

Pikelinia_tambilloi matched to subfamily,
Tarlina_woodwardi
Hersilia_sericea
none (taxonomy)
none (taxonomy)
Hypochilus_pococki
=
Liphistius sp
=
Australomimetus_sp_NS112
Argoctenus_sp_CG26
=
=
Nuliodon_fishburni
none (taxonomy)
none (taxonomy)
Oncodamus_decipiens
Oecobius_sp_TAB2009
Tasmanoonops_sp_MR690
Oxyopes_salticus
=
=
Tibellus_chamberlini
=
Tupua_sp_CG299
Pimoa_altioculata
Dendrolycosa_cruciata
Dolomedes_sp_CG96
Opisthoncus_kochi
=
=
=
Ariadna_boesenbergi
none (taxonomy) Matched to subfamily S
Segestria_senoculata
Isopeda_parnabyi
Neolana_sp_CG121 (probably S. dalmasi, identified through BOLD engine)
Stiphidion_sp_CG91 (S. facetum, identified through BOLD engine)
none (taxonomy)
none (taxonomy) Matched to family Stip
Therlinya_sp_CG297
Leucauge_venusta
Meta_sp_GH47
Tetragnatha_sp_GH19_GH27
Cryptachaea_riparia
Episinus_antipodianus
Dipoena_cf_hortoni
=
Sidymella_angulata
Stephanopis_cambridgei
Tharpyna_campestrata
Goeldia_sp_MR17

Toxops_sp_CG278
none (taxonomy)
Trechalea_bucculenta
none (taxonomy)
=
=
=
=

ng Scharff and Coddington (1997). Scharff, N. & Coddington, J. A. (1997). A phylogenetic analysis of the c

Castianeirinae, following Baehr and Raven (2013). Baehr, B. C. & Raven, R. J. (2013). The new Australian

a, following Milledge (2011) and Davies (1986). Milledge, G. A. (2011). A revision of Sterenosoma Hogg a

Metaltellinae, following Gray (1983). Gray, M. R. (1983). A new genus of spiders of the subfamily Metalte

Matachiinae, following Lehtinen (1967). Lehtinen, P. T. (1967). Classification of the cribellate spiders anc

Dictyninae, following Forster (1970). Forster, R. R. (1970). The spiders of New Zealand. Part III. Otago Mu

following Ramírez and Grismado (1997). Ramírez, M. J. & Grismado, C. J. (1997). A review of the spider f

Segestriinae, following Giroti and Brescovit (2017). Giroti, A. M. & Brescovit, A. D. (2017). Revision of the

hidiidae, following Gray (2005). Gray, M. R. (2005). A revision of the spider genus Taurongia (Araneae, St

orb-weaving spider family Araneidae (Arachnida, Araneae). Zoological Journal of the Linnean Society 12(

ground-hunting spider genus Leichardteus (Araneae: Corinnidae). Memoirs of the Queensland Museum,

and description of a new genus, Oztira (Araneae: Amaurobiidae). Records of the Australian Museum 63:

ellinae (Araneae, Amaurobioidea) from southeastern Australia. Proceedings of the Linnean Society of Ne

d some allied families, with notes on the evolution of the suborder Araneomorpha. Annales Zoologici Fer

useum Bulletin 3: 1-184.

family Filistatidae in Argentina (Arachnida, Araneae), with a cladistic reanalysis of filistatid genera. Enton

e spider genus Gippsicola Hogg, 1900 (Araneae: Segestriidae). Zootaxa 4227(3): 390-406.

tiphidioidea) from south-eastern Australia. Journal of Arachnology 33: 490-500.

0: 355-434.

, Nature 58: 339-358.

1-32. Davies, V. T. (1986). New Australian species of Otira Forster & Wilton, 1973 and Storenosoma Hog

ew South Wales 106: 275-285.

nnici 4: 199-468.

nologica Scandinavica 28: 319-349.

ɜg, 1900 (Araneae: Amaurobiidae). Memoirs of the Queensland Museum 22: 237-251.

ESM.11. Genbank identifiers of sequences used for the phylogenetic analysis.

Family	Species	H3	COI
Agelenidae	Tegenaria domestica	DQ628648	GU682888
Amaurobiidae	Amaurobius fenestralis	---	FN554820
Antrodiaetidae	Antrodiaetus unicolor	KY018105	KY017574
Anyphaenidae	Amaurobioides maritima	KR558771	KR558954
Anyphaenidae	Anyphaena accentuata	KR558829	KR559012
Araneidae	Arachnura_logio	KJ957997	KJ957944
Araneidae	Argiope bruenicchi	KY018114	KY017585
Araneidae	Cyrtophora citricola	KC849030	KC849071
Araneidae	Cyrtophora_moluccensis	FJ607599	FJ607560
Araneidae	Eriophora sp. GH7-GH21	KY018115	KY017587
Araneidae	Gasteracantha cancriformis	EU003319	FJ525321
Araneidae	Nephila pilipes	KC849045	JF835935
Araneidae	Phonognatha graeffei	KC849059	FJ607582
Araneidae	Poecilopachys_australasia	---	AB910444
Arkyidae	Arkys cornutus	KY018125	FJ607556
Arkyidae	Arkys_lancearius	---	---
Austrochilidae	Hickmania troglodytes	KY018130	KY017601
Clubionidae	Clubiona huttoni	KY018136	KY017608
Corinnidae	Nyssus cf. coloripes	---	KY017624
Cycloctenidae	Cycloctenus sp. CG98	KY018172	KY017657
Cycloctenidae	Pakeha sp. CG169	KY018175	KY017660
Deinopidae	Deinopis spinosa	FJ525337	KY017668
Deinopidae	Menneus camelus	KY018181	KY017669
Desidae	Badumna insignis	KY018184	KY017673
Desidae	Badumna longinqua	KY018185	KY017674
Desidae	Barahna sp. CG293	KY018187	KY017677
Desidae	Cambridgea sp. CG97	KY018188	KY017679
Desidae	Metaltella sp. CG60	KY018200	KY017690
Desidae	Paramatachia sp. CG277	KY018205	KY017694
Dictynidae	Brigittea latens	---	KY017698
Dysderidae	Harpactea hombergi	EU139752	KY017707
Eresidae	Eresus walckenaeri	FJ949037	DQ973154
Eresidae	Stegodyphus lineatus	FJ949053	AY611803
Eutichuridae	Calamoneta sp. MR661	KY018222	---
Filistatidae	Filistata insidiatrix	KY018231	KY017720
Filistatidae	Kukulcania hibernalis	JX240303	JX240233
Filistatidae	Pikelinia tambilloi	KY018233	KY017722
Gradungulidae	Tarlina woodwardi	KY018251	KY017743
Hersiliidae	Hersilia sericea	KY018255	KY017746
Hypochilidae	Hypochilus pococki	---	KY017756
Linyphiidae	Linyphia triangularis	AY078702	FR775771
Liphistiidae	Liphistius bicoloripes	---	---
Liphistiidae	Liphistius laoticus	KP229944	KP229913
Megadictynidae	Megadictyna thilenii	KY018298	KY017789
Mimetidae	Australomimetus sp. NS112	KY018304	KY017794
Miturgidae	Argoctenus sp. CG26	KY018306	KY017795
Miturgidae	Mituliodon tarantulinus	KY018307	KM225114
Miturgidae	Miturga lineata	KY018308	KY017796
Miturgidae	Nuliodon fishburni	KY018310	KY017797
Nicodamidae	Oncodamus decipiens	FJ949048	FJ949011

Oecobiidae	Oecobius sp. TAB-2009	---	FJ607579
Orsolobidae	Tasmanoonops sp. MR690	---	KY017828
Oxyopidae	Oxyopes salticus	---	KY017830
Philodromidae	Philodromus aureolus	---	JN817234
Philodromidae	Tibellus chamberlini	KY018351	KY017845
Philodromidae	Tibellus oblongus	KY018352	KY017846
Pholcidae	Pholcus phalangioides	---	DQ029233
Physoglenidae	Tupua sp. CG299	KY018368	KY017862
Pimoidae	Pimoa altioculata	KC849060	KC849104
Pisauridae	Dendrolycosa cruciata cruciata	KY018375	KY017871
Pisauridae	Dolomedes sp. CG96	KY018376	KY017872
Salticidae	Opisthoncus_kochi	---	EU815584
Salticidae	Sandalodes_bipenicillatus	---	EU815587
Salticidae	Servaea_incana	---	JF949752
Scytodidae	Scytodes thoracica	---	KY269347
Segestriidae	Ariadna boesenbergi	KY018416	KY017903
Segestriidae	Segestria senoculata	---	KY017905
Sparassidae	Isopeda parnabyi	KY018430	KY017921
Stiphidiidae	Neolana sp. CG121	KY018441	KY017935
Stiphidiidae	Stiphidion sp. CG91	KY018446	KY017942
Stiphidiidae	Therlinya sp. CG297	---	KY017944
Tetragnathidae	Leucauge venusta	FJ525341	FJ607568
Tetragnathidae	Meta sp. GH47	---	KY017954
Tetragnathidae	Tetragnatha sp. GH19-GH27	KY018459	KY017958
Theridiidae	Cryptachaea_riparia	KT894369	KT894356
Theridiidae	Dipoena cf. hortoni	---	AY231038
Theridiidae	Episinus antipodianus	KY018469	KY017970
Thomisidae	Australomisidia_pilula	---	KM495290
Thomisidae	Sidymella angulata (sp. CG211, identified w	KY018489	KY017991
Thomisidae	Stephanopis_cambridgei	KY703595	KY703494
Thomisidae	Tharpina_campestrata	KY703601	KY703519
Titanoecidae	Goeldia sp. MR17	KY018504	KY018008
Toxopidae	Toxops sp. CG278	---	KY018018
Trechaleidae	Trechalea_bucculenta	KY190282	KY190311
Uloboridae	Philoponella_variabilis	KM486513	---
Uloboridae	Waitkera waitakerensis	FJ607625	KY018043
Zoropsidae	Kilyana hendersoni	KY018561	KY018072
Zoropsidae	Zoropsis spinimana	KY018569	KY018081

28S	18S	16S	12S
AY633852	DQ628719	DQ628566	---
FR694066	---	---	---
KY016915	KY016296	KY015727	KY015289
KR558888	KY016298	KR558837	KY015291
KR558945	KY016299	KR558880	KY015292
KJ958092	---	---	---
KY016927	KY016316	KY015736	KY015303
---	KC848942	KC849115	KC848910
FJ607525	FJ607486	FJ607451	JQ087466
KY016928	KY016317	KY015738	---
EU003407	EU003348	EU003256	EU003235
JN018407+KC849004	JN018310	KC849130	AF145035
KY016934	KY016323	KY015742	KY015309
AB910501	AB910470	---	---
KY016938	KY016327	KY015749	KY015314
KM486346	---	KM486279	KM486218
KY016945	KY016333	KY015757	KY015320
KY016954	KY016341	---	---
KY016974	KY016361	KY015778	---
KY017009	KY016387	KY015807	KY015355
KY017012	KY016390	KY015810	---
KY017020	KY016396	KY015818	KY015360
KY017021	KY016397	KC849122	KY015361
KY017025	KY016400	KY015822	---
FJ607523	KY016401	KY015823	---
KY017028	KY016404	KY015826	---
KY017030	KY016406	KY015827	KY015367
KY017042	KY016418	KY015836	KY015379
KY017047	KY016423	KY015839	KY015383
---	---	KY015843	KY015386
KY017066	KY016440	KY015855	KY015396
FJ948959	FJ948875	AF374182	---
FJ948976	FJ948892	AF374183	JQ955684
---	---	KY015866	---
KY017088	KY016452	KY015874	KY015403
JX240273	JX240253	AY560684	AY560726
KY017090	KY016454	KY015876	KY015405
KY017115	KY016479	KY015899	KY015426
KY017119	KY016484	KY015903	KY015429
KY017132	KY016493	KY015913	KY015437
EU153170	EU003390	EU333943	EU003239
KY017162	KY016520	KY015942	KY015459
---	---	---	---
KY017183	KY016542	KY015956	---
KY017192	KY016547	KY015963	---
KY017196	KY016550	KY015967	KY015471
KY017197	---	KY015968	KY015472
KY017199+KY017198	KY016551	KY015969	KY015473
KY017201	KY016553	KY015971	KY015474
FJ948971	FJ948887	---	---

FJ607540	FJ607505	FJ607466	---
KY017242	KY016585	KY016009	---
KY017244	KY016587	KY016011	---
JN817021	JN816816	JN816600	---
KY017262	KY016608	KY016030	---
KY017263	KY016609	KY016031	---
KY017268	KY016614	KY016036	KY015509
KY017283	---	KY016051	KY015518
KC849019	KC848947	KC849144	KC848939
KY017295	KY016640	KY016059	---
KY017296	KY016641	KY016060	KY015525
EU815468	EU815528	---	---
EU815471	---	---	---
---	---	---	---
JN816867	JN816653	JN816436	---
KY017341	KY016688	KY016102	KY015556
KY017343	KY016690	KY016104	KY015558
KY017362	KY016706	KY016119	KY015572
KY017377	KY016718	KY016128	KY015583
KY017384	KY016725	KY016134	KY015589
KY017386	KY016727	KY016136	KY015591
EU003409	EU003350	EU003263	EU003238
KY017398	KY016739	KY016148	---
HM030427	KY016743	KY016151	HM030399
KT894296	KT894328	KT894335	---
AY231095	---	AY230961	---
KY017417	KY016757	KY016165	KY015613
---	---	---	---
KY017440	KY016780	---	KY015632
---	---	---	---
---	---	---	---
KY017455	KY016795	KY016193	---
KY017466	KY016805	KY016204	KY015648
---	KY190266	KY190249	KY190233
KM486399	---	---	KM486257
KY017496	KY016834	FJ607474	---
KY017533	KY016869	KY016253	---
KY017542	KY016878	KY016262	KY015694